Reference Model for MERIS Level 2 Processing

Third MERIS reprocessing: Ocean Branch

Doc. no: PO-TN-MEL-GS-0026-Ocean

Issue: 5.0

Date: July 2011

Function	Name	Company	Signature	Date
Editor:	K. Barker	ARGANS		July 2011
Approved:	L. Bourg	ACRI-ST		
Released:	P. Goryl	ESA		

Contributors:

- D. Antoine (LOV, France)
- L. Bourg (ACRI-ST, France)
- C. Brockmann (Brockmann-Consult, Germany)
- R. Doerffer (HGZ, Germany)
- J. Fischer (FUB, Germany)
- G. Moore (Bio-Optika, UK)
- R. Santer (LISE. France)
- F. Zagolski (ParBleu, Canada)

Acknowledgement

To all MERIS QWG members who have all contributed to the MERIS Third Reprocessing and who have provided feedback on the Reference Model Document, and to ACRI-ST as contract manager (ESA Contract numbers: 21091/07/I-OL).

Table of Contents

List Of Figures

List Of Tables

1. Purpose and Scope

The specifications provided in this document define the parameters to be used to generate inherent optical properties for the oceanic and atmospheric components as a function of geophysical properties and wavelengths, which can be the basis upon which to generate test data and auxiliary parameters needed for operation and end-to-end tests of the MERIS ground-segment processor (i.e. mostly to generate water reflectances or total reflectances at top of the atmosphere level). Parameters have been selected from various measurements and models in water, surface and atmosphere. The underlying geo-physical models are the same as those of the MERIS geophysical algorithms, as described in the "MERIS Algorithm Theoretical Basis Document" (ATBD), PO-TN-MEL-GS-0005, Iss. 4.1.

Parts of the model might be subject to evolution in the future, thanks to more field and research works. In its current state, this model has severe limitations when used as a predictive tool. The inherent and/or apparent optical properties computed with this model for given geophysical properties may deviate from locally measured properties. This is due in general to deviation between parameter values or parameterizations adopted in the model and those that may be derived locally in any given water body.

This model is intended to apply to the generation of operational auxiliary parameters for the MERIS processing, and accompanies the third MERIS reprocessing.

1.1 CAUTION: ATBD REFERENCING WITHIN THE RMD

A caution is here provided in relation to the referencing to the ATBD's in this document.

At the time of preparation this RMD is to be considered the most up to date reference source for the scientific content detailed in regard to the MERIS reprocessing. Any discrepancies with the original science and/or the ATBD documents should be made known to the QWG.

2. References, Abbreviations, Definitions

2.1 REFERENCES

ANTOINE, D. and MOREL, A. 1999. A multiple scattering algorithm for atmospheric correction of remotely sensed ocean color (MERIS instrument): Principle and implementation for atmospheres carrying various aerosols including absorbing ones, *International Journal of Remote Sensing*, **20 (9)**, 1875-1916.

AUSTIN, R.W. 1974. The remote sensing of spectral radiance from below the ocean surface, in *Optical aspects of Oceanography*, *Ed. N.G. Jerlov and E. Steemann Nielsen*, *Academic*, London, 317-344 .

BABIN, M., STRAMSKI, D., FERRARI, G. M., CLAUSTRE, H., BRICAUD, A., OBLENSKY, G. And HOEPFFNER, N. 2003. Variations in the light absorption coefficients of phytoplankton nonalgal particles, and dissolved organic matter in coastal waters around Europe. *J. Geophys. Res*., **108**, No. C7, 3211

BARKER, K., HUOT, J-P and MVT Coauthors. 2009. The MERIS Optical Measurement Protocols. Doc No. PO-TN_MEL-GS_0043.

BRICAUD, A., A. MOREL, M. BABIN, K. ALLALI and H. CLAUSTRE, 1998. Variations of light absorption by suspended particles with Chlorophyll-a concentration in oceanic (case 1) waters: Analysis and implications for bio-optical models, *Journal of Geophysical Research*, **103**: 31033-31044

BROGNIEZ, G., J-C. BURIEZ, V. GIRAUD, F. PAROL, C. VANBAUCE, 1995. *Monthly Weather Review*, **123**, 1025.

COX, C., and W. MUNK, 1954**.** Measurements of roughness of the sea surface from photographs of the sun glitter, *Journal of Opt. Soc. Am.,* **44** (11): 838-888.

DEUZÉ, J.L., HERMAN, M. And SANTER, R. 1989. Fourier series expansion of the transfer equation in the atmosphere-ocean system. *Journal of Quantitative Spectroscopy & Radiative Transfer*, **41 (6)**, 483-494.

DOERFFER, R. And SCHILLER, H. 2007. The MERIS Case 2 Water Algorithm. *International Journal of Remote Sensing* **28 (3-4):** 517-535.

ELTERMAN, L. 1968. UV, visible, and IR attenuation for altitudes to 50 km, Air Force Cambridge Research Laboratories, *Environmental Research papers, N° 285, AFCRL-68-0153*, 49pp.

GORDON, H.R. 1979. Diffuse reflectance of the ocean : the theory of its augmentation by Chl-a fluorescence, *Applied Optics*, **18:** 1161-1166.

GORDON, H. R., and W. R. McLUNEY., 1975. Estimation of the depth of sunlight penetration in the sea for remote sensing, *Applied Optics*, **14**: 413-416.

GORDON, H. R. and CLARK, D. K. 1981. Clear water radiances for the atmospheric correction of coastal zone scanner imagery. Applied Optics **20:** 4175-4180

GORDON, H. R. and A. MOREL, 1983. Remote assessment of ocean color for interpretation of satellite visible imagery: A review, *Lecture Notes on Coastal and Estuarine Study*, Vol. 4, Springer Verlag.

HANSEN, J.E. and L. TRAVIS, 1974**.** Light scattering in planetary atmospheres, *Space Science Reviews*, **16**: 527-610.

KATTAWAR G.W., and J.C. VALERIO, 1982. Exact 1-D solution to the problem of the Chl-a fluorescence from the ocean, *Applied Optics*, **21**: 2489-2492.

KISHINO, M., S. SUGIHARA, and N. OKAMI, 1984. Influence of fluorescence of Chl-a on underwater upward irradiance spectrum, *La Mer*, **22**: 224-232.

KOU, L. LABRIE, D. and CHEYLEK, P. 1993. Refractive indices of water and ice in the 0.65- to 2.5-µm spectral range. *Applied Optics*, **32**, No. 19, pp. 3531-3541.

LOISEL, H., and A. MOREL, 1998. Light scattering and chlorophyll concentration in Case 1 waters: A re-examination, *Limnology and Oceanography*, **43**(5): 847-858.

MARITORENA S., A. MOREL, and B. GENTILI, 2000. Determination of the fluorescence quantum yield by oceanic phytoplankton in their natural habitat, *Applied Optics*, **39**, in press.

MIE, G., 1908. Beitraege zur optik trüber medien, speziell kolloidaler metallösungen", *Ann. Physik.*: 25, 377-445.

MOBLEY, C.D., 1994. Light and water: Radiative transfer in natural waters, *Academic Press.*

MOREL, A., 1966. Etude expérimentale de la diffusion de la lumière par l'eau, les solutions de chlorure de sodium et l'eau de mer optiquement pure, *Journal of Physical Chemistry*, 10: 1359-1366.

MOREL, A., 1974. Optical properties of pure water and sea water. In : *Optical aspects of Oceanography*, *N. G. Jerlov and E. Steemann-Nielsen, N. G. Jerlov and E. Steemann-Nielsen*, Academic: 1-24.

MOREL, A., 1987. Chlorophyll-specific scattering coefficient of phytoplankton. A simplified theoretical approach, *Deep-Sea Research*, **34**: 1093-1105.

MOREL A., 1988. Optical modelling of the upper ocean in relation to its biogenous matter content (case 1 waters). *Journal of Geophysical Research*, **93**: 10749-10768.

MOREL A., and D. ANTOINE. 1994. Heating rate within the upper ocean in relation to its bio-optical state, *Journal Physical Oceanography*, **24**: 1652-1665.

MOREL, A. and GENTILLI, B. 1996. Diffuse Reflectance of Oceanic Waters. 3. Implications of Bidirectionality for the Remote-Sensing Problem. *Applied Optics* 35:4850-62

MOREL, A. and ANTOINE, D. 2000. ATBD 2.9: Pigment Index Retrieval in Case 1 Waters. ESA Doc. No. PO-TN-MEL-GS-0005, pp. 9-1 - 9-26.

MOREL, A., and S. MARITORENA, 2001. Bio-optical properties of oceanic waters : a reappraisal. *Journal of Geophysical Research* **106(C4)**: 7163-7180

MOULIN, C., H.R. GORDON, V.F. BANZON, AND R.H. EVANS, 2001. Assessment of Saharan dust absorption in the visible from SeaWiFS imagery, *Geophysical Research Letters*, 106D(18), 239-249.

PETZOLD, T. L., 1972. Volume scattering functions for selected ocean waters. San Diego: Scripps Inst. Oceanogr., Ref. 72-78, 79 pp.

POPE, R. M., and E. S. FRY, 1997. Absorption spectrum (380-700 nm) of pure water. II. integrating cavity measurements, *Applied Optics*, **36**: 8710-8723.

ROTHMAN, L. S. and CoAuthors. 2009. The *HITRAN* 2008 molecular spectroscopic database. *Journal of Quantitative Spectroscopy and Radiative Transfer*. **110:** 533-572

SATHYENDRANATH, S., and T. PLATT, 1998. An ocean color model incorporating trans-spectral processes, *Applied Optics*, **27**, 2216-2227.

SANTER, R., CARRÈRE, V., DUBUISSON, P and ROGER, J. C. 1999. Atmospheric corrections over land for MERIS. *International Journal of Remote Sensing*, **20 (9)**, 1819-1840.

SANTER, R., and ZAGOLSKI, F., 2010. Extraction of the blue aerosols with an approach combining the micro-physical properties of these small particles and their inherent optical properties derived from CIMEL sun/sky radiance measurements, MERIS Technical Note PO-TN-PAR-GS-0004 1 - BLUE_AEROSOLS.

SHETTLE, E.P. and R.W. FENN, 1979. Models for the aerosols of the lower atmosphere and the effects of humidity variations on their optical properties. *Environmental Research Papers, AFGL-TR-79-0214*, 20 September 1979, AFGL, Hanscom (Mass.).

SIEGEL, H., GERTH, M., OHDE, T. and HEENE, T. 2005. Ocean colour remote sensing relevant water constituents and optical properties of the Baltic Sea. *International Journal of Remote Sensing* **26(2)**: 315-330

TASSAN, S. and FERRARI, G. M. 1995. An alternative approach to absorption measurements of aquatic particles retained on filters*, Limnol. Oceanogr.* 40: 1358-1368, 1995.

THUILLIER, G., HERSÉ, M., LABS, D., FOUJOLS, T., PEETERMAN, W., GILLOTAY, D., SIMON, P. C. and MANDEL, H. 2003. The solar spectral irradiance from 200 to 2400 nm as measured by the SOLSPEC spectrometer from the ATLAS and EURECA missions. *Solar Physics*, **214**: 1-22.

VERMONTE, E., TANRÉ, D., DEUZÉ, J. L., HERMAN, M. and MORCETTE, J. J. 1997. Second simulation of the satellite signal in the solar spectrum, 6S: an overview. *I.E.E.E. Transactions on Geoscience and Remote Sensing*, **35 (3)**, 675-687.

WALRAFEN, G.E., 1967. Raman studies of the effect of temperature on water structure, *Journal of Physical Chemistry*, **47**: 114-126.

WORLD CLIMATE RESEARCH PROGRAM, 1986. A preliminary cloudless standard atmosphere for radiation computation, *Int. Ass. for Meteor. and Atm. Phys.*, Radiation Commission, March 1986, WCP-112, WMO/TD-N° 24.

2.2 ABBREVIATIONS AND DEFINITIONS

AOP	Apparent Optical Property
AOT	Aerosol Optical Thickness
AU	Astronomical Unit
ATBD	Algorithm Theoretical Basis Document
BOA	Bottom Of the Atmosphere
BPAC	Bright Pixel Atmospheric Correction
CDOM	Coloured Dissolved Organic Matter
FUB	Freie Universität Berlin (Berlin, Germany)
GS	Ground-Segment
IOP	Inherent Optical Property
LBL	Line-By-Line code to compute the gaseous absorption coefficients
LUT	Look-Up Table
MERIS	MEdium Resolution Imaging Spectrometer (*http://envisat.esa.int/instruments/meris/*)
MOMO	Matrix-Operator MethOd code (RTC/FUB)
NN	Neural Network tool
NIR	Near-InfraRed part of the solar spectrum
QWG	Quality Working Group
RH	Relative Humidity (expressed as percent)
RTC	Radiative Transfer Code
SAM	Standard Aerosol Model
SO	Successive Orders of the scattering code (RTC/LISE)
SPM	Suspended Particulate Matter
STP	Standard Temperature and Pressure (T_o=273.5 K; P_o=1013.25 hPa)
TBD	To Be Defined
TGRD	Table Generation Requirements Document
TOA	Top Of the Atmosphere
TSM	Total Suspended Matter
VIS	Visible part of the solar spectrum
VSF	Volume Scattering Function
WCRP	World Climate Research Programme

Case 2(S) water: Case 2 water dominated by SPM (see ATBD: PO-TN-MEL-GS-0005)

Case 2(Y) water:	Case 2 water dominated by yellow substances (see ATBD: PO-TN-MEL-GS-0005)

2.3 NOTATIONS AND CONVENTIONS

The Geometry notations and conventions in this document are recalled here. In a Cartesian frame linked to the Earth ellipsoid at a given point, the directions of the Sun and of the observer are represented in Figure 2-1 below.

Equations in this document are numbered. The number sequence does *not* reflect a model or algorithm logic.

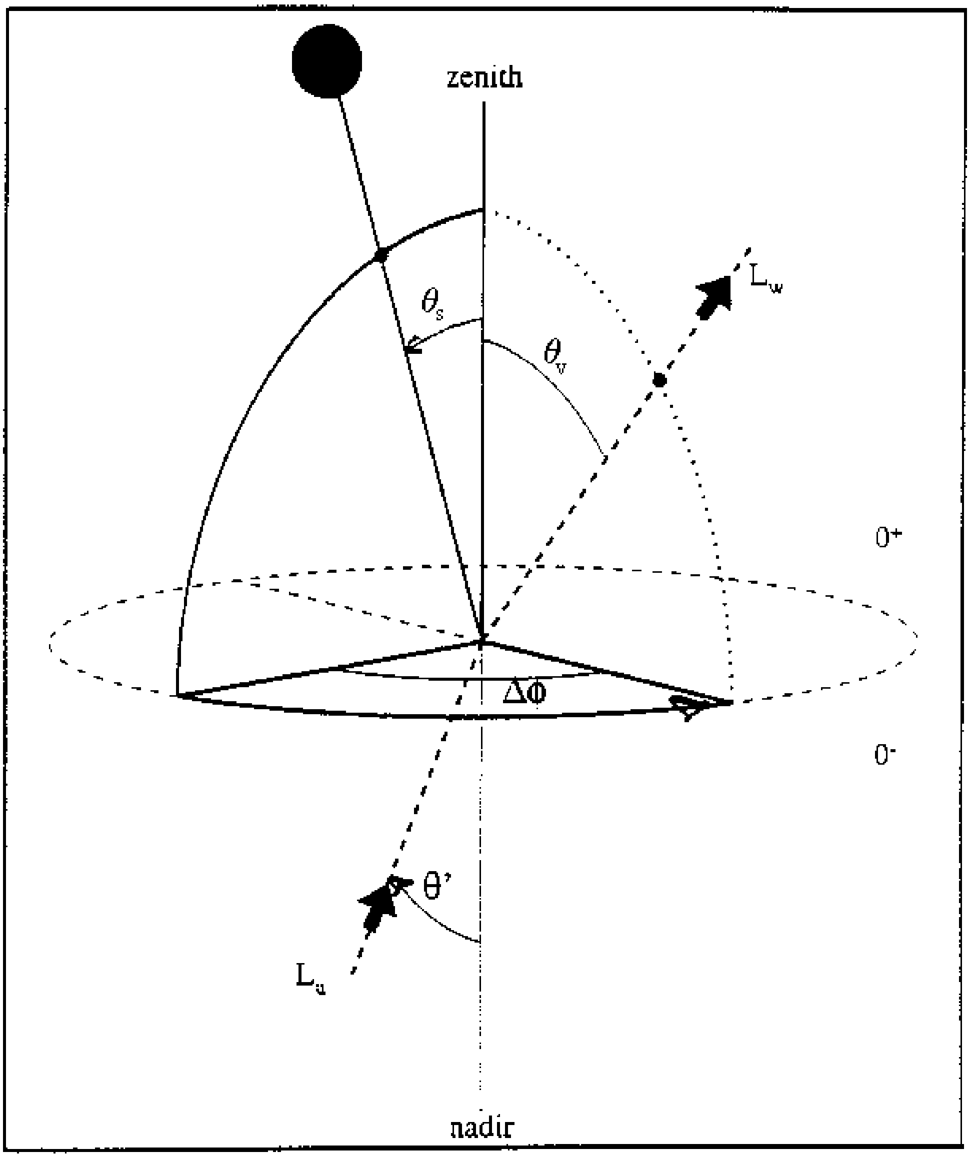

Figure 2-1: Geometry notations (see table of symbols)

2.4 TABLE OF SYMBOLS

Symbol	*Definition*	*Dimension / units*
Geometry (see fig. 2.1)		
λ	Wavelength	nm
θ_S	Solar zenith angle ($\mu_S = \cos(\theta_S)$)	degrees
θ_V, θ	Satellite or view zenith angle ($\mu_V = \cos(\theta_V)$)	degrees
θ'	Refracted view zenith angle ($\theta' = \sin^{-1}(n.\sin(\theta_V))$)	degrees
$\Delta\phi$	Relative azimuth angle between the sun-pixel and pixel-sensor directions	degrees
ψ	Scattering angle (not represented)	degrees
Radiometric quantities		
$L(\lambda,\theta_S,\theta_V,\Delta\phi)$	Spectral radiance	W m^{-2} sr^{-1} nm^{-1}
Inherent Optical Properties (IOPs)		
$\beta(\theta,\lambda)$	Volume scattering function (VSF)	sr^{-1}
$\widetilde{\beta}(\theta)$	Normalised volume scattering function	sr^{-1} m^{-1}
$a(\lambda)$	Absorption coefficient	m^{-1}
$b(\lambda)$	Scattering coefficient	m^{-1}
$c(\lambda)$	Attenuation coefficient for wavelength λ	m^{-1}
$b_b(\lambda)$	Backscattering coefficient	m^{-1}
Apparent Optical Properties (AOPs) and derived quantities		
$\rho_w(\lambda,\theta_S,\theta_V,\Delta\phi)$	Reflectance	dimensionless
$\rho_{wn}(\lambda)$	Normalised water reflectance (i.e. the reflectance if there were no atmosphere, and for $\theta_S = \theta_V = 0$)	dimensionless
$E_u(\lambda)$	Upwelling irradiance	W m^{-2} nm^{-1}
$E_d(\lambda)$	Downwelling irradiance	W m^{-2} nm^{-1}
$E_s(\lambda)$	Total downwelling irradiance just above the sea surface, denoted also as Ed(0+).	W m^{-2} nm^{-1}
$R(\lambda, 0^-)$	Diffuse reflectance at null depth, or irradiance reflectance (E_u / E_d)	dimensionless
$F_0(\lambda)$	Mean extraterrestrial spectral irradiance	W m^{-2} nm^{-1}
f	Ratio of $R(0^-)$ to (b_b/a); subscript 0 when $\theta_S = 0$	dimensionless
f'	Ratio of $R(0^-)$ to $(b_b/(a + b_b))$; subscript 0 when $\theta_S = 0$	dimensionless
$Q(\lambda,\theta_S,\theta_V,\Delta\phi)$	Factor describing the bidirectionality character of $R(\lambda, 0^-)$ Subscript 0 when $\theta_S = \theta_V = 0$; $Q = E_u/L_u$	sr^{-1}
Other atmosphere and aerosol properties		

$f_a(\lambda)$	Aerosol forward scattering proportion (section 15)	dimensionless
$\tau_a(\lambda)$	Aerosol optical thickness	dimensionless
$\tau_r(\lambda)$	Rayleigh (or molecular) optical thickness	dimensionless
$\varpi_a(\lambda)$	Aerosol single scattering albedo	dimensionless
$\varpi_r(\lambda)$	Rayleigh or molecular single scattering albedo	dimensionless
ν	Exponent from the Junge's law used to describe the vertical distribution of particle (aerosol) size.	dimensionless
	RH Relative humidity	percent
$t_d(\lambda,\theta_s)$	Total downwelling transmittance at sea surface level $t_d(\lambda,\theta_s) = E_d(0^+) / (\mu_s\ \varepsilon_c\ F_0)$, where $E_d(0^+)$ is the downwelling irradiance just above the sea surface	dimensionless

Geophysical properties

chl	Chlorophyll concentration	mg m^{-3}
TSM	Total Suspended Matter concentration	g m^{-3}
YS	Yellow Substance absorption coefficient	m^{-1}

Air-water interface

$\Re(\theta')$	Geometrical factor, accounting for multiple reflections and refractions at the air-sea interface (Morel and Gentilli, 1996; defined further in Section 5.1.2)	dimensionless
n	refractive index of sea water	dimensionless
$\rho_F(\theta)$	Fresnel reflectance at the air-sea interface for the scattering angle θ	dimensionless
$\bar{\rho}$	mean reflection coefficient for the downwelling irradiance at the sea surface	dimensionless
$\bar{r}$	average reflection for upwelling irradiance at the air-water interface	dimensionless
σ	Root-mean square of wave facet slopes	dimensionless
β	Angle between the local normal and the normal to a wave facet	
p	probability density function of facet slopes for the illumination and viewing configurations (θ_s, θ_v, $\Delta\phi$)	dimensionless

Miscellaneous

W	Wind-speed just above sea level	m/s
ln	Natural (or Neperian) logarithm	
$\log_{10}$	Decimal logarithm	

3. MERIS Spectral bands and refractive index of seawater

3.1 MERIS SPECTRAL BANDS

The following MERIS spectral bands are considered in this document:

Table 3-1: MERIS Spectral bands

Band number	Wavelength (nm)	Width (nm)
1	412.5	10
2	442.5	10
3	490.0	10
4	510.0	10
5	560.0	10
6	620.0	10
7	665.0	10
8	681.25	7.5
9	708.75	10
10	753.75	7.5
11	761.875	3.75
12	778.75	15
13	865.0	20
14	885.0	10
15	900.0	10

NOTE: Due to the programmable spectral mode of the MERIS sensor and the optimisation of the processing, this list of 15 bands may evolve in the future.

3.2 REFRACTIVE INDEX OF SEAWATER

The refractive index of sea water and fresh water shall be taken from Table 3-2. Values are extracted from Mobley's database (Mobley, 1994) and extrapolated to the MERIS wavelengths, for a standard surface pressure of 1013 hPa, a sea water salinity of 35 psu (and 0 psu for freshwater). Values have been computed at 12 °C. However, because of the small spectral variation of the refractive index of sea water between the MERIS spectral bands, a mean refractive index (at 15 °C) of 1.34 was used for generating atmospheric correction LUT's over the ocean.

Table 3-2: Refractive Index of sea water (35 psu) and for freshwater (0 psu).

Band	λ (nm)	*35* psu	*0* psu
1	412.5	1.349	1.342
2	442.5	1.347	1.340
3	490.0	1.345	1.338
4	510.0	1.344	1.337
5	560.0	1.341	1.335
6	620.0	1.339	1.333
7	665.0	1.338	1.331
8	681.25	1.337	1.331
9	708.75	1.337	1.330
12	778.75	1.335	1.329
13	865.0	1.334	1.327
14	885.0	1.333	1.327

4. Water Optical Properties and water constituents

At a given λ, the optical properties described below apply to Case 1 and Case 2 ocean waters (tentatively to inland waters). Water optical properties shall be computed at least for the following MERIS bands:

1, 2, 3, 4, 5, 6, 7, 9, 12, 13 for algorithms which include the atmospheric correction;
1, 2, 3, 4, 5, 6, 7, 9 for algorithms based on the water-leaving radiance, L_w, (or water reflectance, ρ_w).

4.1 REMOTELY SENSED LAYER

The geometrical thickness of the vertical water layer from which 90% of the remotely sensed ocean colour signal emerges [denoted $Z_{90}(\lambda)$; m] can be approximated by Gordon and McCluney (1975):

$$Z_{90}(\lambda) = 1/K_d(\lambda) \qquad \textbf{Equation 1}$$

where $K_d(\lambda)$ (m^{-1}) is the vertical attenuation coefficient for downward irradiance. Here, we assume that, whatever the wavelength (λ),

$$z >> Z_{90}(\lambda) \qquad \textbf{Equation 2}$$

where z (m) is the geometrical thickness of the water column. In other words, bottom effect is not accounted for in the present model.

4.2 WATER CONSTITUENTS

4.2.1 OVERVIEW

This section presents the concepts and terminology used through the discussion and specification of the water optical properties models.

The apparent optical properties of sea waters can be determined according to the inherent optical properties (absorption and scattering) of 5 groups of substances (cf. Figure 4-1):

1. pure sea water, denoted "w"
2. phytoplankton and other associated particles (detritus, bacteria, …), denoted "p_1"
3. endogenous coloured dissolved organic matter (associated with biological activity), denoted "y_1"
4. terrestrial (exogenous) particles (sediment resuspended from the bottom, brought by rivers), denoted "p_2"
5. exogenous coloured dissolved organic matter from land drainage (present in Case 2 waters only), denoted "y_2".

While only groups 1, 2 and 3 are present in Case 1 waters, all of them (1 to 5 above) co-exist in Case 2 waters. In this case, however, the individual components y_1 and y_2 cannot be practically separated (a measure of CDOM absorption provides the sum $y_1 + y_2$).

IOPs of groups 2, 3, 4 and 5 are related to the following "concentrations":

1. p_1 and y_1 IOPs will be a function of the concentration of chlorophyll-*a* (including the divinyl form and pheopigments) denoted "[*chl*]" and with units as mg m^{-3}
2. p_2 IOPs will be ideally related to the sea water particles dry weight (denoted "*TSM*" and with units as g m^{-3}) from which the contribution of p_1 has been subtracted; practically it is related to the corresponding scattering coefficient (units m^{-1}).
3. y_2 IOPs will be a function of the CDOM concentration as determined by its absorption coefficient at 443 nm, denoted indifferently "$a_{y2}(443)$" or CDOM and with units as m^{-1} (i.e. the total measured CDOM absorption from which a_{y1} has been subtracted).

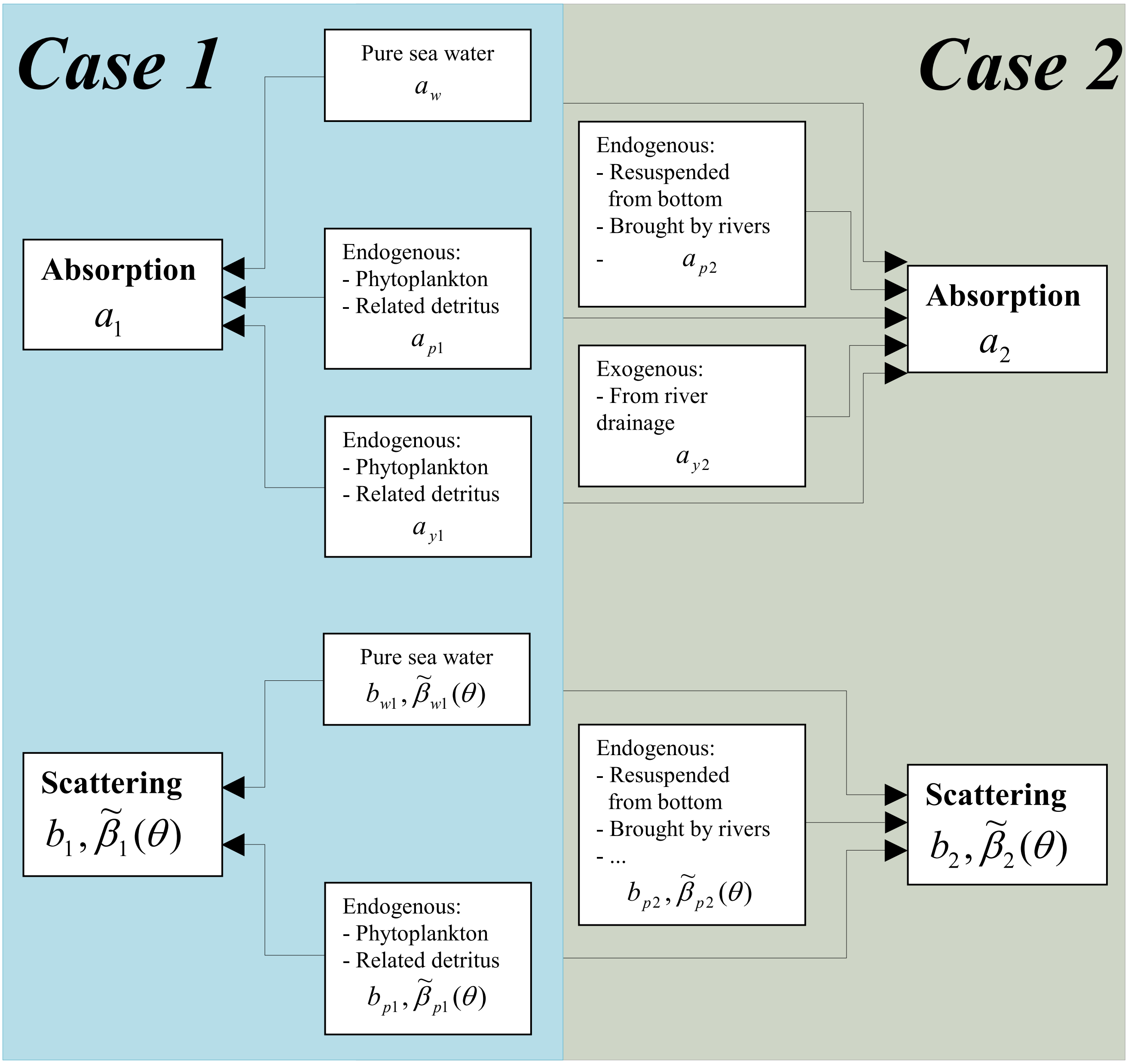

Figure 4-1: Schematic representation of IOP compartments.

Comments on Figure 4-1

Case 2 waters are seen as Case 1 waters to which other optically active substances are added. In other words, Case 1 waters can be seen as particular Case 2 waters when these additional substances are lacking.

Case 1 waters include 3 components:

- *pure sea water for which 2 spectral IOPs must be specified:* $a_w(\lambda)$ *and* $\tilde{\beta}_w(\theta)$.
- *all particulate matter found in open ocean, such as living algal cells, heterotrophic bacteria and organisms, various debris, ... Again, this compartment is described by its absorption and scattering properties:* $a_{p1}(\lambda)$, $b_{p1}(\lambda)$ *and* $\tilde{\beta}_{p1}(\theta)$
- *coloured dissolved organic material presumably generated in open ocean (through processes like excretion, organism decay, ...), and likely related to the particulate matter abundance. This compartment comes into play through its absorption coefficient* $a_{y1}(\lambda)$
  In summary, there are 3 components in forming the absorption coefficient of Case 1 waters and 2 components in forming the scattering properties.

Case 2 waters include the three above components and in addition:

- *exogenous particles, mainly sediment, either transported by rivers, or re-suspended from the bottom in shallow waters. The proportions between organic and mineral particles is varying according to the location and origin; the mineral particles are also geographically differing (clay, calcareous, ...). Therefore, several types of particles may be simultaneously present, and to each type corresponds a couple of properties like* $a_{p2}(\lambda)$ *and* $\tilde{\beta}_{p2}(\theta)$.
- *exogenous CDOM resulting from land drainage which acts only as absorber:* $a_{y2}(\lambda)$. *As for particles, it is likely that several types may be distinguished depending on the location.*

4.2.2 RELATIONSHIP WITH MERIS LEVEL 2 PRODUCTS

The way the IOPs presented above will be practically related to the MERIS Level 2 products is explained separately for Case 1 and Case 2 waters in Sections 4.5 and 4.6 below, respectively.

To summarise:

- The Algal Pigment Index 1 product corresponds to p_1 (and take y_1 into account), *in Case 1 waters*.
- The Algal Pigment Index 2 product corresponds to the absorption of p_1.
- The Total Suspended Matter product corresponds to the aggregate scattering of p_1 and p_2.
- The Yellow Substance product corresponds to the aggregate absorption of p_2, y_1 and y_2.

4.3 VERTICAL DISTRIBUTION

It is assumed that all substances are homogeneously distributed in the upper part of the water column. For many coastal waters, this is a realistic assumption, especially when considering the $Z_{90}(\lambda)$ layer; this may be false for river plumes, where very strong vertical gradients associated with fresh water spreading may be observed.

4.4 INHERENT OPTICAL PROPERTIES (IOPS) OF PURE SEA WATER

These IOPs are involved in both Case 1 and Case 2 waters and include absorption, scattering, and emission (Raman) properties.

4.4.1 ABSORPTION COEFFICIENT

The absorption coefficients of pure water, (a_{W}), are taken from Pope and Fry (1997) for wavelengths up to 682 nm, i.e. up to and including MERIS band 8 (Table 4-1). For band 9 the combined values of Kou *et al.* (1993) and Pope and Fry (1997) are used to ensure consistency of NIR with higher wavelength NIR bands. Values above 709nm are taken from Kou *et al.* (1993). The combined values of Kou *et al.* (1993) and Pope and Fry (1997) are given in Table 4-2, where they have been linearly interpolated onto a 1 nm scale. The values from Pope and Fry (1997) are measured at 2.5 nm intervals and those from Kou *et al.* (1993) at approximately 1.2 nm intervals (20 cm^{-1}). The pure water values are measured at temperature of 22 $^{\mathrm{o}}$C, and appropriate corrections are needed for temperature and salinity when calculations are applied to pure seawater in the NIR region. These corrections are *not* applied for the third MERIS reprocessing, but are intended for inclusion in the next reprocessing.

Table 4-1: Absorption coefficient of pure water, a_w(l), from Pope and Fry (1997). Percent denotes the combined uncertainty from the authors.

λ(nm)	a_w(m^{-1})	Percent	λ(nm)	a_w(m^{-1})	Percent
380.0	0.01137	14.0	500.0	0.02040	6.0
382.5	0.01044	15.0	502.5	0.02280	6.0
385.0	0.00941	13.0	505.0	0.02560	6.0
387.5	0.00917	16.0	507.5	0.02800	5.0
390.0	0.00851	15.0	510.0	0.03250	4.0
392.5	0.00829	14.0	512.5	0.03720	4.0
395.0	0.00813	13.0	515.0	0.03960	4.0
397.5	0.00775	15.0	517.5	0.03990	5.0
400.0	0.00663	11.0	520.0	0.04090	3.0
402.5	0.00579	12.0	522.5	0.04160	4.0
405.0	0.00530	14.0	525.0	0.04170	4.0
407.5	0.00503	13.0	527.5	0.04280	5.0
410.0	0.00473	13.0	530.0	0.04340	4.0
412.5	0.00452	13.0	532.5	0.04470	5.0
415.0	0.00444	13.0	535.0	0.04520	4.0
417.5	0.00442	14.0	537.5	0.04660	4.0
420.0	0.00454	14.0	540.0	0.04740	3.0
422.5	0.00474	13.0	542.5	0.04890	4.0
425.0	0.00478	14.0	545.0	0.05110	3.0
427.5	0.00482	13.0	547.5	0.05370	4.0
430.0	0.00495	12.0	550.0	0.05650	3.0
432.5	0.00504	11.0	552.5	0.05930	3.0

Table 4-1: Continued

435.0	0.00530	11.0	555.0	0.05960	3.0
437.5	0.00580	10.0	557.5	0.06060	4.0
440.0	0.00635	9.0	560.0	0.06190	3.0
442.5	0.00696	9.0	562.5	0.06400	4.0
445.0	0.00751	8.0	565.0	0.06420	3.0
447.5	0.00830	7.0	567.5	0.06720	3.0
450.0	0.00922	6.0	570.0	0.06950	3.0
452.5	0.00969	6.0	572.5	0.07330	4.0
455.0	0.00962	5.0	575.0	0.07720	3.0
457.5	0.00957	5.0	577.5	0.08360	3.0
460.0	0.00979	6.0	580.0	0.08960	3.0
462.5	0.01005	6.0	582.5	0.09890	3.0
465.0	0.01011	7.0	585.0	0.11000	3.0
467.5	0.01020	6.0	587.5	0.12200	3.0
470.0	0.01060	6.0	590.0	0.13510	3.0
472.5	0.01090	8.0	592.5	0.15160	3.0
475.0	0.01140	7.0	595.0	0.16720	3.0
477.5	0.01210	8.0	597.5	0.19250	3.0
480.0	0.01270	7.0	600.0	0.22240	3.0
482.5	0.01310	7.0	602.5	0.24700	3.0
485.0	0.01360	6.0	605.0	0.25770	3.0
487.5	0.01440	6.0	607.5	0.26290	3.0
490.0	0.01500	5.0	610.0	0.26440	3.0
492.5	0.01620	9.0	612.5	0.26650	3.0
495.0	0.01730	6.0	615.0	0.26780	3.0
497.5	0.01910	8.0	617.5	0.27070	3.0

Table 4-2: Absorption coefficient of pure water, from Pope and Fry (1997) combined with that of Kou *et al.* (1993) where a_w, is computed as $4\pi k/l$, with l in meters. Percent denotes the combined uncertainty from the authors.

λ(nm)	a_w(m^{-1})	Percent	λ(nm)	a_w(m^{-1})	Percent
600	0.22240	3.0	650	0.34000	3.0
601	0.23329	3.0	651	0.34650	3.0
602	0.24305	3.0	652	0.35451	3.0
603	0.25012	3.0	653	0.36078	3.0
604	0.25448	3.0	654	0.36539	3.0
605	0.25770	3.0	655	0.37100	3.0
606	0.26035	3.0	656	0.37939	3.0
607	0.26218	3.0	657	0.38878	3.0
608	0.26343	3.0	658	0.39677	3.0
609	0.26393	3.0	659	0.40366	3.0
610	0.26440	3.0	660	0.41000	3.0
611	0.26524	3.0	661	0.41625	3.0
612	0.26612	3.0	662	0.42182	3.0
613	0.26679	3.0	663	0.42554	3.0
614	0.26720	3.0	664	0.42729	3.0
615	0.26780	3.0	665	0.42900	3.0
616	0.26875	3.0	666	0.43185	3.0
617	0.26997	3.0	667	0.43482	3.0
618	0.27153	3.0	668	0.43725	3.2
619	0.27344	3.0	669	0.43867	3.4
620	0.27550	3.0	670	0.44076	3.6
621	0.27780	3.0	671	0.44479	3.7
622	0.28009	3.0	672	0.44919	3.9
623	0.28160	3.0	673	0.45136	4.0
624	0.28226	3.0	674	0.45147	4.1
625	0.28340	3.0	675	0.45309	4.2
626	0.28615	3.0	676	0.45782	4.3
627	0.28930	3.0	677	0.46401	4.4
628	0.29090	3.0	678	0.46751	4.4
629	0.29092	3.0	679	0.46976	4.5
630	0.29160	3.0	680	0.47253	4.6
631	0.29458	3.0	681	0.47758	4.7
632	0.29821	3.0	682	0.48239	4.9
633	0.30016	3.0	683	0.48710	4.8
634	0.30047	3.0	684	0.49100	5.0
635	0.30120	3.0	685	0.49554	5.0
636	0.30362	3.0	686	0.50105	5.0
637	0.30654	3.0	687	0.50799	4.9
638	0.30841	3.0	688	0.51459	5.0
639	0.30914	3.0	689	0.52027	5.0
640	0.31080	3.0	690	0.52754	5.0
641	0.31509	3.0	691	0.53750	5.1
642	0.32016	3.0	692	0.54751	4.9
643	0.32301	3.0	693	0.55654	5.0
644	0.32369	3.0	694	0.56627	4.9
645	0.32500	3.0	695	0.57710	4.9
646	0.32874	3.0	696	0.58944	4.8
647	0.33321	3.0	697	0.60279	4.7
648	0.33611	3.0	698	0.61693	4.9
649	0.33730	3.0	699	0.63072	4.6

Table 4-2: Continued

λ(nm)	a_w(m^{-1})	Percent	λ(nm)	a_w(m^{-1})	Percent
700	0.64540	4.5	750	2.85331	1.4
701	0.66111	4.6	751	2.86199	1.4
702	0.67804	4.5	752	2.85847	1.3
703	0.69508	4.5	753	2.87041	1.4
704	0.71421	4.4	754	2.86611	1.4
705	0.73216	4.4	755	2.87610	1.3
706	0.75239	4.4	756	2.87625	1.3
707	0.77364	4.2	757	2.87184	1.3
708	0.79680	4.1	758	2.86805	1.3
709	0.82328	4.1	759	2.86383	1.4
710	0.85045	4.0	760	2.86147	1.3
711	0.88298	4.0	761	2.87326	1.4
712	0.91417	3.8	762	2.86970	1.3
713	0.95116	3.7	763	2.86573	1.3
714	0.98900	3.6	764	2.86197	1.3
715	1.02991	3.4	765	2.85906	1.3
716	1.07551	3.4	766	2.85116	1.3
717	1.11880	3.3	767	2.83386	1.2
718	1.16501	3.2	768	2.83071	1.3
719	1.21627	3.1	769	2.82702	1.4
720	1.26652	2.9	770	2.82456	1.3
721	1.31808	2.9	771	2.81256	1.3
722	1.37438	2.8	772	2.79373	1.3
723	1.43092	2.7	773	2.77913	1.3
724	1.48762	2.6	774	2.77629	1.4
725	1.54773	2.5	775	2.75845	1.3
726	1.61257	2.4	776	2.75354	1.4
727	1.69050	2.5	777	2.74233	1.4
728	1.77644	2.4	778	2.72433	1.4
729	1.85493	2.5	779	2.70754	1.3
730	1.97385	2.3	780	2.69049	1.4
731	2.08007	2.2	781	2.66158	1.4
732	2.18600	2.1	782	2.64123	1.5
733	2.30218	2.0	783	2.62508	1.5
734	2.42636	1.7	784	2.60909	1.5
735	2.50845	1.7	785	2.59189	1.5
736	2.58251	1.6	786	2.56239	1.4
737	2.64692	1.5	787	2.53203	1.5
738	2.70610	1.4	788	2.51188	1.5
739	2.75339	1.4	789	2.49212	1.5
740	2.78132	1.5	790	2.46361	1.5
741	2.80403	1.4	791	2.44892	1.6
742	2.81442	1.5	792	2.42220	1.5
743	2.82607	1.4	793	2.39243	1.5
744	2.83757	1.4	794	2.36846	1.6
745	2.83287	1.4	795	2.35411	1.6
746	2.84299	1.4	796	2.33868	1.7
747	2.84247	1.3	797	2.32448	1.7
748	2.84854	1.4	798	2.30231	1.7
749	2.85249	1.4	799	2.27308	1.7

Table 4-2: Continued

λ(nm)	a_w(m^{-1})	Percent	λ(nm)	a_w(m^{-1})	Percent
800	2.24624	1.6	850	4.19789	1.1
801	2.24388	1.7	851	4.20351	1.1
802	2.23274	1.7	852	4.22543	1.0
803	2.21638	1.7	853	4.26296	1.0
804	2.20312	1.7	854	4.29016	1.0
805	2.20097	1.7	855	4.31793	1.0
806	2.19948	1.7	856	4.35468	1.1
807	2.18857	1.7	857	4.37120	1.0
808	2.17855	1.7	858	4.39207	1.0
809	2.18975	1.7	859	4.42876	1.0
810	2.18681	1.7	860	4.45472	1.0
811	2.19116	1.7	861	4.47775	1.0
812	2.20123	1.7	862	4.50133	1.0
813	2.21023	1.7	863	4.53366	1.0
814	2.21810	1.7	864	4.56791	1.0
815	2.23486	1.7	865	4.60137	1.0
816	2.25625	1.7	866	4.63476	1.0
817	2.27656	1.6	867	4.66806	1.0
818	2.29676	1.6	868	4.70129	1.0
819	2.31496	1.6	869	4.73236	1.0
820	2.34218	1.6	870	4.77352	1.0
821	2.38694	1.6	871	4.82781	1.0
822	2.42825	1.7	872	4.87160	1.0
823	2.47588	1.7	873	4.91275	1.0
824	2.53536	1.7	874	4.95499	1.0
825	2.61217	1.8	875	5.01166	1.0
826	2.71748	1.8	876	5.06478	1.0
827	2.82486	1.8	877	5.10457	1.0
828	2.93831	1.7	878	5.16173	1.0
829	3.08026	1.7	879	5.22291	1.0
830	3.22208	1.7	880	5.27880	1.0
831	3.35180	1.5	881	5.33915	1.0
832	3.46488	1.4	882	5.39711	1.0
833	3.57271	1.3	883	5.44204	1.1
834	3.65559	1.3	884	5.49960	1.1
835	3.72123	1.2	885	5.56612	1.0
836	3.78077	1.1	886	5.62673	1.0
837	3.83235	1.1	887	5.68424	1.0
838	3.87605	1.1	888	5.73926	1.0
839	3.91190	1.1	889	5.79463	1.0
840	3.93804	1.0	890	5.84989	1.0
841	3.97268	1.0	891	5.90503	1.0
842	4.00851	1.0	892	5.96005	1.0
843	4.03446	1.1	893	6.01494	1.0
844	4.06097	1.1	894	6.06970	1.0
845	4.08745	1.1	895	6.12435	1.0
846	4.11378	1.0	896	6.17887	0.9
847	4.13889	1.0	897	6.23328	0.9
848	4.17315	1.0	898	6.28736	0.9
849	4.20536	1.0	899	6.34086	0.9

4.4.2 WATER ABSORBANCE: BAND INTEGRATED VALUES

These are the current harmonic means that have been derived by merging Pope and Fry (1997) and Kou *et al*. (1993). The RMD has been updated with these.

Table 4-3 shows the change with wavelength is together with the percentage effect for consideration for future smile effect corrections.

Table 4-3: the band integrated values for water absorption at 22°C. The rate of change with wavelength is shown for future smile effect corrections.

Band	λ(nm)	Width	a_w(22°C)	$da_w/d\lambda$	%/nm
1	412.500	10.00	0.00460	-0.000055	-1.19
2	442.500	10.00	0.00688	0.000250	3.63
3	490.000	10.00	0.01518	0.000366	2.41
4	510.000	10.00	0.03185	0.001358	4.26
5	560.000	10.00	0.06202	0.000467	0.75
6	620.000	10.00	0.27554	0.001565	0.57
7	665.000	10.00	0.42828	0.003327	0.78
8	681.250	7.50	0.47929	0.004006	0.84
9	708.750	10.00	0.81911	0.026110	3.19
10	753.750	7.50	2.86712	0.001879	0.07
11	761.875	3.75	2.86710	0.000335	0.01
12	778.750	15.00	2.69492	-0.017334	-0.64
13	865.000	20.00	4.61577	0.034267	0.74
14	885.000	10.00	5.55930	0.057044	1.03
15	900.000	10.00	6.40580	0.059348	0.93

In Table 4-4 are the current temperature coefficients.

Table 4-4: temperature dependence of the water absorption for bands 7-15. The temperature effects at wavelengths below 665 nm are not significant.

Band	λ(nm)	da_w=/dT	a_w(T=5)	a_w(T=15)	%Change
7	665.000	0.00017	0.4254	0.4271	-0.40
8	681.250	0.00015	0.4767	0.4782	-0.32
9	708.750	0.00180	0.7885	0.8065	-2.24
10	753.750	0.00894	2.7153	2.8047	-3.19
11	760.625	0.00568	2.7705	2.8273	-2.01
12	778.750	0.00055	2.6857	2.6912	-0.20
13	865.000	0.00394	4.5489	4.5883	-0.86
14	885.000	-0.00488	5.6423	5.5935	0.87
15	900.000	0.00049	6.3975	6.4024	-0.08

4.4.3 NORMALISED VSF, TOTAL SCATTERING AND BACKSCATTERING COEFFICIENTS

The normalised volume scattering function of pure sea water is that published by Morel (1966, 1974), which can be expressed as:

Equation 3

$$\tilde{\beta}_w(\theta) = \frac{3}{4\pi(3+p)}(1 + p\cos^2\theta)$$

where the parameter p (polarisation factor at 90°) equals 0.84.

The backscattering probability corresponding to this normalised VSF is

Equation 4

$$\tilde{b}_{bw} = \frac{1}{2}$$

The total scattering coefficient for sea water (in the salinity range 35-38 psu), $b_w(\lambda)$, is determined from Morel (1974):

Equation 5

$$b_w(\lambda) = 0.00288.\left(\frac{\lambda}{500}\right)^{-4.32}$$

Note that for fresh water it is

Equation 6

$$b_w(\lambda) = 0.00222.\left(\frac{\lambda}{500}\right)^{-4.32}$$

Also note, the variation of b_w with salinity is roughly a linear function of salinity.

4.4.4 EMISSION

See Section 4.5.4.1

4.5 CASE 1 WATERS IOPS

4.5.1 TOTAL ABSORPTION COEFFICIENT (PURE SEA WATER AND PHYTOPLANKTON[1])

Here, the analytical approach suggested by Figure 4-1, and which consists of explicitly modelling a_1 as the sum $[a_w + a_{p1} + a_{y1}]$ is not used, by lack of knowledge of a stable relationship (if any) between [*chl*] and the associated endogenous yellow substance. The indirect approach used here relies on the consideration of $K_d(\lambda)$. Indeed, this coefficient merges the influences of all absorbing substances, without discriminating their separate

---

[1] Here, “phytoplankton” means the living algal cells as well as all other particulate or dissolved matter found in open ocean, such as heterotrophic bacteria and organisms, various debris, yellow substances etc. (see comments on Figure 4-1).

contributions. Therefore a_1 is globally determined as a function of [*chl*] as described in Morel and Maritorena (2000):

$$a_1(\lambda) = K_d(\lambda)\,u(\lambda) \qquad \textbf{Equation 7}$$

where $K_d(\lambda)$ is given as a function of $[chl]$:

$$K_d(\lambda) = K_w(\lambda) + \chi(\lambda)[chl]^{e(\lambda)} \qquad \textbf{Equation 8}$$

Values for K_w are given in Table 4-5 below.

The factor *u* is determined by iterations as described in Morel (1988) and Morel and Maritorena (2000). This scheme consists of introducing of $b_b(\lambda)$ in the following equation:

$$R(\lambda) = f(\lambda)\frac{b_b(\lambda)}{a_1(\lambda)} \qquad \textbf{Equation 9}$$

where R is the irradiance reflectance (E_u/E_d), and $b_b = b_{bw} + b_{bp1}$. The coefficient b_{bw} is calculated according to Equation 4and Equation 5 above, and b_{bp1} according to Equation 19 below (§4.5.2.2). Then $a_1(\lambda)$ is replaced by u_1 $K_d(\lambda)$, with u_1=0.75, whatever the wavelength and *f* is set to 0.33. A first set of $R(\lambda)$ values is thus derived. Then, an exact relationship (derived from the Gershun's equation), namely:

$$a_1 = K_d\,\mu_d\,[1 + R\left(\frac{\mu_d}{\mu_u}\right)]^{-1}[1 - R + (K_d)^{-1}\left(\frac{dR}{dZ}\right)] \qquad \textbf{Equation 10}$$

is operated by letting μ_u equal to 0.42, by interpolating μ_d from the values given in table 4.5.1-2 below as a function of the chlorophyll concentration and wavelength, and by neglecting *dR/dZ*, which results in:

$$a_1(\lambda) = K_d(\lambda)\,\mu_d\,[1 + R(\lambda)\left(\frac{\mu_d}{0.42}\right)]^{-1}[1 - R(\lambda)] \qquad \textbf{Equation 11}$$

or

$$a_1(\lambda) = K_d(\lambda)\,\mu_2(\lambda) \qquad \textbf{Equation 12}$$

The first set of $R(\lambda)$ values is used to produce the spectrally varying $u_2(\lambda)$ values through Equation 11 and a new set of $a_1(\lambda)$ values through Equation 12. The value of a_1 shall be constrained to be higher than or equal to $a_w(\lambda)$ (from §4.4.1). With these adjusted $a_1(\lambda)$ values, through a second loop using Eq. (10), a more accurate set of $R(\lambda)$ values is derived, and so forth. Stable $R(\lambda)$ values (then stable $a_1(\lambda)$ values) are obtained within three loops in this iterative process. The final $a_1(\lambda)$ values are given in Table 4-7.

Table 4-5: K_w, x and e values. Values are reproduced from Morel and Maritorena (2000), and from Morel and Antoine (1994). Above 775nm, only $a(\lambda)$ is specified (unit: m^{-1}).

λ	K_w	e	χ	λ	K_w	e	χ	λ	$a(\lambda)$
350	0.0271	0.6523	0.19031	**530**	0.04454	0.55863	0.06402	**775**	2.40
355	0.0238	0.65786	0.1809	**535**	0.0463	0.55144	0.06301	**800**	1.96
360	0.0216	0.65298	0.1731	**540**	0.04846	0.54385	0.06227	**825**	2.77
365	0.0188	0.653	0.1669	**545**	0.05212	0.5332	0.0603	**850**	4.33
370	0.0177	0.6534	0.16131	**550**	0.05746	0.53029	0.05711	**875**	5.61
375	0.0159	0.6595	0.15625	**555**	0.06053	0.525	0.0561	**900**	6.78
380	0.0151	0.66268	0.15132	**560**	0.0628	0.52	0.0555		
385	0.01376	0.6651	0.146	**565**	0.06507	0.515	0.0551		
390	0.01271	0.661	0.142	**570**	0.07034	0.505	0.0545		
395	0.01208	0.642	0.138	**575**	0.07801	0.501	0.0542		
400	0.01042	0.638	0.134	**580**	0.09038	0.501	0.0535		
405	0.0089	0.628	0.1333	**585**	0.11076	0.502	0.0525		
410	0.00812	0.628	0.1347	**590**	0.13584	0.502	0.0522		
415	0.00765	0.631	0.1346	**595**	0.16792	0.502	0.0521		
420	0.00758	0.63424	0.13223	**600**	0.2331	0.495	0.0522		
425	0.00768	0.6378	0.12961	**605**	0.25838	0.491	0.0525		
430	0.00771	0.63656	0.12728	**610**	0.26506	0.489	0.05228		
435	0.00792	0.63739	0.12485	**615**	0.26843	0.482	0.0538		
440	0.00885	0.64339	0.12065	**620**	0.27612	0.481	0.0555		
445	0.0099	0.645	0.1157	**625**	0.28401	0.48	0.056		
450	0.01148	0.64317	0.1103	**630**	0.29218	0.483	0.057		
455	0.01182	0.637	0.1068	**635**	0.30176	0.488	0.0585		
460	0.01188	0.6345	0.10384	**640**	0.31134	0.49	0.0598		
465	0.01211	0.6394	0.1005	**645**	0.32553	0.501	0.0605		
470	0.01251	0.63255	0.09704	**650**	0.34052	0.505	0.062		
475	0.0132	0.62869	0.09333	**655**	0.3715	0.508	0.0615		
480	0.01444	0.63262	0.0891	**660**	0.41048	0.51	0.064		
485	0.01526	0.62689	0.08618	**665**	0.42947	0.513	0.0675		
490	0.0166	0.625	0.08323	**670**	0.43946	0.51	0.0705		
495	0.01885	0.62364	0.08028	**675**	0.44844	0.495	0.0735		
500	0.02188	0.62459	0.07742	**680**	0.46543	0.465	0.074		
505	0.02701	0.62553	0.07333	**685**	0.48643	0.432	0.067		
510	0.03385	0.625	0.06911	**690**	0.5164	0.405	0.058		
515	0.0409	0.615	0.0675	**695**	0.55939	0.365	0.046		
520	0.04214	0.592	0.06602	**700**	0.62438	0.33	0.027		
525	0.04287	0.575	0.06578	**705**	0.74200	0.60000	0.02500		
				710	0.83400	0.60000	0.02000		
				715	1.00200	0.60000	0.01500		
				720	1.17000	0.60000	0.01000		
				725	1.48500	0.60000	0.00700		
				730	1.80000	0.60000	0.00500		
				735	2.09000	0.60000	0.00200		
				740	2.38000	0.60000	0.00000		
				745	2.42000	0.60000	0.00000		
				750	2.47000	0.60000	0.00000		

Note that the K_w values in Table 4-5 have been obtained by using the absorption and scattering coefficients of pure sea water as described in Sections 4.4.1 and 4.4.2 ($K_w = a_w + 0.5b_w$).

Table 4-6: mean cosines of the downwelling irradiance (μ_d) as a function of wavelength (lines) and chlorophyll concentration (columns), sun zenith angle: 30°, no Raman emission

	0.03	*0.1*	*0.3*	*1.*	*3.*	*10.*
350.	0.770	0.769	0.766	0.767	0.767	0.767
400.	0.770	0.769	0.766	0.767	0.767	0.767
412.	0.765	0.770	0.774	0.779	0.782	0.782
443.	0.800	0.797	0.796	0.797	0.799	0.799
490.	0.841	0.824	0.808	0.797	0.791	0.791
510.	0.872	0.855	0.834	0.811	0.796	0.796
555.	0.892	0.879	0.858	0.827	0.795	0.795
620.	0.911	0.908	0.902	0.890	0.871	0.871
670.	0.914	0.912	0.909	0.901	0.890	0.890
700.	0.914	0.912	0.909	0.901	0.890	0.890
710.	0.914	0.912	0.909	0.901	0.890	0.890

Table 4-7: total absorption coefficients a_1 (m^{-1}), computed as function of *chl* and λ through Equation 7 to Equation 12, with μ_d from Table 4-6.

	0.03	*0.1*	*0.3*	*1*	*3*	*10*
412.5	0.0115643	0.0228673	0.0445606	0.095627	0.194528	0.425296
442.5	0.0126095	0.0223262	0.0415189	0.0877143	0.179471	0.399036
490.0	0.0173563	0.0234732	0.0358357	0.0663681	0.128137	0.280947
510.0	0.0325	0.0372764	0.0470969	0.0713008	0.120455	0.244057
560.0	0.0619	0.0619	0.0672771	0.0807731	0.106826	0.174669
620.0	0.2755	0.2755	0.2755	0.276348	0.301871	0.375383
665.0	0.429	0.429	0.429	0.429	0.467546	0.58095
681.25	0.4715	0.4715	0.4715	0.4715	0.504934	0.617897
708.5	0.7915	0.7915	0.7915	0.7915	0.7915	0.7915

4.5.2 NORMALISED VSF, TOTAL SCATTERING, AND BACKSCATTERING COEFFICIENTS

4.5.2.1 Pure Sea Water

See Section 4.4 above.

4.5.2.2 Case 1 Waters Particles (phytoplankton and its retinue)

The normalised VSF for Case 1 waters particles is obtained as a mixture of two separately computed VSFs (Figure 4-2). The first one (Table 4-8) corresponds to a population of “small” non-absorbing particles of spheroidal shape, with a relative index of refraction equal to 1.06, and assumed to obey Junge’s law with an exponent ν equal to -4.2. The second population corresponding to “large” particles (Table 4-9) is identical except that ν is equal to -3. The weighted sum of these two VSFs provides,

$$\widetilde{\beta}_{p1}(\theta, chl) = w_s[chl]\,\widetilde{\beta}_{p1,s}(\theta) + w_l[chl]\,\widetilde{\beta}_{p1,l}(\theta)$$ **Equation 13**

where the subscripts s and l stand for small and large particles, respectively, and where the weights w_s and w_l are such that :

$$w_s[chl] + w_1[chl] = 1$$ **Equation 14**

$$w_s[chl] = 0.855(0.5 - 0.25\log_{10}[chl])$$ **Equation 15**

The normalised VSF computed through Equation 13 are assumed to be wavelength independent (no change in shape).

The backscattering efficiency for Case 1 water particles that derives from the use of the above chlorophyll-varying normalised VSF exactly matches the following expression (from Morel and Maritorena, 2000):

$$\widetilde{b}_{bp1}(\lambda) = 0.002 + \left[0.01\ \left[0.5 - 0.25\log_{10}[chl]\right]\right]$$ **Equation 16**

At 550 nm, the particle scattering coefficient, $b_{p1}(550)$, is taken from Loisel and Morel (1998):

$$b_{p1}(550) = A_{bp1}\left[chl\right]^{b_{p1}}$$ **Equation 17**

where A_{bp1} and b_{p1} equal 0.416 and 0.766, respectively. The factor of variation in A_{bp1} equals 1.3.

Table 4-8: Normalised VSF for small particles (see text)

θ	$\widetilde{\beta}(\theta)$	θ	$\widetilde{\beta}(\theta)$	θ	$\widetilde{\beta}(\theta)$	θ	$\widetilde{\beta}(\theta)$
0.	42.282829537580	47.0	2.2451516277360D-02	94.0	2.7766892922530D-03	141.0	2.0547500762672D-03
1.0	34.958732391211	48.0	2.1023504641344D-02	95.0	2.7211555064079D-03	142.0	2.0626834742451D-03
2.0	23.065450213275	49.0	1.9706560577018D-02	96.0	2.6576883225850D-03	143.0	2.0626834742451D-03
3.0	15.406801674179	50.0	1.8492750686405D-02	97.0	2.6021545367400D-03	144.0	2.0706168722230D-03
4.0	10.720368953898	51.0	1.7382074969504D-02	98.0	2.5545541488728D-03	145.0	2.0706168722230D-03
5.0	7.6237177877997	52.0	1.6358666630359D-02	99.0	2.5069537610056D-03	146.0	2.0785502702008D-03
6.0	5.5174720252582	53.0	1.5406658873015D-02	100.0	2.4593533731384D-03	147.0	2.0785502702008D-03
7.0	4.0755214089952	54.0	1.4533985095450D-02	101.0	2.4196863832490D-03	148.0	2.0864836681787D-03
8.0	3.0647033724414	55.0	1.3716845103730D-02	102.0	2.3800193933597D-03	149.0	2.0944170661566D-03
9.0	2.3450331082773	56.0	1.2971105693810D-02	103.0	2.3482858014483D-03	150.0	2.0944170661566D-03
10.0	1.8249354036444	57.0	1.2272966671758D-02	104.0	2.3165522095368D-03	151.0	2.1023504641344D-03
11.0	1.4415460129661	58.0	1.1622428037573D-02	105.0	2.2848186176253D-03	152.0	2.1023504641344D-03
12.0	1.1551186123732	59.0	1.1019489791255D-02	106.0	2.2530850257139D-03	153.0	2.1102838621123D-03
13.0	0.93748963904439	60.0	1.0464151932805D-02	107.0	2.2292848317803D-03	154.0	2.1102838621123D-03
14.0	0.76994420714985	61.0	9.9405476662657D-03	108.0	2.2054846378467D-03	155.0	2.1182172600901D-03
15.0	0.63911454109686	62.0	9.4566103896159D-03	109.0	2.1896178418909D-03	156.0	2.1182172600901D-03
16.0	0.53574236544527	63.0	9.0044067048776D-03	110.0	2.1658176479573D-03	157.0	2.1261506580680D-03
17.0	0.45312395890378	64.0	8.5760032140728D-03	111.0	2.1499508520016D-03	158.0	2.1340840560459D-03
18.0	0.38633268132813	65.0	8.1793333151796D-03	112.0	2.1340840560459D-03	159.0	2.1340840560459D-03
19.0	0.33187783760806	66.0	7.7985302122420D-03	113.0	2.1182172600901D-03	160.0	2.1420174540237D-03
20.0	0.28700653864525	67.0	7.4494607012159D-03	114.0	2.1023504641344D-03	161.0	2.1420174540237D-03
21.0	0.24977510193512	68.0	7.1162579861456D-03	115.0	2.0944170661566D-03	162.0	2.1499508520016D-03
22.0	0.21861271467807	69.0	6.7989220670309D-03	116.0	2.0785502702008D-03	163.0	2.1499508520016D-03
23.0	0.19234523397335	70.0	6.5053863418499D-03	117.0	2.0706168722230D-03	164.0	2.1499508520016D-03
24.0	0.17006031905353	71.0	6.2277174126246D-03	118.0	2.0626834742451D-03	165.0	2.1578842499795D-03
25.0	0.15102809730463	72.0	5.9579818813772D-03	119.0	2.0547500762672D-03	166.0	2.1578842499795D-03
26.0	0.13469323086820	73.0	5.7041131460855D-03	120.0	2.0468166782894D-03	167.0	2.1658176479573D-03
27.0	0.12058764926356	74.0	5.4661112067495D-03	121.0	2.0468166782894D-03	168.0	2.1658176479573D-03
28.0	0.10834641618371	75.0	5.2360426653914D-03	122.0	2.0388832803115D-03	169.0	2.1658176479573D-03
29.0	9.7675995903483D-02	76.0	5.0218409199890D-03	123.0	2.0388832803115D-03	170.0	2.1737510459352D-03
30.0	8.8330453085557D-02	77.0	4.8235059705424D-03	124.0	2.0309498823336D-03	171.0	2.1737510459352D-03
31.0	8.0119386178466D-02	78.0	4.6331044190736D-03	125.0	2.0309498823336D-03	172.0	2.1737510459352D-03
32.0	7.2868260426697D-02	79.0	4.4506362655827D-03	126.0	2.0309498823336D-03	173.0	2.1816844439131D-03
33.0	6.6442208064625D-02	80.0	4.2840349080475D-03	127.0	2.0230164843558D-03	174.0	2.1816844439131D-03
34.0	6.0730161520562D-02	81.0	4.1253669484902D-03	128.0	2.0230164843558D-03	175.0	2.1816844439131D-03
35.0	5.5636920018772D-02	82.0	3.9746323869107D-03	129.0	2.0230164843558D-03	176.0	2.1816844439131D-03
36.0	5.1091082977455D-02	83.0	3.8397646212870D-03	130.0	2.0230164843558D-03	177.0	2.1816844439131D-03
37.0	4.7005383018854D-02	84.0	3.7048968556633D-03	131.0	2.0309498823336D-03	178.0	2.1896178418909D-03
38.0	4.3332219755103D-02	85.0	3.5858958859953D-03	132.0	2.0309498823336D-03	179.0	2.1896178418909D-03
39.0	4.0016059400355D-02	86.0	3.4748283143052D-03	133.0	2.0309498823336D-03	180.0	2.1975512398688D-03
40.0	3.7025168362699D-02	87.0	3.3637607426151D-03	134.0	2.0309498823336D-03		
41.0	3.4311946254269D-02	88.0	3.2606265689028D-03	135.0	2.0388832803115D-03		
42.0	3.1852592881131D-02	89.0	3.1654257931684D-03	136.0	2.0388832803115D-03		
43.0	2.9615374651373D-02	90.0	3.0781584154119D-03	137.0	2.0388832803115D-03		
44.0	2.7576491371061D-02	91.0	2.9988244356332D-03	138.0	2.0468166782894D-03		
45.0	2.5712142846263D-02	92.0	2.9194904558546D-03	139.0	2.0468166782894D-03		
46.0	2.4014395679000D-02	93.0	2.8480898740538D-03	140.0	2.0547500762672D-03		

Table 4-9: Normalised VSF for large particles (see text)

θ	$\tilde{\beta}(\theta)$	θ	$\tilde{\beta}(\theta)$	θ	$\tilde{\beta}(\theta)$	θ	$\tilde{\beta}(\theta)$
0.	99.652707830456	47.0	5.4847330202340D-03	94.0	4.9069761508587D-04	141.0	1.8994746390421D-04
1.0	73.481769997167	48.0	5.1127525700883D-03	95.0	4.6695418209784D-04	142.0	1.8994746390421D-04
2.0	36.927670628662	49.0	4.7803445082559D-03	96.0	4.5112522677249D-04	143.0	1.8203298624153D-04
3.0	20.353147764054	50.0	4.4795943570742D-03	97.0	4.2738179378447D-04	144.0	1.8203298624153D-04
4.0	12.851924552535	51.0	4.2184165942059D-03	98.0	4.1155283845912D-04	145.0	1.8203298624153D-04
5.0	8.5125509962107	52.0	3.9809822643257D-03	99.0	3.9572388313377D-04	146.0	1.8203298624153D-04
6.0	5.7523452534420	53.0	3.7752058450961D-03	100.0	3.7989492780842D-04	147.0	1.8203298624153D-04
7.0	4.0082080674853	54.0	3.5852583811919D-03	101.0	3.7198045014574D-04	148.0	1.8203298624153D-04
8.0	2.8410204741822	55.0	3.4269688279384D-03	102.0	3.5615149482039D-04	149.0	1.8203298624153D-04
9.0	2.0484251086536	56.0	3.2765937523476D-03	103.0	3.4823701715771D-04	150.0	1.8203298624153D-04
10.0	1.5064337638360	57.0	3.1499621097448D-03	104.0	3.3240806183236D-04	151.0	1.8203298624153D-04
11.0	1.1225736827185	58.0	3.0312449448046D-03	105.0	3.2449358416969D-04	152.0	1.8203298624153D-04
12.0	0.85049768410875	59.0	2.9283567351899D-03	106.0	3.1657910650701D-04	153.0	1.8203298624153D-04
13.0	0.65265948597486	60.0	2.8333830032378D-03	107.0	3.0866462884434D-04	154.0	1.8203298624153D-04
14.0	0.50766625519465	61.0	2.7463237489483D-03	108.0	3.0075015118166D-04	155.0	1.8203298624153D-04
15.0	0.39944368763522	62.0	2.6671789723216D-03	109.0	2.9283567351899D-04	156.0	1.8203298624153D-04
16.0	0.31787708084369	63.0	2.5880341956948D-03	110.0	2.8492119585631D-04	157.0	1.8203298624153D-04
17.0	0.25567720089273	64.0	2.5168038967308D-03	111.0	2.8492119585631D-04	158.0	1.8203298624153D-04
18.0	0.20747803192703	65.0	2.4455735977667D-03	112.0	2.7700671819364D-04	159.0	1.8203298624153D-04
19.0	0.17005838153790	66.0	2.3664288211399D-03	113.0	2.6909224053096D-04	160.0	1.8203298624153D-04
20.0	0.14039491925820	67.0	2.2872840445132D-03	114.0	2.6909224053096D-04	161.0	1.8203298624153D-04
21.0	0.11692057851070	68.0	2.2081392678864D-03	115.0	2.6117776286829D-04	162.0	1.8203298624153D-04
22.0	9.8052463762885D-02	69.0	2.1210800135970D-03	116.0	2.5326328520561D-04	163.0	1.8203298624153D-04
23.0	8.2753778440933D-02	70.0	2.0340207593076D-03	117.0	2.5326328520561D-04	164.0	1.8203298624153D-04
24.0	7.0351791943521D-02	71.0	1.9390470273555D-03	118.0	2.4534880754293D-04	165.0	1.8203298624153D-04
25.0	6.0102543370356D-02	72.0	1.8361588177407D-03	119.0	2.4534880754293D-04	166.0	1.8203298624153D-04
26.0	5.1681539137270D-02	73.0	1.7332706081259D-03	120.0	2.3743432988026D-04	167.0	1.8203298624153D-04
27.0	4.4661397450477D-02	74.0	1.6303823985111D-03	121.0	2.3743432988026D-04	168.0	1.8203298624153D-04
28.0	3.8780940547109D-02	75.0	1.5274941888963D-03	122.0	2.3743432988026D-04	169.0	1.8203298624153D-04
29.0	3.3858135440925D-02	76.0	1.4246059792816D-03	123.0	2.2951985221758D-04	170.0	1.8203298624153D-04
30.0	2.9663462279707D-02	77.0	1.3296322473295D-03	124.0	2.2951985221758D-04	171.0	1.8203298624153D-04
31.0	2.6125690764491D-02	78.0	1.2425729930400D-03	125.0	2.2160537455491D-04	172.0	1.8203298624153D-04
32.0	2.3094445819687D-02	79.0	1.1555137387506D-03	126.0	2.2160537455491D-04	173.0	1.8203298624153D-04
33.0	2.0490582668666D-02	80.0	1.0842834397865D-03	127.0	2.2160537455491D-04	174.0	1.8203298624153D-04
34.0	1.8258699967792D-02	81.0	1.0130531408224D-03	128.0	2.1369089689223D-04	175.0	1.8203298624153D-04
35.0	1.6319652940437D-02	82.0	9.4973731952104D-04	129.0	2.1369089689223D-04	176.0	1.8994746390421D-04
36.0	1.4641783675949D-02	83.0	8.9433597588231D-04	130.0	2.1369089689223D-04	177.0	1.8994746390421D-04
37.0	1.3185519786017D-02	84.0	8.3893463224358D-04	131.0	2.0577641922956D-04	178.0	1.8994746390421D-04
38.0	1.1903374404664D-02	85.0	7.9144776626753D-04	132.0	2.0577641922956D-04	179.0	1.8994746390421D-04
39.0	1.0787433054226D-02	86.0	7.5187537795416D-04	133.0	2.0577641922956D-04	180.0	2.1369089689223D-04
40.0	9.8060378240547D-03	87.0	7.0438851197810D-04	134.0	1.9786194156688D-04		
41.0	8.9433597588231D-03	88.0	6.6481612366473D-04	135.0	1.9786194156688D-04		
42.0	8.1756554255436D-03	89.0	6.2524373535135D-04	136.0	1.9786194156688D-04		
43.0	7.5029248242162D-03	90.0	5.9358582470065D-04	137.0	1.8994746390421D-04		
44.0	6.9093389995156D-03	91.0	5.6192791404995D-04	138.0	1.8994746390421D-04		
45.0	6.3790689961163D-03	92.0	5.3818448106192D-04	139.0	1.8994746390421D-04		
46.0	5.9042003363558D-03	93.0	5.1444104807390D-04	140.0	1.8994746390421D-04		

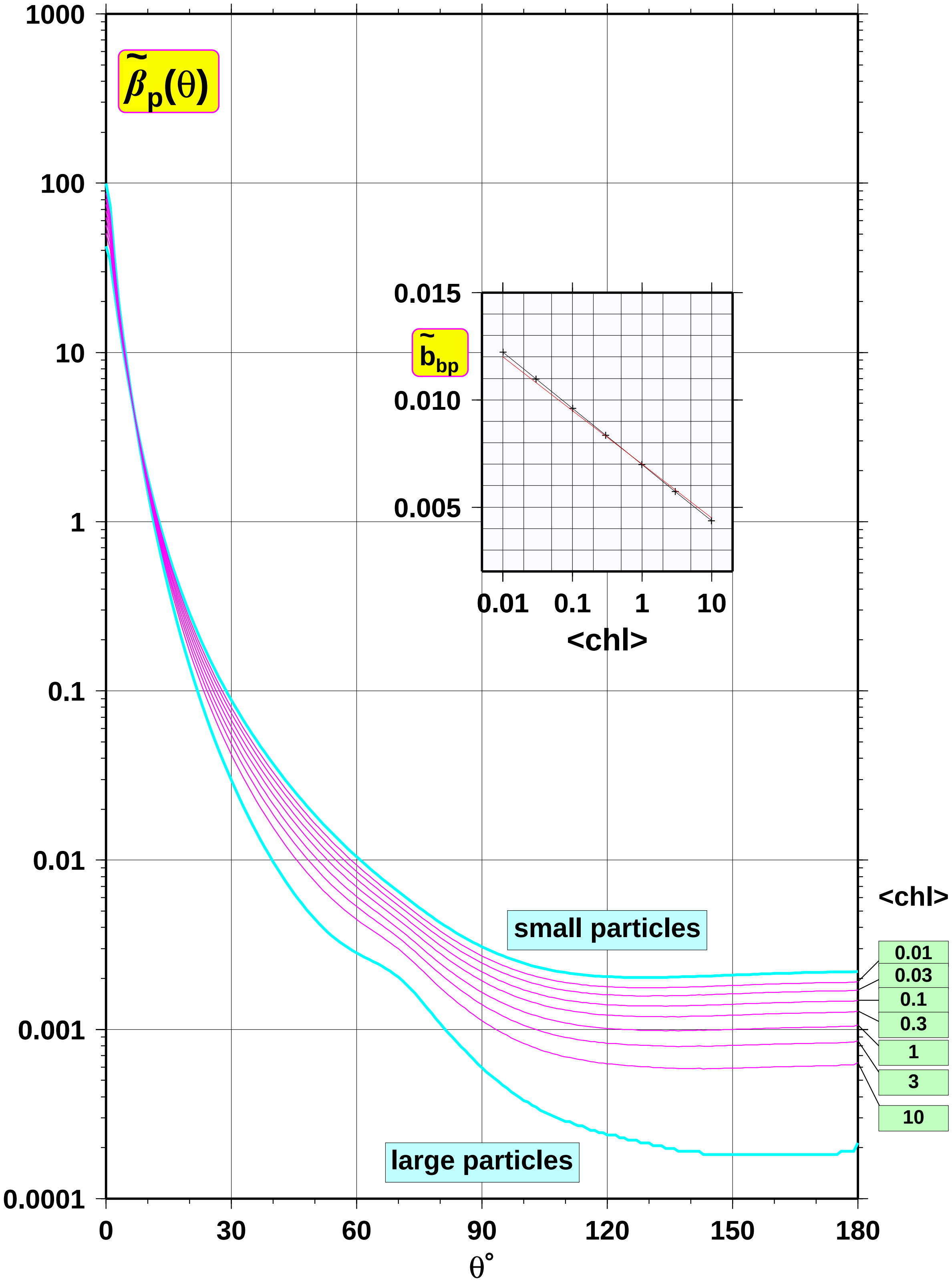

Figure 4-2: Normalised VSFs of large, small particles (blue curves; tables 4.5.2-1 & 4.5.2-2), and of mixed populations following a mixing rule depending on chl (Eqs. (12) & (13)). These "mixed VSFs" are shown as red curves, and the corresponding chl concentration is indicated in the green box on the side of the figure. In insert is shown the resulting backscattering probability, as a function of the chl concentration (Equation 16)

At any other wavelength, the particle scattering coefficient, $b_{p1}(\lambda)$, is expressed from its value at 550 nm according to :

Equation 18

$$b_{p1}(\lambda) = b_{p1}(550)\left(\frac{\lambda}{550}\right)^{-v}$$

where: $v = 0.5\ \ \left[0.3 - \log_{10}(chl)\right]$ when $[chl] < 2$ mg m^{-3}

and: $v = 0$ when $[chl] \geq 2$ mg m^{-3}

From the above equations, it results that the backscattering coefficient for Case 1 water particles is expressed as :

Equation 19

$$b_{bp1}(\lambda) = \left[0.002 + 0.01 \cdot \left(0.5 - 0.25 \log_{10}(chl)\right)\right] b_{p1}(550)\left(\frac{\lambda}{550}\right)^{-v}$$

4.5.3 TOTAL IOPS IN CASE 1 WATERS

Case 1 water absorption and backscattering coefficients, denoted $a_1(\lambda)$ and $b_{b1}(\lambda)$, respectively, can be expressed as:

$a_1(\lambda)$ as per section 4.5.1

$$b_{b1}(\lambda) = 0.5 b_w(\lambda) + b_{bp1}(\lambda) b_{p1}(\lambda)$$

Equation 20

where the normalised VSF for these waters is denoted $\tilde{\beta}(\theta)$:

$$\tilde{\beta}_1(\theta,\lambda) = \eta(\lambda)\tilde{\beta}_{\mathrm{w}}(\theta) + (1 - \eta(\lambda))\tilde{\beta}_{\mathrm{p1}}(\theta)$$

Equation 21

and where:

$$\eta(\lambda) = \mathrm{b_w}(\lambda) \,/\, \left(\mathrm{b_w}(\lambda) + \mathrm{b_{p1}}(\lambda)\right)$$

Equation 22

4.5.4 WARNING CONCERNING THE USE OF THE MODEL FOR CASE 1 WATERS IOPS: STATE-OF-THE-ART AND UNCERTAINTIES

4.5.4.1 Raman Emission

The Raman emission by water molecules is a trans-spectral (or inelastic) scattering process by which absorbed energy at a given wavelength λ' is re-emitted as radiation at longer wavelengths around λ. The Raman VSF $\beta^R(\theta)$ is symmetrical with respect to $\theta = \pi/2$ and expresses as :

$$\beta^R(\theta) = 0.067\,(1 + 0.55\cos^2(\theta))$$

Equation 23

The Raman emission undergoes a frequency shift that is independent on the incident frequency and thus occurs within the whole (visible) spectrum. According to Walrafen (1967), the shape of the redistribution function $f^R(\kappa_R)$ is the sum of four Gaussian functions (i = 1 to 4) :

Equation 24

$$f^R(\kappa_R) = \left[\left(\frac{\pi}{4 \ln(2)} \right)^{1/2} \sum_1^4 A_i \right]^{-1} \sum_1^4 A_i \frac{1}{\Delta\kappa_i} \exp\left(-\frac{(\kappa_R - \kappa_i)^2}{\Delta\kappa_i^{\,2}} \right)$$

where κ_R is the wavenumber shift of the Raman emission, κ_i is the centre of the i^{th} Gaussian function, $\Delta\kappa_i$ the width at half maximum of this function and the A_i's are the weights of each function (see Table 4-10).

Table 4-10: Data from Walrafen (1967)

i	A_i	κ_i (cm^{-1})	$\Delta\kappa_i$ (cm^{-1})
1	0.41	3250	210
2	0.39	3425	175
3	0.10	3530	140
4	0.10	3625	140

To an incident (exciting) radiation with a wavelength λ' and a wavenumber κ' will correspond a Raman emission within a spectral band described by Equation (5) such as $\kappa = \kappa' - \kappa^R$, leading to redistribution functions expressed in terms of wavelengths $f^R(\lambda' \rightarrow \lambda)$ as shown in Figure 4-3 below.

The magnitude of the phenomenon is expressed through the Raman coefficient $a^R(\lambda')$ through:

Equation 25

$$a^R(\lambda') = \int_{\lambda'}^{\infty} b^R(\lambda' \rightarrow \lambda)\, d\lambda$$

where b^R is the Raman scattering coefficient for an exciting wavelength λ' and an emission at wavelength λ ($\lambda > \lambda'$). This coefficient, according to recent determinations at 488 nm, is :

Equation 26

$$a^R(448) = 2.610^{-4}\, m^{-1}$$

it varies according to a law in λ^{-5}.

This phenomenon is important in clear Case 1 waters (low [c*hl*]) to the extent that the elastic scattering is low, in the red part of the spectrum in particular. With an almost isotropic function (Equation 23), it strongly modifies the upward radiance distribution and thus affects the Q (and f/Q) behaviour.

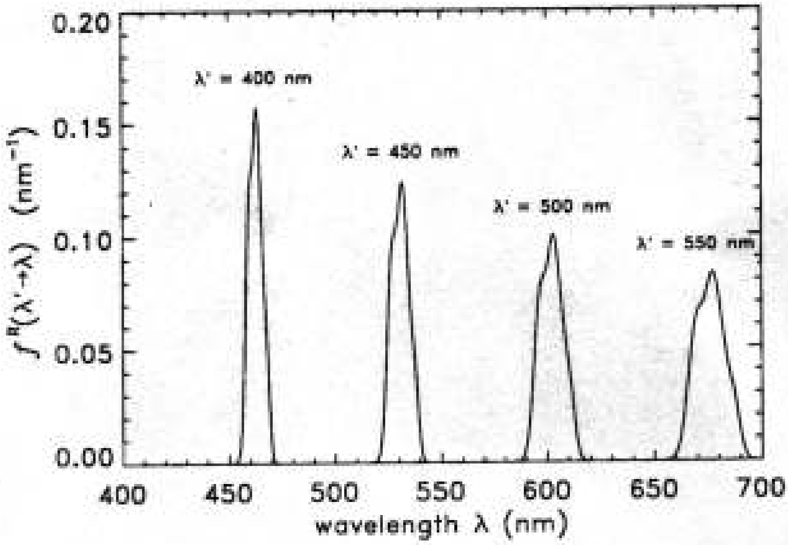

Figure 4-3: the Raman wavelength redistribution function $f^R(\lambda' \to \lambda)$, for selected incident wavelengths λ'. Figure reproduced from Mobley (1994). Conversely the Raman emission at a fixed wavelength λ is excited by a spectral band centred on λ', the shape of which is approximately the reverse image of those shown in this figure.

4.5.4.2 Fluorescence by Phytoplankton

The emission of fluorescence by phytoplankton is isotropic ($\tilde{\beta}^F(\theta)$=constant). Its intensity depends on the chlorophyll-*a* concentration and on the quantum yield for fluorescence, ϕ_f. This yield ϕ_f is defined as the number of photons emitted divided by the number of photons absorbed by the algal cells. It is known as being varying within a factor of 10, approximately with the lower values observed near the surface (Maritorena *et al.* 2000). If ϕ_f is fixed, this emission can be (but has not been) incorporated into the IOP model for Case 1 waters. Any radiation within the 380-680 nm domain, after being weighted by the algal absorption spectrum, is able to excite the *chl-a* fluorescence around 683 nm. In contrast, the emission spectrum is independent from the excitation spectrum and is currently modelled (*e.g.*, see Gordon, 1979; Kattawar and Valerio, 1982; Kishino *et al.*, 1984; Sathyendranath and Platt, 1998) as a Gaussian spectral distribution, peaked around 683 nm, and with a standard deviation σ = 10.64 nm, corresponding to a width of about 25 nm at half maximum (see Figure 4-4). This curve, modelled through $\exp(-(\lambda-683)/2\sigma^2)$ accounts very well for observations for natural populations as well as for algae grown in culture, except beyond 710 nm where a weak shoulder (around 730 nm) often appears.

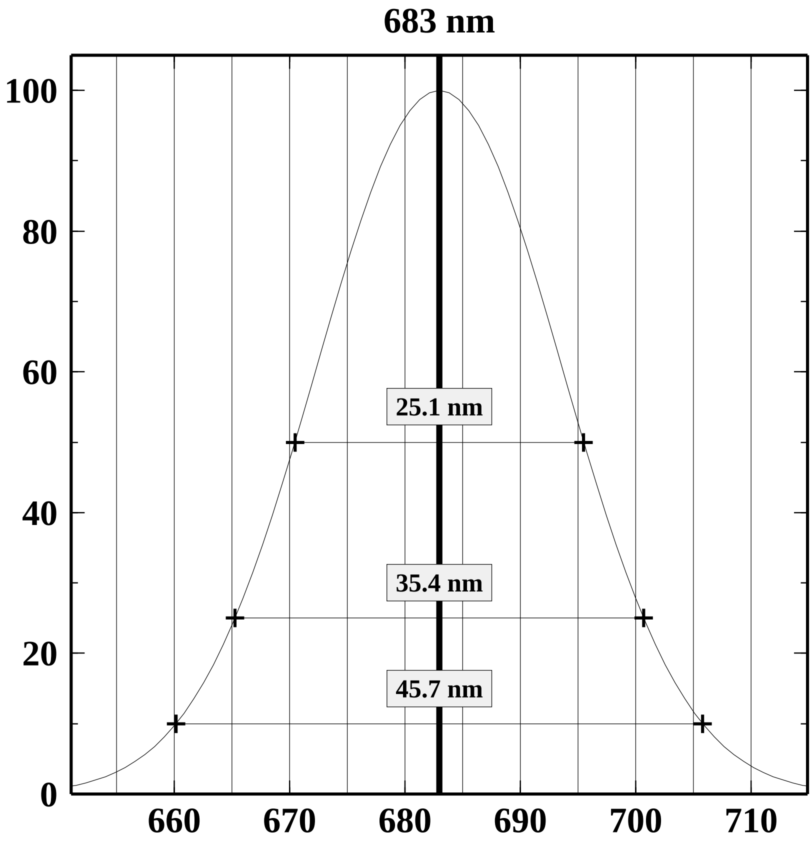

Figure 4-4: Typical Gaussian spectral distribution for the chl-a fluorescence, peaked around 683 nm, and with a standard deviation $\sigma = 10.64$ nm, corresponding to a width of about 25 nm at half maximum

4.5.4.3 Fluorescence by Endogenous Yellow Substance

This term, which may be important in presence of high amount of yellow substance, is less documented than the chlorophyll-*a* fluorescence and depends on the chemical composition of the organic matter collectively forming the "yellow substance". This emission is believed to be negligible in Case 1 waters, and has not been incorporated within the IOP model for Case 1 waters.

4.5.4.4 Other Warnings and Limitations

The Case 1 waters IOP model include some uncertainties in its parameterization or even some assumptions. These properties with their corresponding uncertainties are listed in Table 4-11 below. The column "Expectation" indicates which scientific evolutions are foreseen.

Table 4-11: Comments on model parameterization

IOP	Equation number or table	Comment	Expectation
$a_w(\lambda)$	Table 4-2	Known with sufficient accuracy	Will not evolve
$a^R(\lambda)$	Equation 25 and Table 4-10	Known with sufficient accuracy	Will not evolve
$a_1 (\lambda)$	Equation 7 to Equation 12, Table 4-5 and Table 4-7	Well documented for world ocean (but see the large variation factor). Seasonal variability under investigation.	Will not evolve significantly
$b_w(\lambda)$	Equation 5 and Equation 6	Known with sufficient accuracy	Will not evolve
$b_{p1}(\lambda)$	Equation 17 and Equation 18	Well documented for world ocean (but see the large variation factor)	Will not evolve significantly
$b_{bp1}(\lambda)$	Equation 16 and Equation 19	Best guess	Could evolve
$\tilde{\beta}_w(\theta)$	Equation 3 and Equation 4	Slight uncertainty on p; very weak influence on the result	Will not evolve
$\beta^R(\theta)$	Equation 23 and Equation 24	Known with sufficient accuracy	Will not evolve
$\tilde{\beta}_p(\theta)$	Equation 13 to Equation 15, Table 4-8 and Table 4-9		Could evolve

As a general warning, the present model is based on statistical relationships (between K_d or b_p and [chl]) that represent "average" situations. Therefore, its use as a predictive tool leads to various results when the large standard errors associated with each input parameters are taken into account; it may fail when compared case by case to actual data (as reflectance for instance).

4.6 CASE 2 WATERS IOPS

4.6.1 INTRODUCTION

This section describes the bio-optical model which is used to simulate a set of water leaving radiance reflectances, which in turn is used to train the neural network (NN) algorithm for the standard processing of MERIS data of case 2 waters (Doerffer & Schiller, 2007).

Water constituents comprise a large number of different substances, which include mineralic dissolved and particulate compounds, a large variety of organic macromolecules, living organisms such as phytoplankton, zooplankton, bacteria etc. and their debris and excrements. All of these constituents of water exhibit different optical properties concerning scattering and absorption.

For the purpose of optical remote sensing this diversity of substances has to be grouped into a small number of classes each of which includes constituents with similar optical properties and / or correlated concentrations. For the majority of the world ocean areas it is sufficient to comprise all substances into one group using phytoplankton chlorophyll-*a* as a proxy. This type of waters is so-called the Case 1 waters. The concentration of this class of substances (in terms of chlorophyll-*a*) can be derived from the blue to green shift of the water colour. In many coastal waters one needs more than one class of substances to describe the variability of water colour. By tradition and experience three classes are defined: (1) phytoplankton pigment with chlorophyll-*a* as a proxy, (2) the dry weight of all particles (total suspended matter, TSM) and (3) the absorption caused by the dissolved fraction of all water constituents (gelbstoff or yellow substance). Dissolved particulate is defined by the pore size of the filter used for separation, which was traditionally about 0.45 µm and nowadays about 0.2 µm.

However, each of the three groups of substances is variable with respect to their composition and thus their chemical, physical and in particular optical properties. Any remote sensing system and retrieval algorithm has to take this variability into account.

4.7 THE MERIS CASE 2 ALGORITHM (NEURAL NETWORK).

The bio-optical model consists of three optical components, which are cartooned in Figure 4-5. Gelbstoff is defined as the absorption, a_y, by all substances in water, which pass a filter with a pore size of 0.2 µm. Total suspended matter (TSM) is defined as all substances, which remain on this filter. The absorption a of TSM, which is measured using the filter pad method by Tassan & Ferrari (1995), is split into two fractions by a bleaching process. The bleachable fraction, i.e. the difference between the TSM absorption before and after bleaching, is defined as phytoplankton pigment absorption, a_{pig}, while the absorption of TSM after bleaching is defined as particle absorption, a_{bp}. The scattering component b was determined in-situ by measuring $b = c - a$, i.e. the difference between the beam attenuation c and absorption coefficient a using an AC-9 instrument. The four components were reduced, as required by the MERIS level 2 product processor, to three by combining the absorption coefficient of Gelbstoff, a_y, and of particles, a_{bp}.

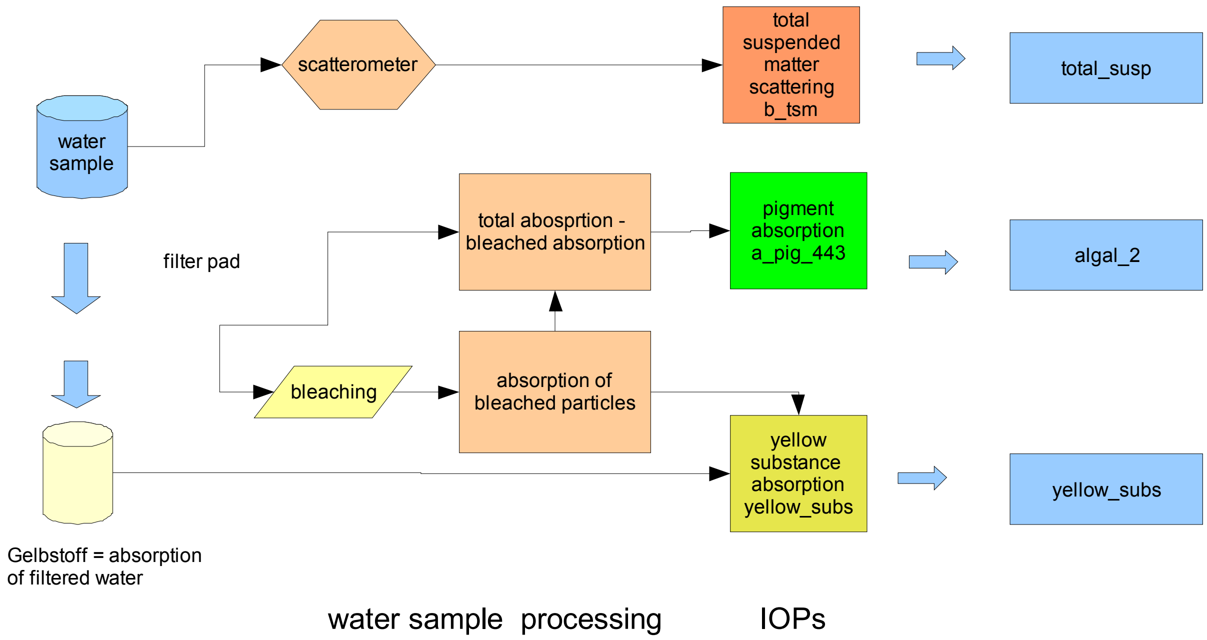

Figure 4-5: Scheme of the bio-optical model used for development of the MERIS Case 2 water algorithm

4.7.1 COMPONENTS

All concentrations are measured according to the MERIS Validation Team (MVT) protocols (PO-TN_MEL-GS_0043).

4.7.2 PURE WATER ABSORPTION

The spectral absorption coefficients for pure water were taken from Pope & Fry (1997). For the relevant MERIS bands the following values were used:

Table 4-12: Absorption coefficients of pure water (Pope & Fry, 1997) for MERIS bands 1-7 and band 9.

Band no.	Wavelength (nm)	*a* (m^{-1})
1	412.5	4.597e-003
2	442.5	6.884e-003
3	490.0	1.492e-002
4	510.0	3.250e-002
5	560.0	6.167e-002
6	620.0	2.746e-001
7	665.0	4.263e-001
9	708.75	8.147e-001

4.7.3 PURE WATER SCATTERING

The spectral scattering coefficients of pure water are calculated according to Morel (1974) using:

$$b_w = 0.00288\left(\frac{\lambda}{500}\right)^{-4.32}$$ **Equation 27**

with λ in nm.

4.7.4 GELBSTOFF AND PARTICLE ABSORPTION

The spectral absorption of both components show similar shapes, i.e. nearly exponential decreases with increasing wavelength. This decrease is described by the spectral exponent *s*, so that:

$$a(\lambda) = a(\lambda_{ref})\exp(-s(\lambda - \lambda_{ref}))$$ **Equation 28**

The two exponents for gelbstoff s_g and particle absorption s_p were determined from the COLORS time series. Since the exponents depend on the wavelength range, which is used for their determination, the interval 400 – 550 nm was used, which is about the most important for remote sensing. The exponents were fitted to each measurements using a non linear fit routine. No subtraction of the absorption at a red wavelength, e.g. at 750 nm, was performed, in contrast to many procedures reported in literature.

The variability of the slopes of the 2 years timeseries at Helgoland are plotted in Figure 4-6. The time series themselves do not show any obvious seasonal patterns, which would require special seasonal treatment.

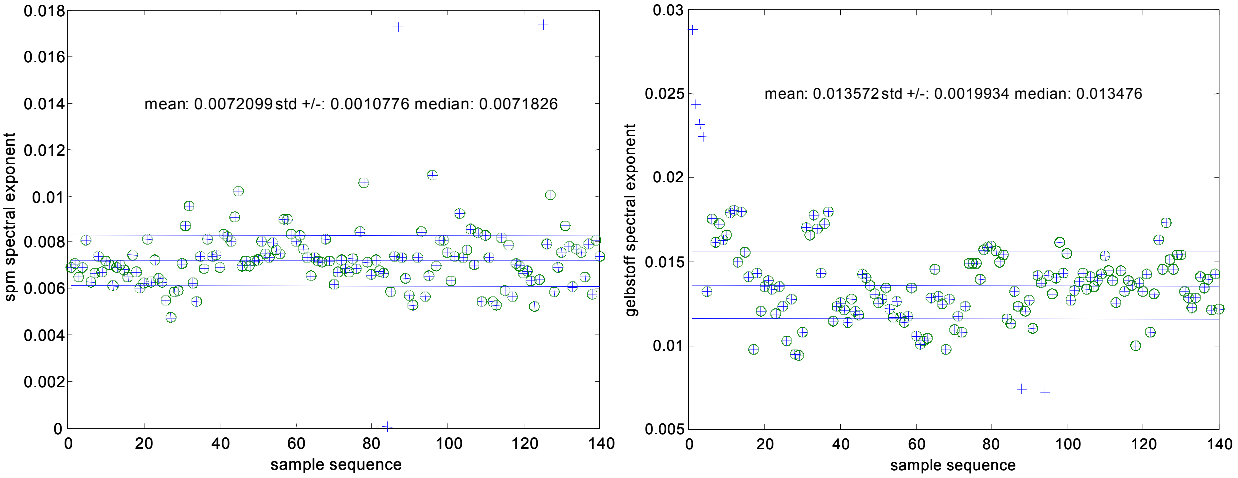

Figure 4-6: Spectral exponent of bleached TSM (left) and gelbstoff (after passing a filter with a pore size of 0.2 µm) for a two years time series of measurements around the island of Helgoland (German Bight, North Sea).

Mean slopes and standard deviations found for this series are for the dissolved part s_g = 0.0138 ± 0.00284 and for the particulate part s_p = 0.0072 ± 0.00108.

4.7.5 PHYTOPLANKTON PIGMENT ABSORPTION

The pigment absorption component is determined from measurements of filter pad absorption. It is the absorption of the bleachable fraction of the material, which does not pass the filter, i.e. the difference between the absorption of the filter pad before and after bleaching.

The time series of Helgoland shows two different types of spectra with all transitions, a typical summer spectrum with a clear maximum around 440 nm and a winter spectrum without a clear maximum but with a nearly exponential decrease in the blue-green spectral range. Since it is assumed that the winter spectra are dominated by detritus, which contain degradation products of chlorophyll, only the summer spectrum have been used for the component model. In order to include the variance of these summer spectra, a set of 77 spectra haven been selected with a clear absorption peak at 442 nm (Figure 4-7). One of these spectra is selected randomly for the computation of the reflectances. The 77 spectra (denoted by a_{pig_n} where n is the spectrum number) were selected after normalisation by $a_{pig}(442)$ according to the following criteria:

$$a_{pign}(442) / a_{pign}(412) > 0.98$$

$$a_{pign}(442) / a_{pign}(448) > 1.0$$

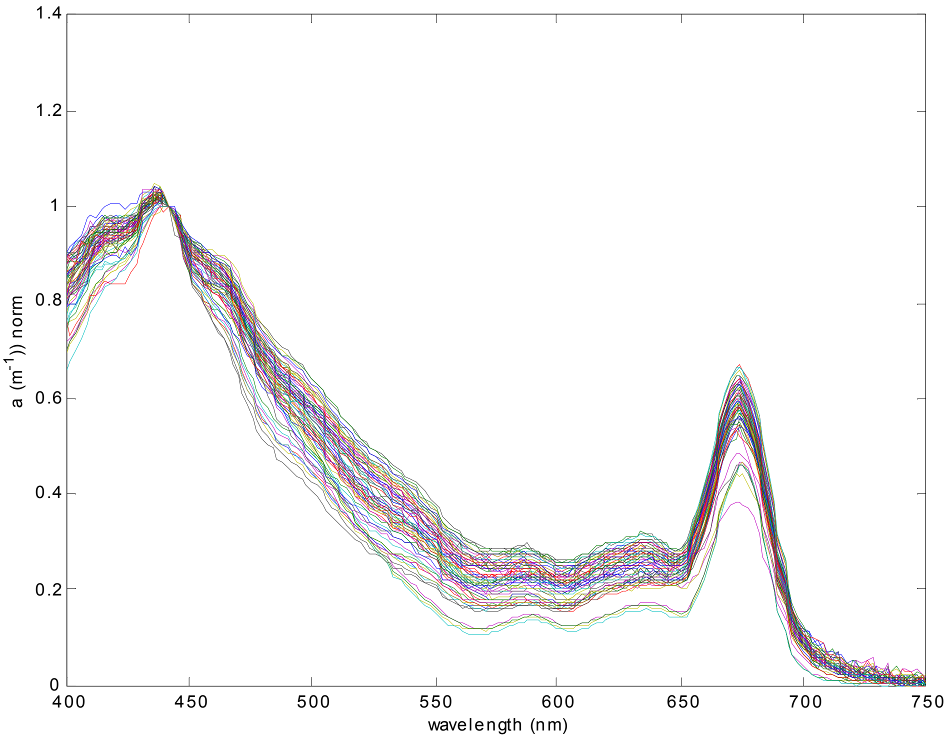

Figure 4-7: Normalized pigment absorption spectra selected from the data base of site Helgoland

This set was complemented by absorption spectra (Figure 4-8) measured from samples of different cruises in the North Sea and from the Skagerrak and North Sea water off the coast of

Norway, which have been provided by K. Sorensen, NIVA. Altogether 221 different spectra were used.

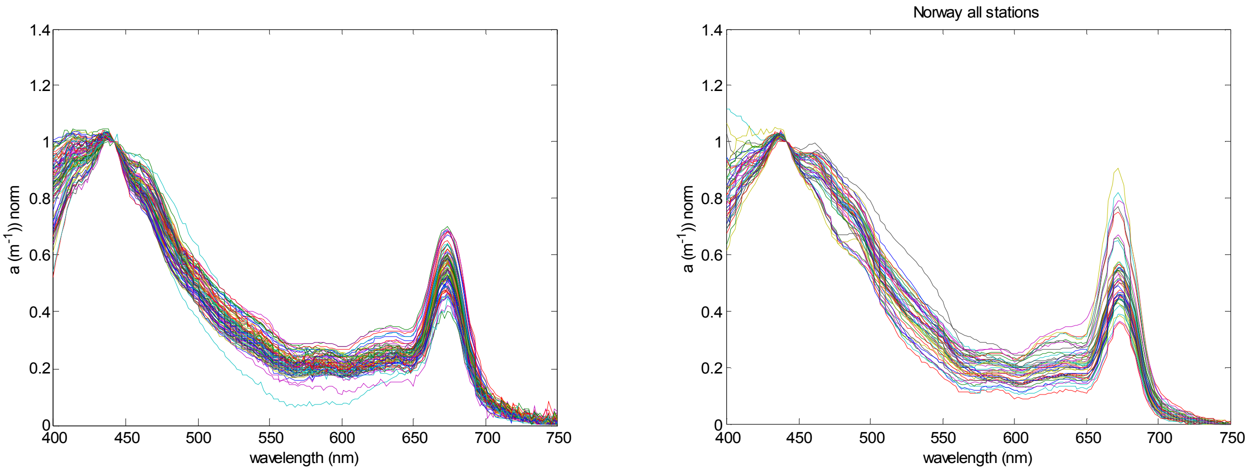

Figure 4-8: Normalized absorption spectra of pigments from the North Sea / German Bight (left) and from waters in the Skagerrak and the North Sea off Norway (right)

4.7.6 PARTICLE SCATTERING

The optical component particles are assumed to be non-absorbing. Their spectral scattering shape is described by:

$$b_p(\lambda) = b_{p(442)}\left(\frac{\lambda}{442}\right)^{-s_b}$$ **Equation 29**

with s_b, the spectral exponent and $b_{p(442)}$ the scattering at 442 nm. An exponent of $s_b = 0.4$ is used with a standard deviation of 0.2 according to the measurements of COASTLOOC (Babin *et al.*, 2003) and COLORS (measurements of GKSS).

Particle scattering is not varied independently from the absorption of particles and phytoplankton in order to exclude unrealistic combinations of high particle absorption without any scattering. Thus, the minimum scattering of the range from which particle scattering is randomly sampled depends on the absorption by particles and phytoplankton, which are sampled first, while the maximum of the particle scattering range is fixed.

Since no measurements of the phase function of particle scattering is available for our reference sites, the phase function of Petzold (1972) as described in Mobley (1994, Table 4-13) is used. This phase function has a backscattering probability:

$$\tilde{b}_{bp} = \frac{b_{bp}}{b_p} = 0.02$$

The value of 0.02 about is the mean backscattering factor of the Helgoland time series measured with the BB-4 backscatterometer instrument, and corresponds to the value for scattering phase function of Petzold (1972).

The total volume scattering *b* [m-1] of all particles has been measured in-situ at 9 wavelength with an AC-9 instrument, which determines absorption and beam attenuation. The spectral exponent was then determined from all wavelengths using a nonlinear fit. Furthermore, the results were checked against data of the COASTLOOC project (Babin 2003), which covered coastal and off shore areas of the Mediterranean, the Atlantic, North and Baltic Sea, and compared to results of Siegel *et al*. (2005) for the Baltic area.

In addition a white scatterer (spectral exponent of 0) was introduced to include the effects of coccolithophorides, which often occurs in the North Sea and Celtic Sea during summer months. However, due to the restrictions of the MERIS products format, the white scatterer is not a separate variable, only the optical effect was introduced so that the NN learned that this kind of material may be present in the water. For this component also the scattering phase function of Petzold (1972) was used (Table 4-13).

Table 4-13: Normalised volume scattering function for marine particles as derived by Mobley (1994) from Petzold's measurements.

$\boldsymbol{\theta}$	$\tilde{\beta}_{p1}(\theta)$	$\boldsymbol{\theta}$	$\tilde{\beta}_{p1}(\theta)$
0.1	1767	50	0.02275
0.12589	1296	55	0.01699
0.15849	950.2	60	0.01313
0.19953	699.1	65	0.01046
0.25119	513.7	70	0.008488
0.31623	376.4	75	0.006976
0.39811	276.3	80	0.005842
0.50119	201.2	85	0.004953
0.63096	144.4	90	0.004292
0.79443	102.2	95	0.003782
1	71.61	100	0.003404
1.2589	49.58	105	0.003116
1.5849	33.95	110	0.002912
1.9953	22.81	115	0.002797
2.5119	15.16	120	0.002686
3.1623	10.02	125	0.002571
3.9811	6.58	130	0.002476
5.0119	4.295	135	0.002377
6.3096	2.807	140	0.002329
7.9433	1.819	145	0.002313
10	1.153	150	0.002365
15	0.4893	155	0.002506
20	0.2444	160	0.002662
25	0.1472	165	0.002835
30	0.08608	170	0.00303
35	0.05931	175	0.003092
40	0.0421	180	0.003154
45	0.03067		0.02275

The concentrations of all particles are determined as the dry weight per volume of water.

4.7.7 CONVERSION FACTORS

Although the prime products of the MERIS Case 2 water algorithm are the IOP coefficients at a wavelength of 442 nm, mean conversion factors were provided to present these properties also in form of concentrations of TSM and chlorophyll *a*. For TSM only the scattering coefficient is used and for phytoplankton only the pigment absorption. However, a combination of scattering and absorption might be more appropriate in some cases.

The conversion factor for TSM was derived from measurements in the German Bight (Figure 4-9) and confirmed by COASTLOOC data (Babin, 2003) and determined as:

$$< TSM >= b_p(442) / \mathrm{bp}^*(442)$$ **Equation 30**

where $1/b_p^*(442) = 1.73$, i.e. $b_p^*(442) = 0.578$.

The conversion factors for chlorophyll *a* from the measurements in the German Bight and in Norwegian waters are:

$$[chl] = 21.0\ [a_{pig}(442)]^{1.04}$$ **Equation 31**

The chlorophyll conversion factors are in good agreement with those found by Bricaud *et al.* (1998) for mainly Case 1 waters.

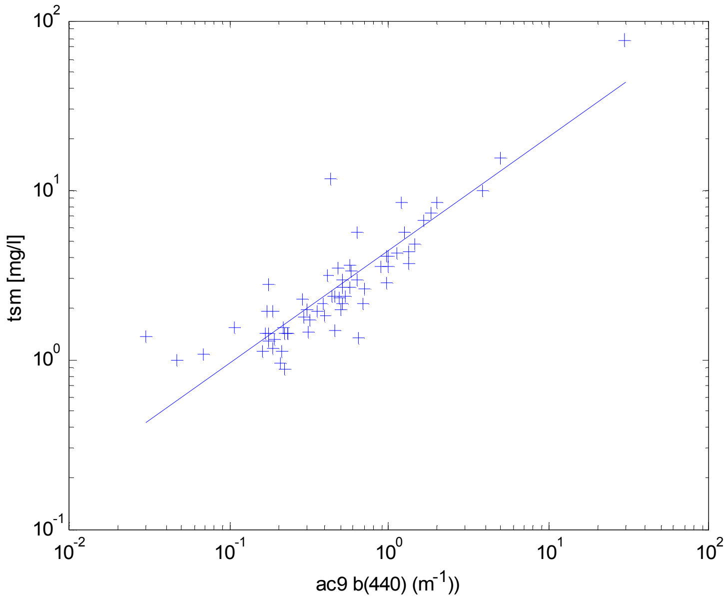

Figure 4-9: Relationship between the scattering coefficient of particles in the North Sea at 440 nm and the dry weight of total suspended matter, used for determining the conversion factor.

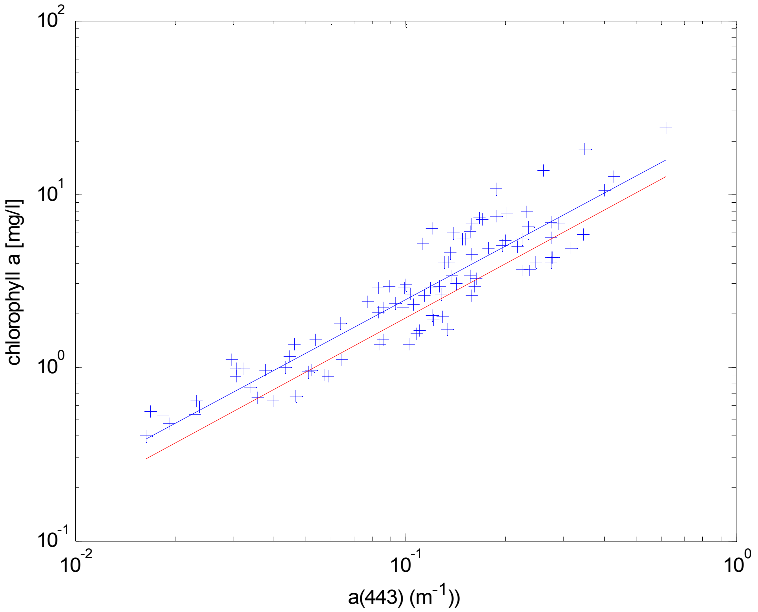

Figure 4-10: Relationship between the pigment absorption at 443 nm and the chlorophyll concentration. Data is from cruise 187 of RV "Heincke". The blue regression line is chl = 23 (a_pig)$^{1.02}$, red line is the algal_2 model for MEGS 7.3: algal_2= 21 (a_pig)$^{1.04}$

4.7.8 SPECTRAL VARIABILITY

The spectral variability, which was found in the Helgoland time series and COASTLOOC data set, as well as the expected measurement error of MERIS and of the atmospheric correction procedure were included into the NN by training in the following way: For the computation of each spectrum of the training set, the spectral exponents for scattering, s_b, and absorption of gelbstoff, s_g, and particles, s_p, were randomly varied according to a Gaussian distribution. The standard deviation was determined from the field measurements. For pigment absorption one of the set of 221 spectra (see above) was randomly selected. The simulated reflectance spectrum was then varied for each band according to a Gaussian distribution with the expected (pre launch) MERIS radiometric and atmospheric correction covariance.

4.7.9 RANGE AND CO-VARIANCES

According to the data from North Sea Water and the concentration ranges in Case 1 water (ATBD: Morel and Antoine 2000) the range for pigment and gelbstoff absorption (a_{pig} and a_y) as well as particle and white particle scattering b_{pw} (442 nm) was set as listed in Table 4-14.

Although all variables should vary as independently as possible within the given ranges, we have introduced some restrictions concerning the minimum scattering associated with the absorption coefficients of phytoplankton pigments and bleached particles in order not produce unrealistic low reflectances.

These minima were determined from the co-variations between absorption and scattering.

The following relationships were determined:

$$b_{tsm\_min} = 0.25\, a_{pig}(442)$$ **Equation 32**

The co-variation between the absorption coefficient of bleached particles (a_{tsm_bl}) and the scattering coefficient of total suspended matter scattering was determined as:

$$a_{tsm\_bl}(442) = 0.1\, b_p(442) + ran\_gauss\, 0.03\, b_p(442)$$ **Equation 33**

where ran_gauss is a random number of a N(0,1) Gaussian probability distribution.

Note that this coupling excludes some extreme combinations, which however might occur in nature.

Table 4-14: Variability of the optical properties and range used for the simulation of water reflectance spectra.

COMPONENT / PROPERTY	VALUE RANGE
Gelbstoff absorption wavelength exponent	0.014 ± 0.002
Bleached particle absorption wavelength exponent	0.008 ± 0.005
Particle scattering wavelength exponent	0.4 ± 0.4
White particle scattering wavelength exponent	0.0
Phytoplankton pigment absorption	Random selection from > 200 absorption spectra, normalised at 442 nm.
Gelbstoff absorption, a_gelb at 442 nm	0.005 – 5.0 m^{-1}
Particle scattering b_p at 442 nm	0.005 – 30.0 m^{-1}
White particle scattering b_{pw} at 442 nm	0.005 – 30 m^{-1}
Phytoplankton pigment absorption a_pig at 442 nm	0.001 – 2.0 m^{-1}
Minimum particle scattering at 442 nm	Equation 32
Bleached particle absorption	Equation 33
Sun zenith angle	0-180°
Viewing zenith angle	0-180°
Difference between sun and viewing azimuth angle	0-180°

4.7.10 ENVIRONMENTAL CONDITIONS

The environment as well as further optical properties were defined in the following way: infinite deep water (no bottom effect), vertical homogenous distribution of all water constituents, rough sea surface according to a wind speed of 3 ms^{-1}.

The downwelling radiance distribution above water has been simulated with Hydrolight, which was adapted for this purpose to simulate an atmosphere with 50 layers for 17 solar zenith angels ranging from 0 to 80 degree.

Furthermore no inelastic scattering (fluorescence or Raman scattering) as well as no polarisation effects have been considered in the simulation.

4.8 SIMULATION OF WATER REFLECTANCES

Following Antoine and Morel, (1999), the directional water reflectance $\rho_w(\theta_v,\phi_v)$ associated with the water-leaving radiance $L_w(\theta,\phi)$ and the downwelling irradiance above the sea surface E_s is defined to be:

$$\rho_w(\theta_v,\phi_v) = \pi L_w(\theta_v,\phi_v) / E_s(\theta_s)$$ **Equation 34**

where θ_v and ϕ_v are the zenith and azimuth observation angles respectively. E_s depends on the solar zenith angle, θ_s, for the pixel under examination and corresponds to $E_d(0+)$. For convenience we denote the wavelength dependence in the following only where necessary.

Since simultaneous measurements of concentrations and water leaving radiance reflectance spectra are rare and, thus, do not cover the data space with sufficient density, the construction of the NN is based on a large table (~550K entries) of simulated data generated by our forward model which was built from the Hydrolight (v3.0) radiative transfer code (Mobley 1994) plus a bio-optical model relating scattering and absorption coefficients to concentrations.

For given concentrations / IOPs of water constituents the forward model calculates the angular distribution of water leaving radiance in eight visible MERIS bands. These angular distributions are sampled in the appropriate angle ranges to derive the entries of the training / test tables for building the NN: three concentrations, three angles and eight water leaving radiance reflectances. The concentrations of the water constituents are randomly sampled from an exponential distribution in order to disentangle small concentration differences in regions of small concentrations. In order to get roughly constant relative concentration errors the logarithm of the IOP's was used as NN output.

4.9 BRIGHT PIXEL ATMOSPHERIC CORRECTION REFLECTANCE MODEL

With even modest concentrations of TSM (>0.2 g m^{-3}), there is significant backscatter and/or coccolithophore reflectance that results in reflectance at near infra-red wavelengths (NIR) that negates the `dark pixel' atmospheric correction (AC) procedures, which assume zero water leaving at NIR wavelengths (> 700 nm). These `bright pixel' waters require a modified bright pixel atmospheric correction (BPAC). Yellow substance has little effect on the atmospheric correction (`dark pixel'), as it primarily absorbs due to its dissolved nature and will be ignored.

The BPAC model is detailed further in ATBD 2.6, and outlined here in the following sections. It is parameterised entirely using particulate IOPs; the algorithm uses the IOPs of pure water (a_w and bb_w) and particulates (bb_p and a_p) with the final value of bb_p used to estimate TSM for Case 2 flagging.

The solution relies on providing estimates from a low band set {709nm, 779nm, 865nm} and a high band set {779nm, 865nm, 885nm}. For the initial estimates, the first two wavelengths of the band sets are used. *Note that 709 and 779 are shorthand notations for MERIS bands at 708.75 and 779.75.*

All parameters are described in Table 4-15.

Table 4-15: BPAC parameters

Symbol	Descriptive Name	I/O	Range/Reference/Remarks
$t([709,779,865,885],\theta_v,\theta_s,\Delta_\phi)$	Atmospheric diffuse transmittance	I	From Rayleigh Correction
$F(\lambda,a,bb_w,bb_p,\theta_v,\theta_s,\Delta_\phi)$[1]	Water reflectance above surface factor - polynomials	I	Database Lookup Table
$a(TSM)$	TSM absorption	I	Database Lookup Table
$b(TSM)$	TSM backscatter	I	Database Lookup Table
C	Aerosol extrapolation parameter	-	Calculated Internally
$\rho_{as}([709,779,865],\theta_v,\theta_s,\Delta_\phi)$	Single scattering reflectance	I	From Rayleigh Correction
$\rho_{as}([709,779,865],\theta_v,\theta_s,\Delta_\phi)$	Single scattering corrected reflectance	O	From Iterative Procedure
$\varepsilon(709,865,\theta)$	ρ_{rc} Ratio	-	Calculated Internally
$\varepsilon(779,865,\theta)$	ρ_{rc} ratio	-	Calculated Internally
TSM	TSM load	-	From Procedure
θ_s	Solar zenith angle	I	From Navigation
Δ_ϕ	Azimuth difference	I	From Navigation
θ_v	Viewing angle	I	From Navigation
$\theta \equiv [\theta_v,\theta_s,\Delta_\phi]$	Viewing / solar angles	-	Naming Convention

4.9.1 BPAC HYDROLOGICAL MODEL

The hydrological optics depends on the IOPs of the TSM, which varies according to wavelength. Parameterisation of reflectance for waters dominated by TSM involves knowledge of three IOPs and their spectral properties: particulate specific absorption, $a_s(TSM,\lambda)$; particulate specific scattering, $b_s(TSM,\lambda)$; particulate backscattering ratio, $\tilde{b}$.

Assuming fixed viewing geometry and wind speed, the quasi-linear relationship between sediment concentration and the reciprocal of remote sensed reflectance allows $\rho_w(\theta_s,\theta_v,\Delta_\phi)$ to be expressed as:

$$\rho_w = F'\left(\frac{bb_w + bb_p}{a_w + a_p + bb_w + bb_p}\right)$$

Equation 35

F' is a function that includes the terms Q, $\Re$ and π and implies geometry. $\Re$ is defined as in Equation 58.

Q is the ratio of upwelling irradiance to radiance (Section 5.1.1).

a_w, bb_w are the absorption and backscatter of water, bb_p is the combined backscatter of TSM, that is phytoplankton, detritus and sediment; a_p is the combined absorption of phytoplankton, detritus, and sediment.

The BPAC aims to include waters with very high turbidities and thus reflectances. The limiting values for these alternative reflectance expressions are important in terms of numerical stability. For a non or very low absorbing sediment, such as coccoliths, the limit is:

$$\frac{\lim}{bb_{pds}\rightarrow\infty} F'\left(\frac{bb_w+bb_p}{a_w+a_p+bb_w+bb_p}\right)=F' \tag{Equation 36}$$

Where: bb_{pds} is equivalent to bb_p (the case 2 model does not differentiate).

ATBD 2.6 explains the distinction; in the NIR there is no differentiation between any of the particulate components.

Thus, the $bb/(a+bb)$ variant is more useable since it provides a defined limiting reflectance of F' for high reflectance waters, which can be used as an error check for computing look-up tables (LUT's) and for their implementation.

The limit for absorbing sediment is also of interest. Here, a^*_{bb} is defined as the specific absorption of the sediment backscatter, or the absorption to backscatter ratio, for a particular sediment and in this case Equation 35 becomes:

$$\rho_w=F'\left(\frac{bb_w+bb_p}{a_w+bb_w+bb_p(1+a^*_{bb})}\right) \tag{Equation 37}$$

And the limiting value becomes:

$$\frac{\lim}{bb_{pds}\rightarrow\infty} F'\left(\frac{bb_w+bb_p}{a_w+bb_w+bb_p(1+a^*_{bb})}\right)=\frac{F'}{(1+a^*_{bb})} \tag{Equation 38}$$

This limit permits the estimation of sediment absorption from above water reflectance in tank experiments and highly turbid water where analytical and *in situ* methods may be problematic.

F' values were computed using Hydrolight 3.0 (Mobley, 1995). The refractive index, and phase functions of pure water and particles are as specified in Table 3-2, and Petzold (1972) respectively (Table 4-13), introducing the notations $a=a_w+a_p$ and $b_b=b_{bw}+b_{bp}$.

The tables were run for four wind speeds (0.25 ms^{-1}, 1.00 ms^{-1}, 2.75 ms^{-1} and 5.00 ms^{-1}) corresponding to sea-state values recorded in MERMAID (MERis MAtchup In-situ Database, http://hermes.acri.fr/mermaid/) metadata, and for solar angles (θ_s) of 0, 15, 30, 45 and 60 degrees that encompasses the MERIS useful viewing geometry. θ_v and Δ_Φ are implicit in the Hydrolight runs and the 'quads' were set to give the following viewing geometry:

$\theta_v = \{0,15,30,45,60\}$
$\Delta_\Phi = \{0,15,30,45,60,75,90,105,120,135,150,165,180\}$

The absorption values were run from a range of a_w values that were below the minimum found in literature, when adjusted for smile and temperature effects, and to the similar greatest value. Thereafter, a log ramp was applied to an absorption value of 30.0 m^{-1}. From the absorption, scattering values were calculated according to a ramp of single scattering albedo (ω) from zero to 0.9999 with the highest density of values at the high ω. In all, for each band around 10,000 table runs were computed according to the number of candidate a_w values. The f' determined from the Hydrolight runs was then fitted to η, where:

$$\eta = \frac{bb_w}{bb_w + bb_p} \qquad \text{Equation 39}$$

The relationship with η proved to be linear for low turbidities. The residuals from the fit to η, were expected to relate to ω from previous work on Case I waters (Morel and Gentili, 1993). This however proved unsuccessful, and instead a polynomial relationship was fitted with F' being a function of $b_b/(a+bb)$.

For any view geometry F' can be expressed as:

$$F' = A0 + C\eta + \sum\left(\frac{b_b}{(a+b_b)}\right)ii \qquad \text{Equation 40}$$

where $A0$ and C are the linear coefficients for η, and $\underline{a_i}$ represents the coefficients of a 4th order polynomial. The F' factors are provided as LUTs containing the polynomials for each band, wind speed and viewing geometry, with the terms varying slowly so that a simple nearest neighbour lookup is sufficient.

4.9.1.1 Hydrological model parameters

At present no account is taken of the effect of increased surface albedo on the atmospheric path radiance, and with the BPAC the figure of merit is the correct retrieval of the $\rho_w(NIR)$. The TSM product is qualitative since it's a scaled $bb_p(NIR)$ product and the relationship between TSM and scattering is known to be highly variable.

Since, in the NIR, there is little difference between the optical properties of phytoplankton, detritus and sediment for Case 1 waters the TSM figures will represent a dry weight or organic material that is closely coupled to chlorophyll concentration. The absorption of CDOM is assumed to be negligible in the NIR.

4.9.1.2 Pure water absorption and scattering

The values of pure water absorption, scattering and the temperature dependence of pure water absorption are taken from Section 4.

4.9.1.3 Particulate properties

In common with the Case 2 model a the spectral slope in the NIR is assumed to be 0.4 (4.7.6, Equation 29). The BPAC uses both an absorbing and non-absorbing sediment model where the model is chosen according to the white scatterer flag. The absorbing sediment model is described in terms of the ratio b_{bp}:a_p and is given in Table 4-16 below. This ratio has been derived by considering the maximum observed reflectance in turbid waters, and the derivation of the figures is described further in the ATBD.

Table 4-16: BPAC sediment absorption properties

Band	λ	b_{bp}:a_p
9	708.75	0.982987
10	753.75	0.88159
12	778.75	0.829859
13	865	0.673561
14	885	0.641754

4.9.2 TSM ESTIMATES

The BPAC is an IOP model, and as such does not use the value of TSM internally. TSM is derived from $b_b(779)$ in order to set the turbid water flag. The derivation is according to the case 2 model. First the backscattering at 779 is transformed into backscattering at 442:

$$bp(442) = \frac{b_{bp}(779)}{\tilde{b}_{bp}}(779/442)^{s_b} \qquad \textbf{Equation 41}$$

where $s_b = 0.4$

TSM is finally derived from the scattering at 442

$$< TSM >= b_p(442)/b_p*(442) \qquad \textbf{Equation 42}$$

with $b_p^*(442) = 0.578$.

5. Bidirectionality conversions for AOPs

The conversions outlined in this section allow for comparison of MERIS products with in-situ data, as can be done with the MERMAID (MERis Matchup Insitu Database; http://hermes.acri.fr/mermaid).

5.1.1 RADIATIVE TRANSFER SIMULATIONS/CALCULATIONS

Using the ocean part of the reference model, one should be able to calculate the directional reflectance just below the sea surface, $\rho_u^{0^-}(\lambda,\theta_s,\theta',\Delta\phi)$ (or other AOPs or derived quantities), using geophysical parameters as inputs ([*chl*] only for Case-1 waters, and [*chl*], *SPM* and $a_{y2}(443)$ for Case 2 waters).

A first approach consists in using the parameterizations presented in Sections 4.2 to 4.6 to derive IOPs and introduce them into radiative transfer simulations with the relevant boundary conditions (sea state, barometric pressure, etc.). The output of these simulations are radiances in all directions, which can be integrated in different manners to derive various plane or scalar irradiances, from which various quantities can be derived, such as $f'(\lambda,\theta_s)$, which is commonly defined as (Morel *et al*., 2002):

$$f'(\lambda,\theta_s)=\left(\frac{E_u(\lambda,\theta_s)}{E_d(\lambda,\theta_s)}\right)\left(\frac{b_b(\lambda)+a(\lambda)}{b_b(\lambda)}\right)$$

Equation 43

$f(\lambda,\theta_s)$, which is defined as:

$$f(\lambda,\theta_s)=\left(\frac{E_u(\lambda,\theta_s)}{E_d(\lambda,\theta_s)}\right)\left(\frac{a(\lambda)}{b_b(\lambda)}\right)$$

Equation 44

In Equations 43 and 44, the E_d is $E_d(0\text{-})$, the downwelling irradiance just below the water-air interface.

$Q(\lambda,\theta',\theta_s,\Delta\phi)$, which is defined as:

$$Q(\lambda,\theta_s,\theta',\Delta\phi)=\frac{E_u(\lambda,\theta_s)}{L_u(\lambda,\theta_s,\theta',\Delta\phi)}$$

Equation 45

and the directional reflectance just below the sea surface, which is:

$$\rho_u^{0^-}(\lambda,\theta_s,\theta',\Delta\phi)=\pi\frac{R(\lambda)}{Q(\lambda,\theta_s,\theta',\Delta\phi)}$$

Equation 46

where $R(\lambda)$ is the irradiance reflectance just below sea surface [defined as the ratio of upward to downward irradiance, $E_u(\lambda)/E_d(\lambda)$], and $Q(\lambda,\theta_s,\theta',\Delta\phi)$ is the bi-directionality factor. Equation 46 is obtained when considering that :

$$\rho_u^{0^-}(\lambda,\theta_s,\theta',\Delta\phi)=\pi\frac{L_u(\lambda,\theta_s,\theta',\Delta\phi)}{E_d^{(0+)}(\lambda,\theta_s)}$$

Equation 47

The water reflectance, $\rho_w^{0+}(\lambda,\theta_s,\theta_v,\Delta\phi)$, (i.e., above the sea surface) is expressed as:

$$\rho_w^{0+}(\lambda,\theta_s,\theta_v,\Delta\phi)=\frac{1-\rho_F(W,\theta')}{n^2}\rho_u^{0^-}(\lambda,\theta_s,\theta',\Delta\phi)$$

Equation 48

where $\rho_F(W,\theta')$ is interpolated bi-linearly from Table 5-1.

Table 5-1: Values of $\rho_F(W,\theta')$, the mean Fresnel reflection coefficient for the water-air interface, as function of wind speed W and view angle θ', (Austin, 1974).

w_s *(m/s)* *θ' (deg)*	*0*	*4*	*10*	*16*
0	0.0211	0.0211	0.0213	0.0217
10	0.0211	0.0213	0.0218	0.0228
20	0.0218	0.0227	0.0255	0.0334
30	0.0265	0.0325	0.0613	0.0961
35	0.0350	0.0602	0.1234	0.1686
40	0.0588	0.1559	0.2367	0.2741
45	0.1529	0.3801	0.4065	0.4131
50	1.0000	0.6718	0.5988	0.5629
55	1.0000	0.8905	0.7715	0.7055
60	1.0000	0.9807	0.8967	0.8277

When the Raman scattering is ignored, the functions $f(\lambda)$, $f'(\lambda)$ and $Q(\lambda,\theta_s,\theta_v,\Delta\phi)$ are obtained through monochromatic radiative transfer calculations using $a_1(\lambda)$ and $b_1(\lambda)$ or $a_2(\lambda)$ and $b_2(\lambda)$ as calculated using the parameterization presented in Sections 4.4 (pure sea water), Section 4.5 (Case 1 waters) and 4.6 (Case 2 waters), and a normalised volume scattering function. When the Raman scattering is accounted for, radiative transfer calculations must include the wavelength domain involved for the excitation of the Raman emission.
In case f'/Q (or f/Q) lookup tables are developed, they should have the following entries:

- the molecular to total scattering ratio (b_w/b) as derived from parameterizations in Section 4.
- the single scattering albedo ($b/[a+b]$) as derived from parameterizations in Section 4
- the solar zenith angle θ_s.
- the view zenith angle θ
- the relative azimuth angle $\Delta\phi$

The atmospheric optical thickness $\tau(550)$ should be specified (it is not necessarily an entry to the look-up table).

5.1.2 SEMI-ANALYTICAL CALCULATIONS

When the reflectance $R(\lambda)$ is replaced by :

$$R(\lambda) = f'(\lambda)\frac{b_b(\lambda)}{a(\lambda)+b_b(\lambda)}$$ **Equation 49**

or by:

$$R(\lambda) = f(\lambda)\frac{b_b(\lambda)}{a(\lambda)} \text{ (only usable when } b_b << a)$$ **Equation 50**

Then $\rho_w^{0+}(\lambda,\theta_s,\theta_v,\Delta\phi)$ can be expressed as :

$$\rho_w^{0+}(\lambda,\theta_s,\theta',\Delta\phi) = \pi\Re(\theta')\left(\frac{f(\lambda,\theta_s)}{Q(\lambda,\theta_s,\theta',\Delta\phi)}\right)\left(\frac{b_b(\lambda)}{a(\lambda)}\right)$$ **Equation 51**

which is also obtained by combining the following basic equations (see also the table of symbols in Section 2.5):

$$R = \frac{E_u}{E_d} = f\,\frac{b_b}{a}$$ **Equation 52**

$$Q = \frac{E_u}{L_u}$$ **Equation 53**

$$L_w = L_u\frac{1-\rho_F}{n^2}$$ **Equation 54**

$$E_d(0^-) = E_d(0^+)\frac{1-\bar{\rho}}{1-\bar{r}R}$$ **Equation 55**

The semi-analytical Equation 51 can be used along with the parameterizations developed in section 4.2 to 4.6.1. In that case, $a(\lambda)$ and $b_b(\lambda)$ can be broken into individual contributions by the different water constituents, following the "analytical approach" (but see introduction to Section 4.5.1).

$$a(\lambda) = \sum_{n=1}^{N} a_n(\lambda)$$ **Equation 56**

$$b_b(\lambda) = \sum_{n=1}^{N} \tilde{b}_{bn}(\lambda) b_n(\lambda)$$ **Equation 57**

where the subscript n indicates a given optically significant seawater constituent, $b_n(\lambda)$ is the scattering coefficient of the n^{th} substance and $\tilde{b}_{bn}(\lambda)$ is the ratio of backscattering to scattering (or backscattering efficiency) of the n^{th} substance.

In Equation 51 above, the “gothic” $\Re$ factor (Morel and Gentili, 1996) is defined by:

$$\Re(\theta') = \left[\frac{(1-\bar{\rho})}{(1-\bar{r}\mathrm{R})} \frac{(1-\rho_{\mathrm{F}}(\theta'))}{\mathrm{n}^2} \right]$$ **Equation 58**

where:

n is the refractive index of sea water (dimensionless)

$\rho_{\mathrm{F}}(\theta)$ is the Fresnel reflectance at the air-sea interface for the scattering angle θ (dimensionless)

$\bar{\rho}$ is the mean reflection coefficient for the downwelling irradiance at the sea surface (dimensionless)

$\bar{r}$ is the average reflection for upwelling irradiance at the water-air interface (dimensionless)

$\Re$ is to be interpolated from Table 5-2.

Table 5-2: Values of $\Re$ as function of wind speed W and view angle θ'

W ($m.s^{-1}$) θ' (deg) \	0	4	8	16
0	0.5287	0.5287	0.5287	0.5287
1	0.5287	0.5287	0.5287	0.5287
2	0.5287	0.5287	0.5287	0.5287
3	0.5287	0.5287	0.5287	0.5287
4	0.5287	0.5287	0.5287	0.5287
5	0.5287	0.5287	0.5287	0.5287
6	0.5287	0.5287	0.5287	0.5287
7	0.5287	0.5287	0.5287	0.5287
8	0.5287	0.5287	0.5287	0.5287
9	0.5287	0.5287	0.5287	0.5287
10	0.5287	0.5287	0.5287	0.5287
11	0.5287	0.5287	0.5287	0.5287
12	0.5287	0.5287	0.5287	0.5286
13	0.5287	0.5287	0.5287	0.5286

W ($m.s^{-1}$) θ' (deg) \	0	4	8	16
14	0.5287	0.5287	0.5287	0.5286
15	0.5287	0.5287	0.5286	0.5286
16	0.5287	0.5286	0.5286	0.5286
17	0.5287	0.5286	0.5286	0.5285
18	0.5286	0.5286	0.5286	0.5285
19	0.5286	0.5286	0.5286	0.5285
20	0.5286	0.5286	0.5285	0.5284
21	0.5286	0.5285	0.5285	0.5284
22	0.5285	0.5285	0.5284	0.5283
23	0.5285	0.5284	0.5284	0.5283
24	0.5285	0.5284	0.5283	0.5282
25	0.5284	0.5283	0.5283	0.5282
26	0.5283	0.5283	0.5282	0.5281
27	0.5283	0.5282	0.5281	0.528
28	0.5282	0.5281	0.5281	0.5279
29	0.5281	0.528	0.528	0.5278
30	0.528	0.5279	0.5279	0.5276
31	0.5279	0.5278	0.5277	0.5275
32	0.5278	0.5277	0.5276	0.5274
33	0.5277	0.5276	0.5274	0.5272
34	0.5275	0.5274	0.5273	0.527
35	0.5274	0.5272	0.5271	0.5268
36	0.5272	0.527	0.5269	0.5265
37	0.527	0.5268	0.5266	0.5263
38	0.5267	0.5266	0.5264	0.526
39	0.5265	0.5263	0.5261	0.5257
40	0.5262	0.526	0.5258	0.5253
41	0.5259	0.5257	0.5254	0.5249
42	0.5255	0.5253	0.525	0.5245
43	0.5251	0.5249	0.5246	0.524
44	0.5247	0.5244	0.5241	0.5235
45	0.5242	0.5239	0.5236	0.5229
46	0.5237	0.5233	0.523	0.5223
47	0.5231	0.5227	0.5223	0.5216
48	0.5224	0.522	0.5216	0.5208
49	0.5217	0.5212	0.5208	0.52
50	0.5209	0.5204	0.52	0.5191
51	0.52	0.5195	0.519	0.518
52	0.519	0.5184	0.5179	0.5169
53	0.5179	0.5173	0.5168	0.5157
54	0.5167	0.5161	0.5155	0.5144
55	0.5153	0.5147	0.5141	0.5129
56	0.5138	0.5131	0.5125	0.5113
57	0.5122	0.5115	0.5108	0.5096
58	0.5103	0.5096	0.5089	0.5077
59	0.5083	0.5076	0.5068	0.5056
60	0.5061	0.5053	0.5045	0.5034

W (m.s^{-1}) θ' (deg) \	0	4	8	16
61	0.5037	0.5028	0.502	0.5009
62	0.5009	0.5001	0.4993	0.4983
63	0.4979	0.4971	0.4964	0.4953
64	0.4946	0.4938	0.4932	0.4923
65	0.491	0.4901	0.4896	0.4889
66	0.4869	0.4861	0.4857	0.4853
67	0.4825	0.4818	0.4815	0.4813
68	0.4775	0.4771	0.4769	0.4771
69	0.4721	0.4719	0.4719	0.4726
70	0.4662	0.4662	0.4666	0.468
71	0.4596	0.46	0.4607	0.4631
72	0.4524	0.4532	0.4544	0.4578
73	0.4446	0.4461	0.4478	0.4523
74	0.4359	0.4381	0.4407	0.4467
75	0.4265	0.4295	0.4333	0.4405
76	0.4161	0.4204	0.4254	0.4341
77	0.405	0.411	0.4172	0.4279
78	0.3929	0.4009	0.4086	0.4212
79	0.3797	0.3903	0.3994	0.4142
80	0.3659	0.3793	0.3905	0.4072
81	0.3514	0.3676	0.3809	0.4
82	0.3362	0.3563	0.371	0.3928
83	0.3206	0.344	0.3613	0.3853
84	0.3049	0.3321	0.3515	0.378
85	0.2884	0.32	0.3416	0.3702
86	0.2728	0.3082	0.3316	0.3628
87	0.2572	0.296	0.3219	0.3554
88	0.2421	0.2847	0.312	0.3476
89	0.2276	0.2732	0.3021	0.3394
90	0.5287	0.5287	0.5287	0.5287

6. Sea surface state

6.1 SPECULAR REFLECTIONS

The effect of the *air-sea* interface shape i.e., the water surface roughness) on the Fresnel reflection and refraction are accounted for by applying statistics from Cox and Munk (1954), assuming an isotropic distribution of wave facet slopes and a variable wind-speed above sea level.

The radiative transfer codes (RTCs) from , used in the algorithms for extracting information about atmospheric and oceanic constituents from MERIS signal, account for these multiple specular reflections (so-called “sunglint”) at sea surface level in the TOA radiance (or reflectance) computation. When generating the look-up table (LUT) with the polynomial coefficients for linking $[\rho_{path}/\rho_R]$ to the total aerosol optical thickness (τ_a) for atmospheric corrections of MERIS data over ocean, the sunglint contribution has to be removed from reflectances computed over pure Rayleigh atmospheres (ρ_R) as well as over realistic atmospheres (molecules + aerosols, ρ_{path}) before to make the ratio between these two reflectances and to relate it to the total aerosol optical thickness. Two RTCs are available for generating the LUTs over wind-roughened sea surface: (1) RTC/SO (Successive Orders code from the Laboratoire Interdiscipli-naire en Sciences de l’Environnement (LISE) in France, Deuzé *at al.,* 1989) in which a flag can be activated to remove or not the sunglint contribution from the TOA reflectances, and (2) RTC/MOMO (Matrix-Operator MethOd code from Freie Universität Berlin (FUB) in Germany), in which the sunglint is included in the TOA reflectances. Both these two RTCs use the Cox-Munk model to compute the sunglint contribution.

In this model, the wave facet slopes are assumed to be normally distributed independently of the wind direction. The probability density function of facet slopes $p(\theta_s, \theta_v, \Delta\phi)$ for the illumination and viewing configurations $(\theta_s, \theta_v, \Delta\phi)$ is expressed as:

$$p(\theta_s, \theta_v, \Delta\phi) = \frac{1}{\pi\,\sigma^2}\ \exp\left(\frac{-\tan^2\beta}{\sigma^2}\right)$$ **Equation 59**

where β is the angle between the local normal and the normal to the facet:

$$\cos\beta = \frac{\cos\theta_v + \cos\theta_s}{2\,\cos\omega}$$ **Equation 60**

with, $\cos 2\omega = \cos\theta_s\ (\cos\theta_v - \sin\theta_s)\,\sin\theta_v\ .\cos\Delta\phi$

and σ is the root mean square of slopes function of the wind speed (w_s) just above sea level:

$$\sigma^2 = 0.003 + 5.12\ 10^{-3}\ w_s$$ **Equation 61**

Shadowing effects are not accounted for. The sun glint ρ_G (i.e., the specular reflection of the sunlight over the ocean waves) just above sea level is then computed as:

$$\rho_G = \rho_F(\omega) \; \frac{\pi \; p(\theta_s,\theta_v,\Delta\phi)}{4\cos\theta_s \; \cos\theta_v \; \cos^4\beta}$$ **Equation 62**

where $\rho_F(\omega)$ is the Fresnel reflectance at the air-sea interface.

$$\begin{cases} \rho_F(\omega) = \dfrac{1}{2}\left[\left(\dfrac{\sin(\omega-\vartheta_t)}{\sin(\omega+\vartheta_t)}\right)^2 + \left(\dfrac{\tan(\omega-\vartheta_t)}{\tan(\omega+\vartheta_t)}\right)^2\right] & for\ \omega \neq \vartheta_t \\ \rho_F(\omega) = \left(\dfrac{n_w-1}{n_w+1}\right)^2 & for\ \omega = \vartheta_t \end{cases}$$ **Equation 63**

with $\vartheta_t = \arcsin(\sin\omega / n_w)$

Finally, the sun glint contribution at TOA is expressed as follows:

$$\rho_G T(\theta_s) T(\theta_v)$$ **Equation 64**

where $T(\theta_s)$ and $T(\theta_v)$ are respectively for the direct downward and upward atmospheric transmittances. The latter are expressed as follows:

$$T(\theta_s) = \exp(-\tau/\mu_s) \quad \text{and} \quad T(\theta_v) = \exp(-\tau/\mu_v)$$ **Equation 65**

with τ the total optical thickness (Rayleigh + aerosols + absorbing gases when applicable).

6.2 WHITE CAPS

White caps are not accounted for.

7. Atmosphere

Atmosphere shall be assumed to be plane and its optical properties shall be provided at least for the following MERIS bands (see wavelengths in Section 3):

- 1, 2, 3, 4, 5, 6, 7, 8, 9, 12 and 13 for all ocean-related processing.
- 11 and 12 for correction of the slight O2 gaseous absorption in band#12 over Ocean.
- 9 and 10 for correction of the slight H_2O gaseous absorption in band 9.

7.1 CONSTITUENTS

The atmosphere shall be considered to be composed of:

1. molecules (*Rayleigh* scattering).
2. aerosols (scattering and absorption).
3. ozone (O_3) gas (absorption).
4. oxygen (O_2) gas (absorption).
5. water-vapour (H_2O) gas (absorption).
6. clouds (scattering and absorption).

All the other atmospheric constituents (N_2, Ar, CO_2, Ne, He, CH_4, Kr, H_2, N_2O, Xe, NO_2, CO and NH_3) are neglected.

The atmospheric gaseous absorption, mainly O_2, O_3 and H_2O but also other gases when relevant, may be separately treated from the rest of the atmospheric constituents (aerosols and molecules). This approach allows to generate a set of absorption coefficients used as inputs to the RTC for estimating the gaseous transmission function. Although the interactions of multiple scattering and the gaseous absorption are accurately accounted for in the radiative transfer computations, this assumption needs to be validated. This particular treatment is used in the RTC/FUB(MOMO) implemented in the MERIS Ground Segment (GS).

7.2 POLARISATION

The radiative transfer within the coupled "*Atmosphere-Land/Ocean*" system should be treated by including the polarization processes. Among the RTCs used in the MERIS-GS, only the RTC/SO (LISE) accounts for polarization.

7.3 SAMPLING

In the RTCs implemented in the MERIS-GS, the radiance field is numerically computed with an angular discretization of the space and the computation with respect to the optical thickness (vertical integration) is accomplished by dividing the atmosphere into sub-layers. Consequently, it shall be possible to parameterize in the RTC:

- the number of discrete directions (zenith and azimuth angles), knowing that the set of zenith angles is derived from a Gauss-Lobatto quadrature in the RTC/FUB(MOMO) and from a Gauss quadrature in the RTC/LISE(SO), and that the set of azimuth angles is specified on a regular grid.

- For the vertical layering of the atmosphere, a user defined profile is employed as input to the RTC/MOMO, and a specific of atmospheric profile using three aerosol layers is available in the RTC/SO.
  For MOMO, an input 2D matrix corresponding to the number of types of scatterers (3 aerosols + 3 clouds) by the number of layers (user defined value) has to be filled for each sub-layer with the type and the density (1/dz, m^{-1}) of aerosols and/or cloud particles. This code presents some flexibilities to compute radiative transfer with more than 3 major aerosol layers by using the clouds layers. This is especially dedicated for the treatment of dusts assemblages (4 aerosols layers).
- For the SO code, a mixing rate between molecules and aerosols is precomputed for each of the atmospheric sub-layers For three major aerosol layers (boundary + troposphere + stratosphere over ocean), the aerosols are assumed to be homogeneously distributed. The atmosphere is discretized into 100 elementary sub-layers and to assure the continuity of the light extinction between two consecutive major aerosol layers, an infinitesimal sub-layer is introduced at the transition (see Figure 7-1).

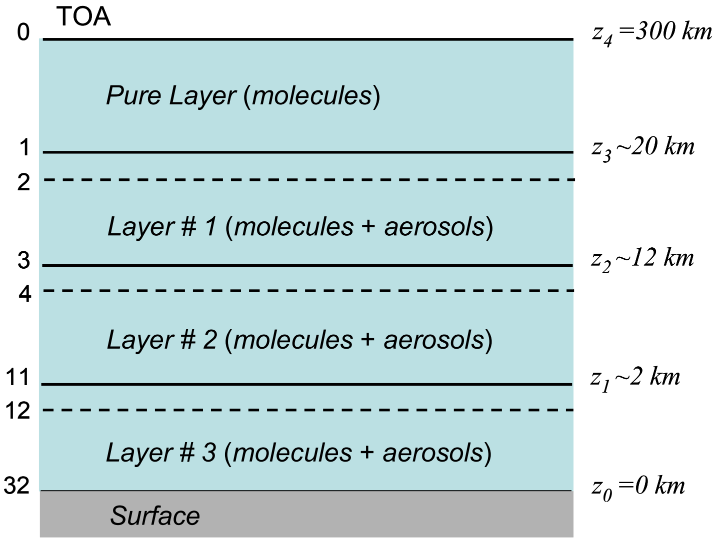

Figure 7-1: Schematic representation of the «3 aerosol-layers» atmosphere

7.4 SURFACE PROPERTIES

The surface below the atmosphere shall be modelled by a water body with optical properties including the Fresnel reflection contribution at the air-sea interface as described in Sections 4 and 6. The surface will be considered as infinite and homogeneous.

7.5 PRESSURE AT GROUND LEVEL

The surface pressure at sea level (elevation of 0 km) shall be equal to 1013.25 hPa.

7.6 RAYLEIGH SCATTERING

The vertical profile of molecules shall be taken from Elterman (1968), scaled so that the total optical thickness (τ_R) has the values from Table 6-1. The sea level pressure is 1013.25 hPa.

The Rayleigh optical thickness (τ_R) shall be taken from Table 7-1. These values are computed with the following approximation from Hansen and Travis (1974):

$$\tau^R = \frac{P_s}{P_o}\left[8.524\ 10^{-3}\ \lambda^{-4} + 9.63\ 10^{-5}\ \lambda^{-6} + 1.1\ 10^{-6}\ \lambda^{-8}\right]$$

Equation 66

where P_s is the surface pressure (hPa), P_o the pressure in the STP conditions, and λ the wavelength expressed as µm.

Table 7-1: Rayleigh optical thickness in the 15 MERIS bands

λ	*412.5*	*442.5*	*490*	*510*	*560*	*620*	*665*	*681.25*	*708.75*	*753.75*	*761.875*	*778.75*	*865*	*885*	*900*
τ_R	0.315280	0.235910	0.155155	0.131714	0.089912	0.059433	0.044730	0.040562	0.034558	0.026944	0.025802	0.023617	0.015459	0.014099	0.013176

Considering the molecular anisotropy, the Rayleigh scattering phase function should be computed as:

$$P(\Theta) = \frac{1}{4\pi}\frac{3}{4\,(1+2\gamma)}\left[(1-\gamma)\ \cos^2\Theta + (1+3\gamma)\right]\ \ with\ \ \gamma = \frac{\delta}{2-\delta}$$

Equation 67

where Θ represents the scattering angle and δ the molecular depolarization factor taken to be equal to 0.0279, whatever the wavelength.

7.7 OXYGEN

The vertical distribution of oxygen follows the pressure and temperature profile of the atmosphere. The latter differs between arctic or tropical atmospheres. The spectral O_2 absorption coefficients shall be computed with a Neural Network tool (NN) combining a Line By Line (LBL) code and the spectroscopic HITRAN database (see Rothman *et al*, 2009) for different states of sea surface, in order to account for O_2 atmospheric-Fresnel transmittances in the residual MERIS absorption bands at 778.75 nm.

7.8 OZONE

The vertical distribution of ozone varies significantly with atmospheric dynamical processes. The impact of different profiles shall be investigated, although the major part of the ozone content is located in the upper atmospheric layers. The spectral O_3 absorption coefficients shall be computed with a LBL code and the spectroscopic HITRAN database (see Rothman *et al*, 2009).

7.9 WATER VAPOUR

Because the vertical distribution of water-vapour is strongly dependent on the temperature-pressure profiles, and the latter has to be considered in the radiative transfer computations. The spectral H_2O absorption coefficients shall be computed with a NN tool combined with LBL code and the spectroscopic HITRAN database (see Rothman *et al*, 2009) for different states of sea surface (i.e., surface roughness levels) to account for the coupling term between the atmospheric scattering and the Fresnel reflection at sea surface.

7.10 AEROSOLS

7.10.1 MODELS AND PROPERTIES

A set of aerosol models shall be taken from ATBD 2.7: Atmospheric corrections over case-1 waters, Section 3.1.1.5.2.

Atmospheric corrections over water rely on a good definition of the aerosol optical properties. Some basic constituents are mixed homogeneously to build-up models which are listed hereafter. Vertical profile of models defines assemblages, as described in Section 12.

Aerosol models shall be defined each as a homogeneous mixture of basic constituents. Each basic constituent shall be a population of spherical particles characterized by:

- its complex refractive index at all wavelengths (see Section 10),
- its particle size distribution function: log-normal, Junge's power-law or modified Gamma distribution (see below),
- the parameters of its particle size distribution (see below).

The 6 basic constituents are the following:

1. sea salt solution in water (oceanic),
2. water soluble particles,
3. dust-like particles,
4. desert dust aerosols (mixing of clay, silt and sand),
5. soot-like particles,
6. sulphuric acid solution in water

An additional constituent, using several models, is built with combination of two constituents from above:

7. rural aerosol mixture (70% of water soluble particles and 30% of dust-like particles)

The standard aerosol models (SAMs) are listed as follows:

1) Maritime model (Shettle and Fenn, 1979)
2) Coastal model (Shettle and Fenn, 1979)
3) Rural model (Shettle and Fenn, 1979)
4) Continental model (WCRP, 1986)
5) Stratospheric model (WCRP, 1986)
6) Desert dust model (Moulin *et al*., 2001)[1]
7) Blue-IOP models composed with a single component from which particles are considered as spherical and from which the size distribution follows a Log-Normal law. The latter are detailed in Section 7.10.2.

Table 7-2 indicates the proportions of constituents in each model, and Figure 7-2 displays the principle of the aerosol assemblages. Distinction between components and models for Desert Dust models from (Moulin *et al*, 2001) is less easy: essential components combine 3 categories of particle sizes (see Table 7-3) associated with two sets of refractive indices (see Table 9-1), referred to as BDS and BDW. Three different combinations (in terms of proportions) of the 3 ranges of particle sizes together with the 2 sets of refractive indices result in 6 elementary models BDS1 to BDS3 (first set of refractive indices) and BDW1 to BDW3 (second set).

Table 7-2: Aerosol components and their respective contributions (as percent of the volume, or as percent of the number of particles) in the composition of the aerosol models. The principle of «external mixing» is applied when calculating the optical properties of the aerosol models. ‡ 70% of water soluble particles, and 30% of dust-like particles.

Aerosol model	*Components*	*Volume [%]*	*Particle [%]*
Maritime	Rural aerosol mixtures‡	-	99.0
(*Shettle and Fenn, 1979*)	Oceanic (Sea-salt solution in water)	-	1.0
Coastal	Rural aerosol mixtures‡	-	99.5
(*Shettle and Fenn, 1979*)	Oceanic (Sea-salt solution in water)	-	0.5
Continental	Water soluble	29	93.876773
	Dust-like	70	$2.27\ 10^{-4}$
(*WCRP, 1986*)	Soot	1	6.123
Blue-IOP	Small particles	-	100
(*Santer and Zagolski, 2010*)	(accumulation mode)	1	

Table 7-2 cont.

Desert -dusts

BDS-1 & BDW-1	Large particles	-	$3.861\ 10^{-5}$
	Medium particles	-	45.78573545
(*Moulin et al, 2001*)	Small particles	-	54.21422594
BDS-2 & BDW-2	Large particles	-	$3.861\ 10^{-4}$
	Medium particles	-	45.785561705
(*Moulin et al, 2001*)	Small particles	-	54.214052195
BDS-3 & BDW-3	Large particles	-	$7.722\ 10^{-4}$
	Medium particles	-	45.785368655
(*Moulin et al, 2001*)	Small particles	-	54.213859145
H_2SO_4	75% solution of	100	100
(WCRP, 1986)	Sulphuric acid in water		

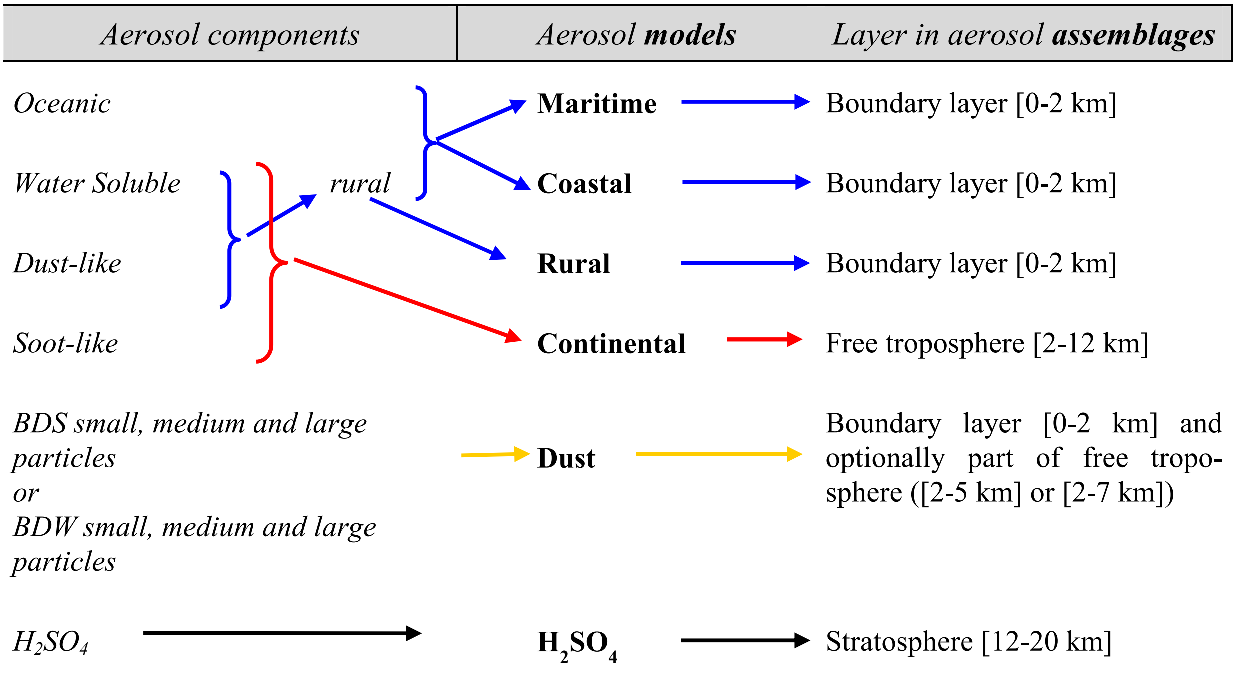

Figure 7-2: Principle of aerosol assemblages

Table 7-3: Parameters defining the size distribution of the aerosol models

Aerosol model or aerosol component		*Parameters of the log-normal distribution*		
		r_{mean} [μm]	$\sigma/ln(10)$ [μm]	$exp(\sigma)$
Rural	RH 50%	0.02748	0.35	2.238721
(water soluble + dust-like)	RH 70%	0.02846	0.35	2.238721
	RH 90%	0.03884	0.35	2.238721
(*Shettle and Fenn, 1979*)	RH 99%	0.05215	0.35	2.238721
Oceanic	RH 50%	0.17110	0.40	2.511886
(sea-salt solution in water)	RH 70%	0.20410	0.40	2.511886
	RH 90%	0.38030	0.40	2.511886
(*Shettle and Fenn, 1979*)	RH 99%	0.75050	0.40	2.511886
Continental		0.00500	0.475671	2.99
(water soluble, dust-like		0.50000	0.475671	2.99
soot) (*WCRP, 1986*)		0.01180	0.301030	2.00
Desert Dust	Large particles	6.240	0.276462	1.89
	Medium particles	0.022	0.505150	3.20
(*Moulin et al., 2001*)	Small particles	0.001	0.328380	2.13

	Parameters of the Modified Gamma size distribution			
	A	α	γ	b
75% H_2SO_4 (*WCRP, 1986*)	324	1	1	18

Tables from Section 9 gives the refractive indices (m) of the aerosol models.

7.10.2 BLUE AEROSOLS

Because of the high temporal and spatial variability of the small particles, the atmospheric correction is a crucial step in the processing of ocean colour satellite imagery. In a classic atmospheric correction scheme, the aerosol reflectance is first estimated at 865 nm. Then a spectral extrapolation from the NIR to the blue region is performed to correct the measured TOA radiance. Accuracy of the atmospheric correction is directly related to the ability of the aerosol model to describe the spectral dependence between the NIR and the blue region.

In the first MERIS processing, a set of four blue aerosol models characterized by a Junge size distribution and a non-absorbing refractive index (m=1.44) was introduced in the set of the 16 SAM's over ocean. They were spectrally described by four Angström exponents ($\alpha = -1.5$, -2.0, -2.5, -3.0). Results derived from the first MERIS validation phase stressed that the first blue model ($\alpha = -1.5$) was whiter than expected. Although the QWG recommendation was to replace this blue model by a more absorbing aerosol (i.e., a maritime model with RH=99%), the atmospheric correction in the second MERIS reprocessing remained unsatisfying.

Furthermore, it clearly appeared that the Junge models do not reproduce accurately the spectral dependence for the small particles. While the normalized extinction coefficient is overestimated with these blue Junge models for the short wavelengths the latter was slightly underestimated for larger wavelengths toward the NIR region. An alternative issue to redefine the blue models was proposed by LISE/ParBleu to the MERIS QWG based on an approach combining the micro-physical properties of these small particles with their IOPs derived from

CIMEL measurements (sky / sun radiances) acquired over ocean sites. A set of 3 blue-IOP models have been proposed then to replace the 3 Junge models from the last set of 16 SAMs. The latter are characterized by a complex refractive index (m=1.44; k=0.003) and a log-normal size distribution (Table 7-4) with a spectral dependence defined by α = -0.3.

Table 7-4: Parameters defining the size distribution of the blue aerosol models.

Aerosol model or aerosol component		*Parameters of the log-normal distribution*		
		r_{mean} *[μm]*	$\sigma / ln(10)$ *[μm]*	$exp(\sigma)$
BLUE	IOP-01	0.039971	2.302585	1.349859
(*Santer and Zagolski, 2010*)	IOP-02	0.034958	2.302585	1.349859
	IOP-03	0.029829	2.302585	1.349859

7.10.3 PHASE FUNCTION AND SINGLE SCATTERING ALBEDO

Aerosol phase function, extinction and scattering coefficients, single scattering albedo, asymmetry factor shall be computed according to Mie theory (Mie, 1908), based on the parameters identified in Section 7.10.1.

Table 10-1 summarizes the results of the Mie computations. For each aerosol model and each wavelength, are displayed the extinction coefficients (Q_{ext}) and the single scattering albedo (ω_0).
The plots in Section 12 display the scattering phase function at 550 nm for the land-aerosol models and at the 15 MERIS wavelengths for the ocean-aerosol assemblages.

7.10.4 VERTICAL PROFILES

Aerosol assemblages over ocean shall be specified by the following 3 major aerosol layers:

- a boundary layer (model, AOT-550) from 0 to 2 km altitude,
- a tropospheric layer (model, AOT-550) from 2 to 12 km altitude,
- a stratospheric layer (model, AOT-550) above 12 km altitude..

34 aerosol assemblages (16 SAMs + 18 Dusts) are available for the atmospheric corrections over oceans. The latter are fully described in Section 11.

7.11 REFERENCE ATMOSPHERE OVER OCEANS

For the purposes of validation and of LUTs computation (i.e., those which do not require variations of the atmosphere properties), a reference atmosphere over ocean has been defined with the following parameters:

- Rayleigh scattering as defined in Section 6.6, with a sea level pressure of 1013.25 hPa,
- boundary aerosol layer: maritime model with a relative humidity = 99%, $\tau_a(550)=0.2$,
- free aerosols both in tropospheric and stratospheric layers,
- no ozone absorption
- no water vapour absorption

7.12 ATMOSPHERIC TRANSMITTANCES OVER OCEAN

7.12.1 GASEOUS ABSORPTION

In the atmospheric correction algorithm over ocean, the first step consists of removing the gaseous absorption. While the ozone absorbs in all the MERIS ocean-related spectral bands (Table 7-5) a slight water-vapour (H_2O) and oxygen (O_2) absorption occurs respectively at 708.75nm (band #9) and at 778.75nm (band#12).

For the first correction, the ozone layer being located above the aerosols, the absorption and scattering processes can be decoupled thanks to the weakness of the coupling between Rayleigh scattering and gaseous absorption at this pressure level. The ozone transmissivity (T_{O3}) is then expressed as:

$$T_{O_3} = \exp(-M \cdot \tau_{O_3} \cdot u_{O_3}) \qquad \textbf{Equation 68}$$

where:

$$M = \frac{1}{\cos(\vartheta_s)} + \frac{1}{\cos(\vartheta_v)} \qquad \textbf{Equation 69}$$

and:

u_{O3} the total amount of ozone (in *cm-atm*)
τ_{O3} the ozone optical thickness
M the airmass.

The actual value of the ozone is provided by the European Centre for Medium range Weather Forecast (ECMWF).

For water vapour (mostly located in the lower troposphere), the correction within a slightly contaminated spectral band is achieved by estimating the water vapour content (u_{H2O}) with a polynomial fit of the ratio of radiances at 900 nm (with absorption) and at 885 nm (without absorption) MERIS wavelengths (Santer *et al.*, 1999). This approach is used to estimate the total water vapour transmittance (T_{H2O}) and accounts for the coupling between scattering and gaseous absorption. To account for the coupling term between the atmospheric scattering and the Fresnel reflection at sea surface, a NN tool (FUB) is then used to get these polynomial coefficients of water-vapour retrieval.

Table 7-5: Ozone optical thickness for a standard amount of 0.32 cm-atm and ozone transmissivities within each of the 15 MERIS spectral bands.

Band	$\lambda(nm)$	$\Delta\lambda(nm)$	τ_{O_3}	*Absorbers*	T_{O_3}
1	412.50	10	$2.1785\ 10^{-4}$	O_3	0.99985
2	442.50	10	$2.8136\ 10^{-3}$	O_3	0.99806
3	490.00	10	$2.0057\ 10^{-2}$	O_3	0.98627
4	510.00	10	$4.0809\ 10^{-2}$	H_2O+O_3	0.97225
5	560.00	10	$1.0399\ 10^{-1}$	O_3	0.93081
6	620.00	10	$1.0903\ 10^{-1}$	O_3	0.92758
7	665.00	10	$5.0504\ 10^{-2}$	O_3	0.96578
8	681.25	7.5	$3.5258\ 10^{-2}$	H_2O+O_3	0.97598
9	708.75	10	$1.8808\ 10^{-2}$	H_2O+O_3	0.98712
10	753.75	7.5	$8.8966\ 10^{-3}$	$H_2O^*+O_3$	0.99388
11	761.875	3.75	$6.6342\ 10^{-3}$	O_2+O_3	0.99544
12	778.75	15	$7.6933\ 10^{-3}$	$H_2O^*+O_2$	0.99471
13	865.00	20	$2.1922\ 10^{-3}$	H_2O^*	0.99849
14	885.00	10	$1.2107\ 10^{-3}$	H_2O	0.99917
15	900.00	10	$1.5167\ 10^{-3}$	H_2O	0.99895

Before applying atmospheric corrections over the ocean, TOA radiance (L), measured by MERIS and delivered as the level-1 product, needs to be converted into normalized radiances (L_n) by an extraterrestrial solar irradiance equal to π:

$$L_n = L \cdot \frac{\pi . d^2}{F_0}, \qquad \textbf{Equation 70}$$

F_0 is the Thuillier *et al.* (2003) mean extraterrestrial solar irradiance, corrected for the Sun-Earth distance d (in AU). $F_0(\lambda)$ can be extracted from the Thuillier database (Thuillier *et al.*, 2003). The corrective factor d depends on the position of the Earth on its orbit and is computed with the following approximation:

$$d = \frac{1}{A - B\cos(\gamma_J \pi / 180) - \varepsilon \cos(\gamma_J \pi / 90)}, \qquad \textbf{Equation 71}$$

where:

ε is the eccentricity of the Earth's elliptic orbit (ε=0.00014)
$\gamma_J = C \cdot J - D$
$A = 1 + \varepsilon$
$B = 0.01671$
$C = 0.9856002831$
$D = 3.4532868$
J = Julian day

A simpler corrective formulation also exists but note that it is ***not*** applied in the atmospheric correction:

$$d = \frac{1}{(1 - 0.01673.\cos M)}$$ **Equation 72**

with:

$$M = 0.9856.(J - 4).\frac{\pi}{180}$$ **Equation 73**

The TOA normalized radiance (L_n) is then corrected for the gaseous absorption as:

$$\rho^* = \frac{L_n}{\mu_s \cdot T_g},$$ **Equation 74**

where:

ρ^* is the apparent reflectance at TOA,
T_g the total gaseous transmittance ($T_{H2O} \times T_{O3}$),
μ_s the cosine of the solar zenith angle.

7.12.2 MARINE REMOTE SENSING REFLECTANCE

In ocean colour remote sensing, ρ^* corrected for gaseous absorption can be linearized as:

$$\rho^* = \rho_{atm} + T \cdot \frac{\rho_w}{1 - \rho_w \cdot S} + \rho_G \cdot e^{-M \cdot \tau},$$ **Equation 75**

where:

ρ_{atm}	stands for the intrinsic atmospheric contribution (multiple scattering contributions from the molecules, the aerosols and the Rayleigh-aerosol coupling, as well as from the coupling between atmospheric scattering and Fresnel surface reflection).
T	is the total atmospheric transmittance (Rayleigh + aerosol) exclusive of gaseous absorption
S	is the spherical albedo relating to the molecules and the aerosols.
τ	is the total optical thickness (Rayleigh + aerosol).
M	is the airmass.
ρ_w	is the water reflectance..
ρ_G	is the direct sun glint reflectance.

The Fresnel reflection is accounted for in the computation of the coupling terms between specular reflections and atmospheric scattering.

The following step in the atmospheric correction algorithm over ocean is to characterize the aerosols. Over case-1 waters, the water body is assumed to be black (ρ_w=0) at 778.75 nm and 865 nm. Moreover, below a wind-speed threshold and outside of the specular direction, the foam and direct sun glint contributions can be neglected. Thus, the signal at TOA corresponds to the intrinsic atmospheric scattering (ρ_{atm}). Consequently, from the two atmospheric path radiances acquired at 778.75 nm and 865 nm we can retrieve the aerosol type and the aerosol optical thickness (AOT) at 865 nm (Antoine and Morel, 1999).

A last step consists of the removal of the atmospheric path reflectance (ρ_{atm}). Because the latter includes also the coupling term between atmospheric scattering and Fresnel surface reflection, its estimation relies on a radiative transfer code (RTC/SO) in which the Fresnel reflection is accounted for with a wind-roughened black sea surface. The apparent contribution of the water body (ρ_w^*) is then expressed as:

$$\rho_w^* = \rho^* - \rho_{atm}\,. \qquad \textbf{Equation 76}$$

ρ_w^* includes three different contributions:

- the water body as seen through the atmosphere,
- the direct sun glint,
- the foam for which no correction is applied..

Moreover, the reflection of the sky dome is accounted for in ρ_{atm}.

In order to derive the water reflectance at sea level (bottom of atmosphere, BOA) from ρ_w^*, a total (diffuse + direct) atmospheric transmittance in upward direction $T(\mu_v)$ is introduced. Following the 5S code (Vermote *et al.*, 1997), this upwelling transmittance corresponds to the ratio between BOA and TOA irradiances for a solar zenith angle (θ_v) measured over a dark surface (without Fresnel reflection). The water reflectance is then computed as:

$$\rho_w = \rho_w^* / T(\mu_v)\,. \qquad \textbf{Equation 77}$$

ρ_w is the geophysical output from atmospheric correction based on a decoupled "atmosphere-ocean" system.

7.12.3 UPWARD AND DOWNWARD ATMOSPHERIC TRANSMITTANCES

Total upwelling ($T(\mu_s)$) and downwelling ($T(\mu_v)$) transmittances have been computed with the RTC/SO for several maritime atmospheres over a black surface, respectively with and without Fresnel reflection, for all illumination/viewing (μ_s, μ_v) configurations defined by a Gauss quadrature (24 discrete directions + nadir) in all the 15 MERIS spectral bands. Scattering atmospheres are characterized by a set of 16 SAMs (corresponding to maritime, coastal, rural and blue-IOP assemblages from Table 7-2 and a set of and a set of 7 AOTs at 550 nm including the case of a pure Rayleigh atmosphere (i.e., $\tau_a(550)$ = 0, 0.04, 0.06, 0.13, 0.33, 0.53, 2.03).

The Fresnel reflection at the air-sea surface is modelled with a Cox-Munk surface with 3 wind-speeds (1.5, 5.0, and 10 m^{-1}). However, the wind-speed was found to have no impact on the transmittance computation and the following figures show only the aerosol and Rayleigh transmittances for a mean wind-speed of 5.0 ms^{-1}.

Figure 7-3 to Figure 7-6 show the logarithm (log) of the total atmospheric transmittance ($T(\mu_s)$ x $T(\mu_v)$) using $\theta_s = \theta_v$, for a purely Rayleigh atmosphere (AOT=0) and a purely aerosol atmosphere, plotted as function of the total airmass, for the 442.5 nm MERIS wavelength, and 3 SAMs (MAR90, COA90, RUR90, BLU-IOP1).

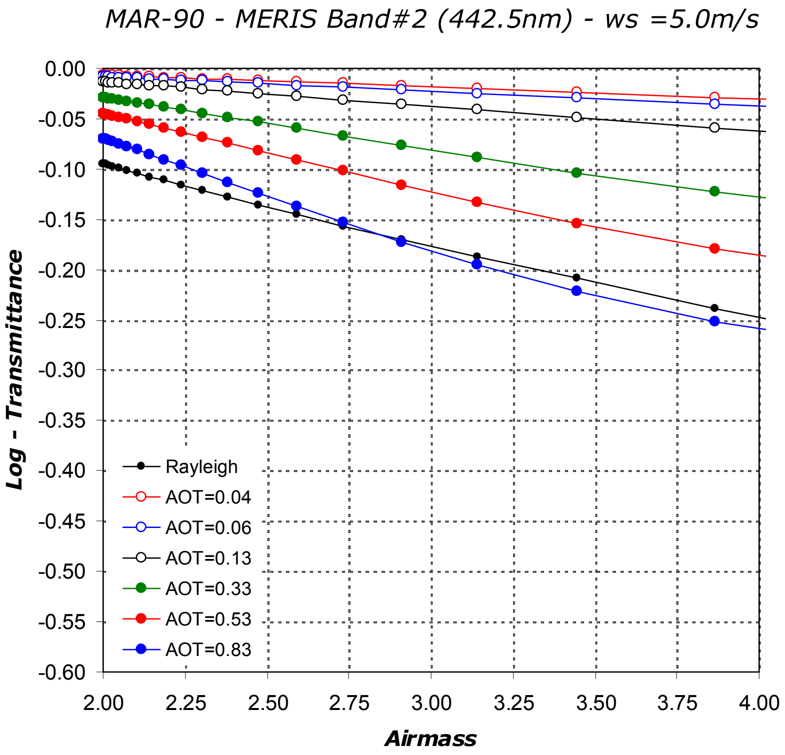

Figure 7-3: Total atmospheric transmittance at 442.5 nm for a purely Rayleigh atmosphere (AOT=0) and a purely aerosol atmosphere for a set of 6 AOTs at 550 nm, as function of the air mass (no unit), using a MAR90 assemblage.

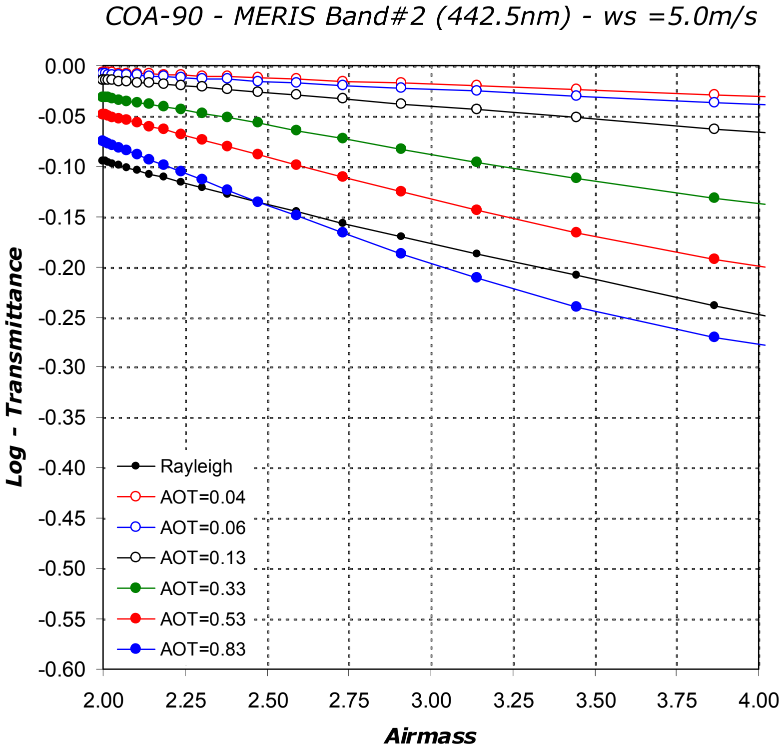

Figure 7-4: Total atmospheric transmittance at 442.5 nm for a purely Rayleigh atmosphere (AOT=0) and a purely aerosol atmosphere for a set of 6 AOTs at 550 nm, as function of the air mass, using a COA90 assemblage.

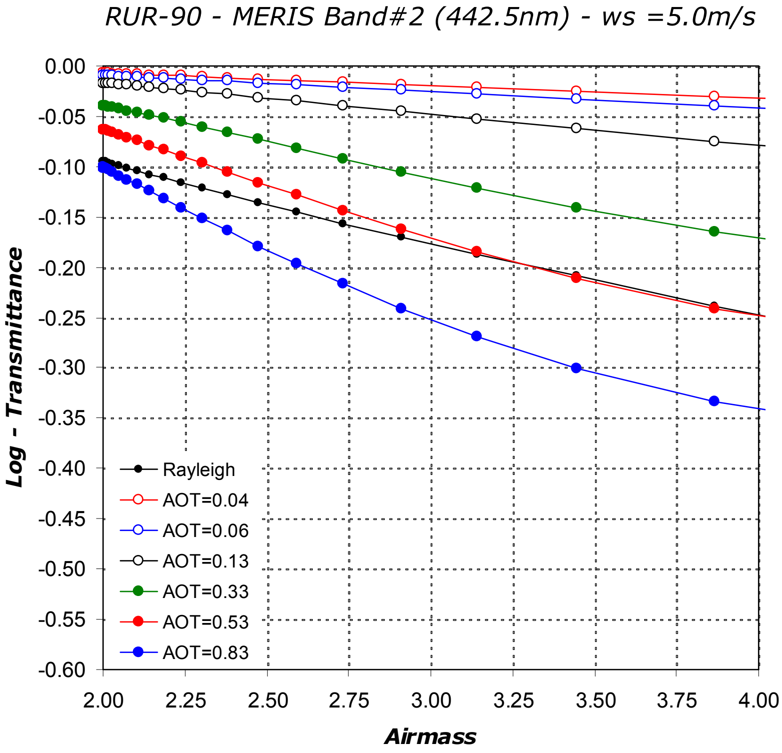

Figure 7-5: Total atmospheric transmittance at 442.5 nm for a purely Rayleigh atmosphere (AOT=0) and a purely aerosol atmosphere for a set of 6 AOTs at 550 nm, as function of the air mass, using a RUR90 assemblage.

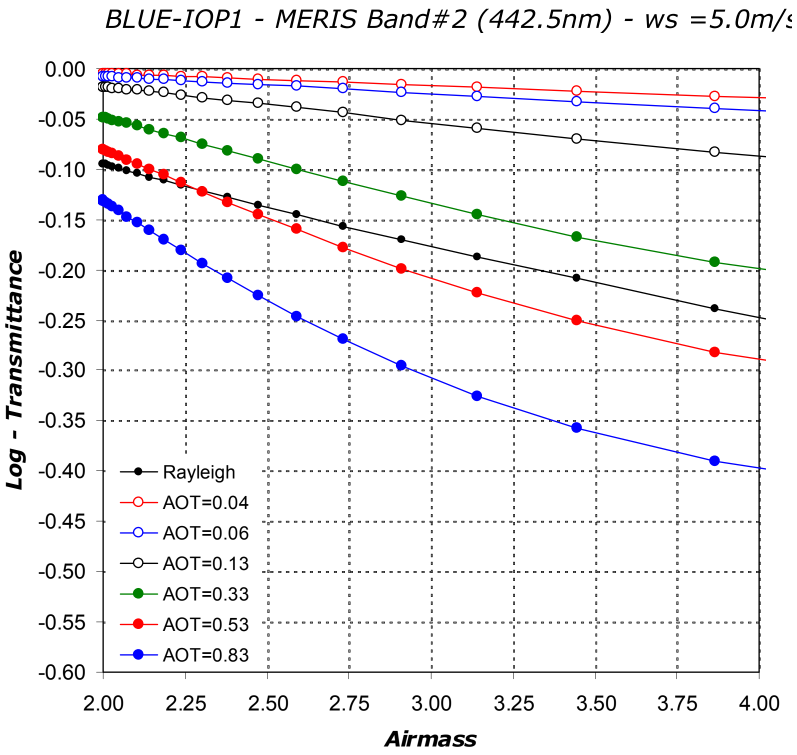

Figure 7-6: Total atmospheric transmittance at 442.5 nm for a purely Rayleigh atmosphere (AOT=0) and a purely aerosol atmosphere for a set of 6 AOTs at 550 nm, as function of the air mass, using a BLUE-IOP1 assemblage.

8. Clouds

8.1 WATER CLOUDS

Cloud types shall be taken from ATBD volume 1, Cloud albedo and optical thickness, Section 3.1.2.1. Each cloud type is specified as a population of water droplets with a modified gamma-function for the vertical distribution, characterized by its effective radius (µm).

The cloud scattering phase function, extinction and scattering coefficients, shall be computed according to the Mie's theory, based on the cloud parameters mentioned above.

Clouds shall be specified by a type and an extinction coefficient (m^{-1}) in each atmospheric layer.

8.2 CIRRUS CLOUDS

It shall be possible to specify layer(s) of cirrus cloud, whose optical properties: scattering phase function, extinction and scattering coefficients, shall be taken from Brogniez *et al.* (1995). At least 1 layer in the atmosphere between 8500m and 9000m should be defined for the radiative transfer simulations.

9. Refractive indices

Table 9-1 provides the complex refractive index of the ocean aerosol models at the 15 MERIS wavelengths (n_r: real part, n_i: imaginary part).

Table 9-1: Refractive index of aerosol components/models

OCEANIC (*Shettle and Fenn, 1979*)								
Wavelength	RH=50%		RH=70%		RH=90%		RH=99%	
(nm)	n_r	n_i	n_r	n_i	n_r	n_i	n_r	n_i
412.50	1.471	-2.403E-08	1.417	-1.468E-08	1.350	-3.750E-09	1.340	-2.000E-09
442.50	1.471	-2.177E-08	1.416	-1.281E-08	1.349	-3.190E-09	1.339	-1.650E-09
490.00	1.470	-1.774E-08	1.415	-9.750E-09	1.347	-2.350E-09	1.337	-1.160E-09
510.00	1.470	-1.012E-08	1.414	-6.220E-09	1.348	-1.930E-09	1.336	-1.240E-09
560.00	1.469	-9.800E-09	1.412	-7.200E-09	1.345	-4.060E-09	1.335	-3.570E-09
620.00	1.462	-1.738E-08	1.409	-1.544E-08	1.344	-1.308E-08	1.334	-1.274E-08
665.00	1.461	-5.481E-08	1.408	-4.170E-08	1.343	-2.584E-08	1.333	-2.334E-08
681.25	1.461	-7.289E-08	1.408	-5.407E-08	1.343	-3.131E-08	1.333	-2.770E-08
708.75	1.460	-2.995E-07	1.407	-1.997E-07	1.343	-7.863E-08	1.333	-5.944E-08
753.75	1.458	-9.602E-07	1.406	-6.223E-07	1.342	-2.123E-07	1.332	-1.474E-07
761.875	1.458	-1.052E-06	1.406	-6.810E-07	1.342	-2.309E-07	1.332	-1.596E-07
778.75	1.457	-1.327E-06	1.405	-8.570E-07	1.341	-2.866E-07	1.331	-1.962E-07
865.00	1.453	-1.156E-05	1.402	-4.042E-06	1.340	-9.848E-07	1.330	-4.981E-07
885.00	1.452	-4.771E-05	1.401	-1.373E-05	1.340	-2.812E-06	1.330	-1.071E-06
900.00	1.451	-7.482E-05	1.401	-2.100E-05	1.339	-4.182E-06	1.329	-1.500E-06

BLUE-IOP (*Santer and Zagolski, 2010*)						
Wavelength	*IOP-1*		*IOP-1*		*IOP-1*	
(nm)	n_r	n_r	n_r	n_r	n_r	n_i
412.50	1.440	-3.00 E-03	1.440	-3.00 E-03	1.440	-3.00 E-03
442.50	1.440	-3.00 E-03	1.440	-3.00 E-03	1.440	-3.00 E-03
490.00	1.440	-3.00 E-03	1.440	-3.00 E-03	1.440	-3.00 E-03
510.00	1.440	-3.00 E-03	1.440	-3.00 E-03	1.440	-3.00 E-03
560.00	1.440	-3.00 E-03	1.440	-3.00 E-03	1.440	-3.00 E-03
620.00	1.440	-3.00 E-03	1.440	-3.00 E-03	1.440	-3.00 E-03
665.00	1.440	-3.00 E-03	1.440	-3.00 E-03	1.440	-3.00 E-03
681.25	1.440	-3.00 E-03	1.440	-3.00 E-03	1.440	-3.00 E-03
708.75	1.440	-3.00 E-03	1.440	-3.00 E-03	1.440	-3.00 E-03
753.75	1.440	-3.00 E-03	1.440	-3.00 E-03	1.440	-3.00 E-03
761.875	1.440	-3.00 E-03	1.440	-3.00 E-03	1.440	-3.00 E-03
778.75	1.440	-3.00 E-03	1.440	-3.00 E-03	1.440	-3.00 E-03
865.00	1.440	-3.00 E-03	1.440	-3.00 E-03	1.440	-3.00 E-03
885.00	1.440	-3.00 E-03	1.440	-3.00 E-03	1.440	-3.00 E-03
900.00	1.440	-3.00 E-03	1.440	-3.00 E-03	1.440	-3.00 E-03

MISCELLANEOUS (*WRCP, 1986*)

Wavelength	*Water soluble*		*Dust-like*		*Soot*		*75 % H2SO4 solution*	
(nm)	n_r	n_i	n_r	n_i	n_r	n_i	n_r	n_i
412.50	1.530	-5.000E-03	1.530	-8.000E-03	1.750	-4.590E-01	1.439	-1.000E-08
442.50	1.530	-5.000E-03	1.530	-8.000E-03	1.750	-4.551E-01	1.436	-1.000E-08
490.00	1.530	-5.000E-03	1.530	-8.000E-03	1.750	-4.500E-01	1.432	-1.000E-08
510.00	1.530	-5.000E-03	1.530	-8.000E-03	1.750	-4.500E-01	1.431	-1.000E-08
560.00	1.530	-6.000E-03	1.530	-8.000E-03	1.750	-4.388E-01	1.430	-1.057E-08
620.00	1.530	-6.000E-03	1.530	-8.000E-03	1.750	-4.316E-01	1.429	-1.396E-08
665.00	1.530	-6.525E-03	1.530	-8.000E-03	1.750	-4.300E-01	1.428	-1.743E-08
681.25	1.530	-6.791E-03	1.530	-8.000E-03	1.750	-4.300E-01	1.428	-1.881E-08
708.75	1.529	-7.444E-03	1.529	-8.000E-03	1.750	-4.300E-01	1.428	-3.404E-08
753.75	1.526	-8.800E-03	1.526	-8.000E-03	1.750	-4.300E-01	1.427	-7.717E-08
761.875	1.526	-9.007E-03	1.526	-8.000E-03	1.750	-4.300E-01	1.427	-8.376E-08
778.75	1.525	-9.553E-03	1.525	-8.000E-03	1.750	-4.300E-01	1.426	-1.011E-07
865.00	1.520	-1.213E-02	1.520	-8.000E-03	1.750	-4.303E-01	1.425	-2.120E-07
885.00	1.520	-1.263E-02	1.520	-8.000E-03	1.750	-4.313E-01	1.424	-3.441E-07
900.00	1.520	-1.300E-02	1.520	-8.000E-03	1.750	-4.320E-01	1.424	-4.432E-07

DUSTS (*Moulin et al., 2001*)

Wavelength	*BDS*		*BDW*	
(nm)	n_r	n_i	n_r	n_i
412.50	1.530	-1.200E-02	1.530	-8.000E-03
442.50	1.530	-9.100E-03	1.530	-4.500E-03
490.00	1.530	-7.900E-03	1.530	-4.000E-03
510.00	1.530	-7.300E-03	1.530	-3.000E-03
560.00	1.530	-5.352E-03	1.530	-1.957E-03
620.00	1.530	-4.778E-03	1.530	-1.435E-03
665.00	1.530	-4.348E-03	1.530	-1.043E-03
681.25	1.530	-4.173E-03	1.530	-9.421E-04
708.75	1.530	-3.860E-03	1.530	-8.000E-04
753.75	1.530	-3.339E-03	1.530	-5.632E-04
761.875	1.530	-3.258E-03	1.530	-5.263E-04
778.75	1.530	-2.940E-03	1.530	-5.000E-04
865.00	1.530	-1.200E-03	1.530	-5.000E-04
885.00	1.530	-1.200E-03	1.530	-5.000E-04
900.00	1.530	-1.200E-03	1.530	-5.000E-04

10. Aerosols optical properties (ATBD 2.7)

Optical properties (scattering phase function, extinction coefficient and single scattering albedo) of a mixing of aerosols are computed with the Mie's theory, assuming the particles as homogeneous isotropic spheres for which the sizes are comparable or larger than the incident wavelength. Each particle size distribution in the aerosols mixing is characterized by a complex refractive index (n_r, n_i) which is assumed to be identical for all the scatterers within the same distribution, and a component mixing ratio.

For each aerosol model used in the assemblage over ocean (see Section 11), single scattering albedo (ω_o) and extinction coefficient (Q_{ext}) at each MERIS wavelength are given in Table 10-1 to Table 10-7.

Table 10-1: Aerosol optical properties (single scattering albedo and scattering coefficient) at the 15 MERIS wavelengths for rural model (RH=50, 70, 90, 99%).

RURAL (*Shettle and Fenn, 1979*)								
Wavelength	RH=50%		RH=70%		RH=90%		RH=99%	
(nm)	ω_o	Q_{ext}	ω_o	Q_{ext}	ω_o	Q_{ext}	ω_o	Q_{ext}
412.50	0.958	1.267E-03	0.967	1.362E-03	0.984	2.787E-03	0.992	5.854E-03
442.50	0.959	1.178E-03	0.967	1.267E-03	0.985	2.609E-03	0.993	5.552E-03
490.00	0.959	1.051E-03	0.968	1.128E-03	0.985	2.353E-03	0.993	5.092E-03
510.00	0.959	1.002E-03	0.968	1.076E-03	0.985	2.250E-03	0.993	4.906E-03
560.00	0.961	8.908E-04	0.964	9.581E-04	0.983	2.022E-03	0.992	4.486E-03
620.00	0.961	7.763E-04	0.964	8.357E-04	0.983	1.788E-03	0.992	4.034E-03
665.00	0.958	7.024E-04	0.961	7.566E-04	0.982	1.629E-03	0.992	3.737E-03
681.25	0.957	6.780E-04	0.960	7.305E-04	0.982	1.577E-03	0.992	3.636E-03
708.75	0.954	6.377E-04	0.957	6.873E-04	0.980	1.495E-03	0.991	3.472E-03
753.75	0.948	5.764E-04	0.952	6.228E-04	0.978	1.363E-03	0.990	3.212E-03
761.875	0.947	5.668E-04	0.951	6.110E-04	0.977	1.342E-03	0.990	3.169E-03
778.75	0.944	5.463E-04	0.948	5.889E-04	0.976	1.296E-03	0.990	3.073E-03
865.00	0.931	4.551E-04	0.936	4.920E-04	0.970	1.100E-03	0.987	2.666E-03
885.00	0.928	4.380E-04	0.933	4.736E-04	0.969	1.062E-03	0.987	2.584E-03
900.00	0.926	4.258E-04	0.931	4.604E-04	0.968	1.034E-03	0.986	2.515E-03

Table 10-2: Aerosol optical properties (single scattering albedo and scattering coefficient) at the 15 MERIS wavelengths for maritime model (RH=50, 70, 90, 99%).

OCEANIC (*Shettle and Fenn, 1979*)								
Wavelength	RH=50%		RH=70%		RH=90%		RH=99%	
(nm)	ω_o	Q_{ext}	ω_o	Q_{ext}	ω_o	Q_{ext}	ω_o	Q_{ext}
412.50	0.979	2.481E-03	0.985	3.064E-03	0.995	8.369E-03	0.998	2.656E-02
442.50	0.980	2.400E-03	0.986	2.982E-03	0.995	8.230E-03	0.998	2.635E-02
490.00	0.981	2.287E-03	0.987	2.862E-03	0.996	8.035E-03	0.999	2.603E-02
510.00	0.982	2.244E-03	0.988	2.818E-03	0.996	7.955E-03	0.999	2.590E-02
560.00	0.984	2.143E-03	0.987	2.715E-03	0.996	7.788E-03	0.999	2.563E-02
620.00	0.985	2.037E-03	0.989	2.607E-03	0.996	7.616E-03	0.999	2.535E-02
665.00	0.985	1.969E-03	0.989	2.535E-03	0.996	7.500E-03	0.999	2.518E-02
681.25	0.985	1.945E-03	0.989	2.511E-03	0.996	7.463E-03	0.999	2.513E-02
708.75	0.985	1.906E-03	0.988	2.471E-03	0.996	7.403E-03	0.999	2.503E-02
753.75	0.984	1.845E-03	0.988	2.410E-03	0.996	7.308E-03	0.999	2.490E-02
761.875	0.984	1.837E-03	0.988	2.398E-03	0.996	7.294E-03	0.999	2.488E-02
778.75	0.983	1.816E-03	0.987	2.377E-03	0.996	7.260E-03	0.999	2.483E-02
865.00	0.982	1.720E-03	0.986	2.278E-03	0.995	7.118E-03	0.999	2.465E-02
885.00	0.981	1.701E-03	0.986	2.258E-03	0.995	7.091E-03	0.999	2.462E-02
900.00	0.980	1.687E-03	0.986	2.243E-03	0.995	7.071E-03	0.999	2.459E-02

Table 10-3: Aerosol optical properties (single scattering albedo and scattering coefficient) at the 15 MERIS wavelengths for coastal model (RH=50, 70, 90, 99%).

COASTAL (*Shettle and Fenn, 1979*)								
Wavelength	RH=50%		RH=70%		RH=90%		RH=99%	
(nm)	ω_o	Q_{ext}	ω_o	Q_{ext}	ω_o	Q_{ext}	ω_o	Q_{ext}
412.50	0.972	1.874E-03	0.980	2.213E-03	0.992	5.578E-03	0.997	1.621E-02
442.50	0.973	1.789E-03	0.981	2.124E-03	0.993	5.420E-03	0.997	1.595E-02
490.00	0.974	1.669E-03	0.982	1.995E-03	0.993	5.194E-03	0.998	1.556E-02
510.00	0.975	1.623E-03	0.982	1.947E-03	0.993	5.103E-03	0.998	1.540E-02
560.00	0.977	1.517E-03	0.981	1.837E-03	0.993	4.905E-03	0.998	1.506E-02
620.00	0.978	1.407E-03	0.982	1.721E-03	0.994	4.702E-03	0.998	1.469E-02
665.00	0.978	1.336E-03	0.982	1.646E-03	0.994	4.564E-03	0.998	1.446E-02
681.25	0.978	1.312E-03	0.982	1.621E-03	0.994	4.520E-03	0.998	1.438E-02
708.75	0.977	1.272E-03	0.982	1.579E-03	0.993	4.449E-03	0.998	1.425E-02
753.75	0.975	1.211E-03	0.980	1.516E-03	0.993	4.335E-03	0.998	1.406E-02
761.875	0.975	1.202E-03	0.980	1.505E-03	0.993	4.318E-03	0.998	1.403E-02
778.75	0.974	1.181E-03	0.979	1.483E-03	0.993	4.278E-03	0.998	1.395E-02
865.00	0.971	1.088E-03	0.977	1.385E-03	0.992	4.109E-03	0.997	1.366E-02
885.00	0.970	1.070E-03	0.977	1.366E-03	0.992	4.077E-03	0.997	1.360E-02
900.00	0.969	1.057E-03	0.976	1.352E-03	0.992	4.053E-03	0.997	1.355E-02

Table 10-4: Aerosol optical properties (single scattering albedo and scattering coefficient) at the 15 MERIS wavelengths for dust-like particles (BDS-1, 2 &3).

BLUE-IOP (*Santer and Zagolski, 2010*)						
Wavelength	*IOP-1*		*IOP-2*		*IOP-3*	
(nm)	ω_o	$Q_{ext}\,(m^{-1})$	ω_o	$Q_{ext}\,(m^{-1})$	ω_o	$Q_{ext}\,(m^{-1})$
412.50	0.9798	3.712E-03	0.9794	2.359E-03	0.9785	1.345E-03
442.50	0.9796	3.377E-03	0.9791	2.124E-03	0.9780	1.196E-03
490.00	0.9793	2.916E-03	0.9784	1.806E-03	0.9769	9.991E-04
510.00	0.9791	2.739E-03	0.9781	1.690E-03	0.9765	9.282E-04
560.00	0.9784	2.363E-03	0.9772	1.436E-03	0.9751	7.763E-04
620.00	0.9775	1.984E-03	0.9760	1.190E-03	0.9734	6.326E-04
665.00	0.9768	1.753E-03	0.9749	1.039E-03	0.9719	5.461E-04
681.25	0.9765	1.674E-03	0.9745	9.904E-04	0.9714	5.185E-04
708.75	0.9760	1.556E-03	0.9738	9.143E-04	0.9704	4.757E-04
753.75	0.9751	1.382E-03	0.9726	8.049E-04	0.9688	4.147E-04
761.875	0.9749	1.353E-03	0.9724	7.870E-04	0.9685	4.048E-04
778.75	0.9745	1.295E-03	0.9719	7.512E-04	0.9678	3.850E-04
865.00	0.9726	1.044E-03	0.9694	5.960E-04	0.9643	3.012E-04
885.00	0.9721	9.950E-04	0.9687	5.672E-04	0.9634	2.851E-04
900.00	0.9717	9.599E-04	0.9682	5.460E-04	0.9627	2.738E-04

Table 10-5: Aerosol optical properties (single scattering albedo and scattering coefficient) at the 15 MERIS wavelengths for dust-like particles (BDS-1, 2 &3).

DUST-BDS (*Moulin et al., 2001*)						
Wavelength	*BDS-1*		*BDS-2*		*BDS-3*	
(nm)	ω_o	$Q_{ext}(m^{-1})$	ω_o	$Q_{ext}(m^{-1})$	ω_o	$Q_{ext}(m^{-1})$
412.50	0.861	2.355E-03	0.837	2.552E-03	0.814	2.771E-03
442.50	0.890	2.329E-03	0.864	2.526E-03	0.839	2.745E-03
490.00	0.907	2.281E-03	0.879	2.479E-03	0.853	2.698E-03
510.00	0.914	2.261E-03	0.886	2.458E-03	0.860	2.678E-03
560.00	0.936	2.209E-03	0.907	2.407E-03	0.881	2.627E-03
620.00	0.945	2.144E-03	0.916	2.342E-03	0.889	2.563E-03
665.00	0.951	2.096E-03	0.922	2.295E-03	0.895	2.516E-03
681.25	0.953	2.078E-03	0.924	2.277E-03	0.898	2.499E-03
708.75	0.957	2.049E-03	0.929	2.248E-03	0.903	2.470E-03
753.75	0.963	2.000E-03	0.936	2.200E-03	0.911	2.422E-03
761.875	0.964	1.991E-03	0.937	2.191E-03	0.912	2.413E-03
778.75	0.967	1.974E-03	0.941	2.173E-03	0.917	2.396E-03
865.00	0.986	1.887E-03	0.970	2.087E-03	0.955	2.310E-03
885.00	0.986	1.867E-03	0.970	2.068E-03	0.956	2.291E-03
900.00	0.986	1.852E-03	0.970	2.053E-03	0.956	2.276E-03

Table 10-6: Aerosol optical properties (single scattering albedo and scattering coefficient) at the 15 MERIS wavelengths for dust-like particles (BDW-1, 2 &3).

DUST-BDW (*Moulin et al., 2001*)						
Wavelength	*BDW-1*		*BDW-2*		*BDW-3*	
(nm)	ω_o	$Q_{ext}(m^{-1})$	ω_o	$Q_{ext}(m^{-1})$	ω_o	$Q_{ext}(m^{-1})$
412.50	0.897	2.359E-03	0.871	2.556E-03	0.846	2.774E-03
442.50	0.937	2.333E-03	0.909	2.530E-03	0.884	2.749E-03
490.00	0.946	2.285E-03	0.918	2.482E-03	0.893	2.702E-03
510.00	0.959	2.264E-03	0.932	2.462E-03	0.908	2.682E-03
560.00	0.973	2.212E-03	0.950	2.410E-03	0.929	2.630E-03
620.00	0.981	2.146E-03	0.961	2.345E-03	0.943	2.565E-03
665.00	0.986	2.098E-03	0.970	2.297E-03	0.955	2.518E-03
681.25	0.987	2.081E-03	0.973	2.280E-03	0.959	2.501E-03
708.75	0.989	2.051E-03	0.976	2.250E-03	0.964	2.472E-03
753.75	0.993	2.002E-03	0.983	2.201E-03	0.974	2.423E-03
761.875	0.993	1.993E-03	0.984	2.193E-03	0.975	2.415E-03
778.75	0.994	1.975E-03	0.985	2.175E-03	0.977	2.397E-03
865.00	0.994	1.887E-03	0.985	2.088E-03	0.978	2.311E-03
885.00	0.994	1.867E-03	0.986	2.068E-03	0.978	2.291E-03
900.00	0.994	1.853E-03	0.986	2.053E-03	0.978	2.277E-03

Table 10-7: Aerosol optical properties (single scattering albedo and scattering coefficient) at the 15 MERIS wavelengths for continental model and H2SO4.

MISCELLANEOUS (*WRCP, 1986*)				
Wavelength	*Continental*		*75 % H2SO4 solution*	
(nm)	ω_o	$Q_{ext}(m^{-1})$	ω_o	$Q_{ext}(m^{-1})$
412.50	0.903	7.556E-05	1.000	1.482E-02
442.50	0.902	7.016E-05	1.000	1.399E-02
490.00	0.900	6.257E-05	1.000	1.262E-02
510.00	0.899	5.969E-05	1.000	1.206E-02
560.00	0.892	5.311E-05	1.000	1.076E-02
620.00	0.888	4.623E-05	1.000	9.318E-03
665.00	0.881	4.184E-05	1.000	8.337E-03
681.25	0.879	4.038E-05	1.000	8.017E-03
708.75	0.872	3.796E-05	1.000	7.501E-03
753.75	0.860	3.431E-05	1.000	6.703E-03
761.875	0.858	3.375E-05	1.000	6.572E-03
778.75	0.853	3.256E-05	1.000	6.285E-03
865.00	0.827	2.723E-05	1.000	5.092E-03
885.00	0.821	2.624E-05	1.000	4.836E-03
900.00	0.817	2.553E-05	1.000	4.668E-03

11. Definition of the aerosol assemblages over ocean (ATBD 2.7)

Table 11-1 gives the description of the aerosol assemblages defined for the MERIS atmospheric corrections over waters. The latter results from different mixtures in aerosol components (i.e. desert dust particles, dust-like particles, oceanic particles, rural aerosol mixtures, soot-like particles, water soluble particles, and H_2SO_4) for each of the 3 aerosol layers (boundary, troposphere and stratosphere). Among these 34 assemblages, the first one, defined for a free aerosol both in the troposphere and the stratosphere, is used for the reference atmosphere (see Section 7.11).

Table 11-1: Description of the 34 aerosol assemblages (*iaer*) defined over oceans (4 maritime + 4 coastal + 4 rural assemblages with 4 relative humidities RH, 18 dust assemblages with 3 scale heights and 4 blue assemblages).

iaer	*Model*	*RH*	*Boundary*	*Troposphere*			*Stratosphere*
		(%)	*[0 - 2 km]*	*[2 - 5 km]*	*[5 - 7 km]*	*[7 - 12 km]*	*[12 - 50 km]*
0	MAR-99	99	*Maritime*	-	-	-	-
1	MAR-50	50	*Maritime*	*Continental*	*Continental*	*Continental*	*H2SO4*
2	MAR-70	70	*Maritime*	*Continental*	*Continental*	*Continental*	*H2SO4*
3	MAR-90	90	*Maritime*	*Continental*	*Continental*	*Continental*	*H2SO4*
4	MAR-99	99	*Maritime*	*Continental*	*Continental*	*Continental*	*H2SO4*
5	COA-50	50	*Coastal*	*Continental*	*Continental*	*Continental*	*H2SO4*
6	COA-70	70	*Coastal*	*Continental*	*Continental*	*Continental*	*H2SO4*
7	COA-90	90	*Coastal*	*Continental*	*Continental*	*Continental*	*H2SO4*
8	COA-99	99	*Coastal*	*Continental*	*Continental*	*Continental*	*H2SO4*
9	RUR-50	50	*Rural*	*Continental*	*Continental*	*Continental*	*H2SO4*
10	RUR-70	70	*Rural*	*Continental*	*Continental*	*Continental*	*H2SO4*
11	RUR-90	90	*Rural*	*Continental*	*Continental*	*Continental*	*H2SO4*
12	RUR-99	99	*Rural*	*Continental*	*Continental*	*Continental*	*H2SO4*
13	MAR-BDS1-1	90	*Maritime* *Dust-BDS1*	*Continental* -	*Continental* -	*Continental* -	*H2SO4* -
14	MAR-BDS1-2	90	*Maritime* *Dust-BDS1*	*Continental* *Dust-BDS1*	*Continental* -	*Continental* -	*H2SO4* -
15	MAR-BDS1-3	90	*Maritime* *Dust-BDS1*	*Continental* *Dust-BDS1*	*Continental* *Dust-BDS1*	*Continental* -	*H2SO4* -
16	MAR-BDS2-1	90	*Maritime* *Dust-BDS2*	*Continental* -	*Continental* -	*Continental* -	*H2SO4* -
17	MAR-BDS2-2	90	*Maritime* *Dust-BDS2*	*Continental* *Dust-BDS2*	*Continental* -	*Continental* -	*H2SO4* -
18	MAR-BDS2-3	90	*Maritime* *Dust-BDS2*	*Continental* *Dust-BDS2*	*Continental* *Dust-BDS2*	*Continental* -	*H2SO4* -
19	MAR-BDS3-1	90	*Maritime* *Dust-BDS3*	*Continental* -	*Continental* -	*Continental* -	*H2SO4* -
20	MAR-BDS3-2	90	*Maritime* *Dust-BDS3*	*Continental* *Dust-BDS3*	*Continental* -	*Continental* -	*H2SO4* -
21	MAR-BDS3-3	90	*Maritime* *Dust-BDS3*	*Continental* *Dust-BDS3*	*Continental* *Dust-BDS3*	*Continental* -	*H2SO4* -
22	MAR-BDW1-1	90	*Maritime* *Dust-BDW1*	*Continental* -	*Continental* -	*Continental* -	*H2SO4* -
23	MAR-BDW1-2	90	*Maritime*	*Continental*	*Continental*	*Continental*	*H2SO4*

			Dust-BDW1	*Dust-BDW1*	-	-	-
24	MAR-BDW1-3	90	*Maritime* *Dust-BDW1*	*Continental* *Dust-BDW1*	*Continental* *Dust-BDW1*	*Continental* -	*H2SO4* -
25	MAR-BDW2-1	90	*Maritime* *Dust-BDW2*	*Continental* -	*Continental* -	*Continental* -	*H2SO4* -
26	MAR-BDW2-2	90	*Maritime* *Dust-BDW2*	*Continental* *Dust-BDW2*	*Continental* -	*Continental* -	*H2SO4* -
27	MAR-BDW2-3	90	*Maritime* *Dust-BDW2*	*Continental* *Dust-BDW2*	*Continental* *Dust-BDW2*	*Continental* -	*H2SO4* -
28	MAR-BDW3-1	90	*Maritime* *Dust-BDW3*	*Continental* -	*Continental* -	*Continental* -	*H2SO4* -
29	MAR-BDW3-2	90	*Maritime* *Dust-BDW3*	*Continental* *Dust-BDW3*	*Continental* -	*Continental* -	*H2SO4* -
30	MAR-BDW3-3	90	*Maritime* *Dust-BDW3*	*Continental* *Dust-BDW3*	*Continental* *Dust-BDW3*	*Continental* -	*H2SO4* -
31	BLUE-IOP1	-	*Blue aerosol*	*Blue aerosol*	*Blue aerosol*	*Blue aerosol*	*H2SO4*
32	BLUE–IOP2	-	*Blue aerosol*	*Blue aerosol*	*Blue aerosol*	*Blue aerosol*	*H2SO4*
33	BLUE-IOP3	-	*Blue aerosol*	*Blue aerosol*	*Blue aerosol*	*Blue aerosol*	*H2SO4*

Optical properties (aerosol optical thickness at 550 nm) of each aerosol layers (boundary, dust, troposphere, and stratosphere) are summarized in the Table 11-2.

Table 11-2: Aerosol optical thickness at 550 nm for each of the 4 aerosol layers (i.e., boundary, dust, troposphere, and stratosphere) and for each of the 34 aerosol assemblages (*iaer*).

Aerosols Assemblage			***Boundary Layer***	***Dust Layer***	***Troposphere***	***Stratosphere***
iaer	***Assemblage***	***RH(%)***	$\tau^{a}_{550,bound}$	$\tau^{a}_{550,dust}$	$\tau^{a}_{550,tropo}$	$\tau^{a}_{550,strato}$
0	MAR-99	99	*0.01,0.03,0.1,0.3,0.5,0.8*	*0*	*0*	*0*
1	MAR-50	50	*0.01,0.03,0.1,0.3,0.5,0.8*	*0*	*0.025*	*0.005*
2	MAR-70	70	*0.01,0.03,0.1,0.3,0.5,0.8*	*0*	*0.025*	*0.005*
3	MAR-90	90	*0.01,0.03,0.1,0.3,0.5,0.8*	*0*	*0.025*	*0.005*
4	MAR-99	99	*0.01,0.03,0.1,0.3,0.5,0.8*	*0*	*0.025*	*0.005*
5	COA-50	50	*0.01,0.03,0.1,0.3,0.5,0.8*	*0*	*0.025*	*0.005*
6	COA-70	70	*0.01,0.03,0.1,0.3,0.5,0.8*	*0*	*0.025*	*0.005*
7	COA-90	90	*0.01,0.03,0.1,0.3,0.5,0.8*	*0*	*0.025*	*0.005*
8	COA-99	99	*0.01,0.03,0.1,0.3,0.5,0.8*	*0*	*0.025*	*0.005*
9	RUR-50	50	*0.01,0.03,0.1,0.3,0.5,0.8*	*0*	*0.025*	*0.005*
10	RUR-70	70	*0.01,0.03,0.1,0.3,0.5,0.8*	*0*	*0.025*	*0.005*
11	RUR-90	90	*0.01,0.03,0.1,0.3,0.5,0.8*	*0*	*0.025*	*0.005*
12	RUR-99	99	*0.01,0.03,0.1,0.3,0.5,0.8*	*0*	*0.025*	*0.005*
13	MAR-BDS1-1	90	*0.05,0.05,0.05,0.05,0.05,0.05*	*0.01,0.05,0.2,0.5,0.8,2*	*0.025*	*0.005*
14	MAR-BDS1-2	90	*0.05,0.05,0.05,0.05,0.05,0.05*	*0.01,0.05,0.2,0.5,0.8,2*	*0.025*	*0.005*
15	MAR-BDS1-3	90	*0.05,0.05,0.05,0.05,0.05,0.05*	*0.01,0.05,0.2,0.5,0.8,2*	*0.025*	*0.005*
16	MAR-BDS2-1	90	*0.05,0.05,0.05,0.05,0.05,0.05*	*0.01,0.05,0.2,0.5,0.8,2*	*0.025*	*0.005*
17	MAR-BDS2-2	90	*0.05,0.05,0.05,0.05,0.05,0.05*	*0.01,0.05,0.2,0.5,0.8,2*	*0.025*	*0.005*
18	MAR-BDS2-3	90	*0.05,0.05,0.05,0.05,0.05,0.05*	*0.01,0.05,0.2,0.5,0.8,2*	*0.025*	*0.005*
19	MAR-BDS3-1	90	*0.05,0.05,0.05,0.05,0.05,0.05*	*0.01,0.05,0.2,0.5,0.8,2*	*0.025*	*0.005*

Aerosols Assemblage			*Boundary Layer*	*Dust Layer*	*Troposphere*	*Stratosphere*
iaer	***Assemblage***	***RH(%)***	$\tau^{a}_{550,bound}$	$\tau^{a}_{550,dust}$	$\tau^{a}_{550,tropo}$	$\tau^{a}_{550,strato}$
20	MAR-BDS3-2	90	*0.05,0.05,0.05,0.05,0.05,0.05*	*0.01,0.05,0.2,0.5,0.8,2*	*0.025*	*0.005*
21	MAR-BDS3-3	90	*0.05,0.05,0.05,0.05,0.05,0.05*	*0.01,0.05,0.2,0.5,0.8,2*	*0.025*	*0.005*
22	MAR-BDW1-1	90	*0.05,0.05,0.05,0.05,0.05,0.05*	*0.01,0.05,0.2,0.5,0.8,2*	*0.025*	*0.005*
23	MAR-BDW1-2	90	*0.05,0.05,0.05,0.05,0.05,0.05*	*0.01,0.05,0.2,0.5,0.8,2*	*0.025*	*0.005*
24	MAR-BDW1-3	90	*0.05,0.05,0.05,0.05,0.05,0.05*	*0.01,0.05,0.2,0.5,0.8,2*	*0.025*	*0.005*
25	MAR-BDW2-1	90	*0.05,0.05,0.05,0.05,0.05,0.05*	*0.01,0.05,0.2,0.5,0.8,2*	*0.025*	*0.005*
26	MAR-BDW2-2	90	*0.05,0.05,0.05,0.05,0.05,0.05*	*0.01,0.05,0.2,0.5,0.8,2*	*0.025*	*0.005*
27	MAR-BDW2-3	90	*0.05,0.05,0.05,0.05,0.05,0.05*	*0.01,0.05,0.2,0.5,0.8,2*	*0.025*	*0.005*
28	MAR-BDW3-1	90	*0.05,0.05,0.05,0.05,0.05,0.05*	*0.01,0.05,0.2,0.5,0.8,2*	*0.025*	*0.005*
29	MAR-BDW3-2	90	*0.05,0.05,0.05,0.05,0.05,0.05*	*0.01,0.05,0.2,0.5,0.8,2*	*0.025*	*0.005*
30	MAR-BDW3-3	90	*0.05,0.05,0.05,0.05,0.05,0.05*	*0.01,0.05,0.2,0.5,0.8,2*	*0.025*	*0.005*
31	BLUE-IOP1	-	*0.01,0.03,0.1,0.3,0.5,0.8*	*0*	*0.025*	*0.005*
32	BLUE-IOP2	-	*0.01,0.03,0.1,0.3,0.5,0.8*	*0*	*0.025*	*0.005*
33	BLUE-IOP3	-	*0.01,0.03,0.1,0.3,0.5,0.8*	*0*	*0.025*	*0.005*

12. Aerosol phase functions

12.1 OCEAN MODELS

Figure 12-1 to Figure 12-7 below display the scattering phase functions for the 23 ocean models in the 15 MERIS bands; CONTI, 4 COA, 4 MAR, 4 RUR, H2SO4, 3 BDS, 3 BDW, and 3 BLU.

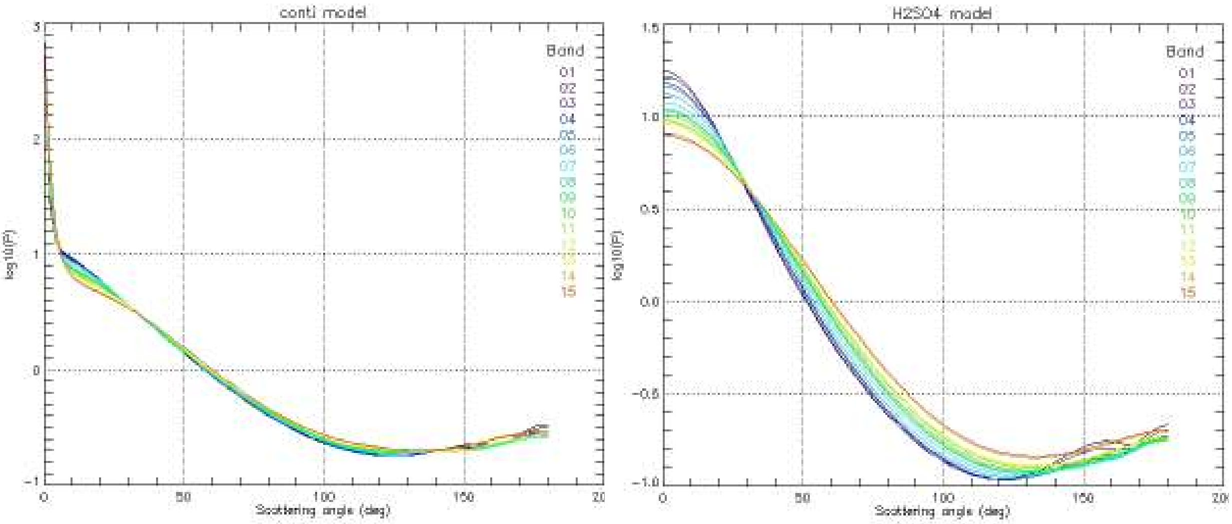

Figure 12-1: Scattering phase functions for the Conti and H2SO4 models in the 15 MERIS bands.

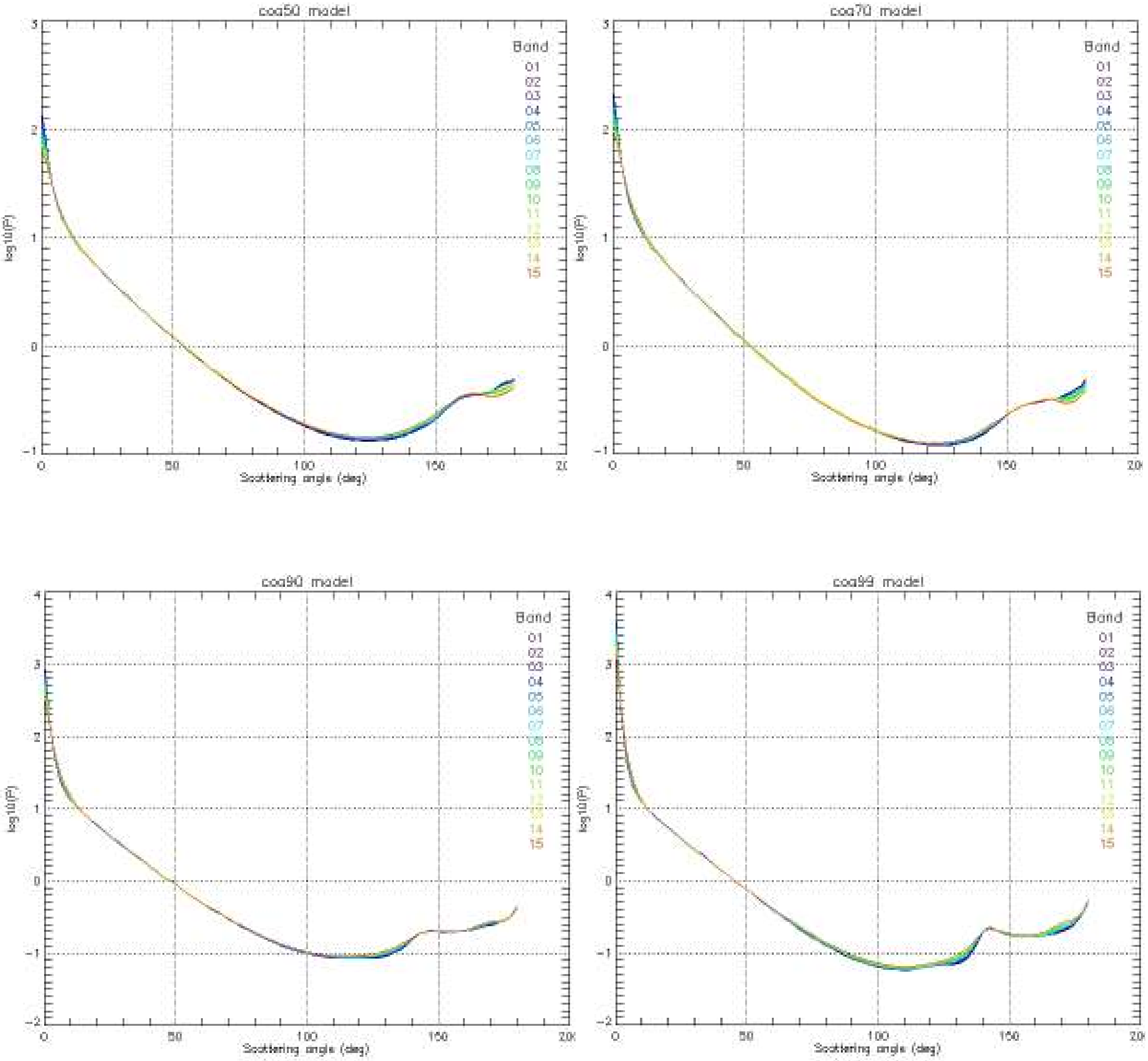

Figure 12-2: Scattering phase functions for the COA models in the 15 MERIS bands.

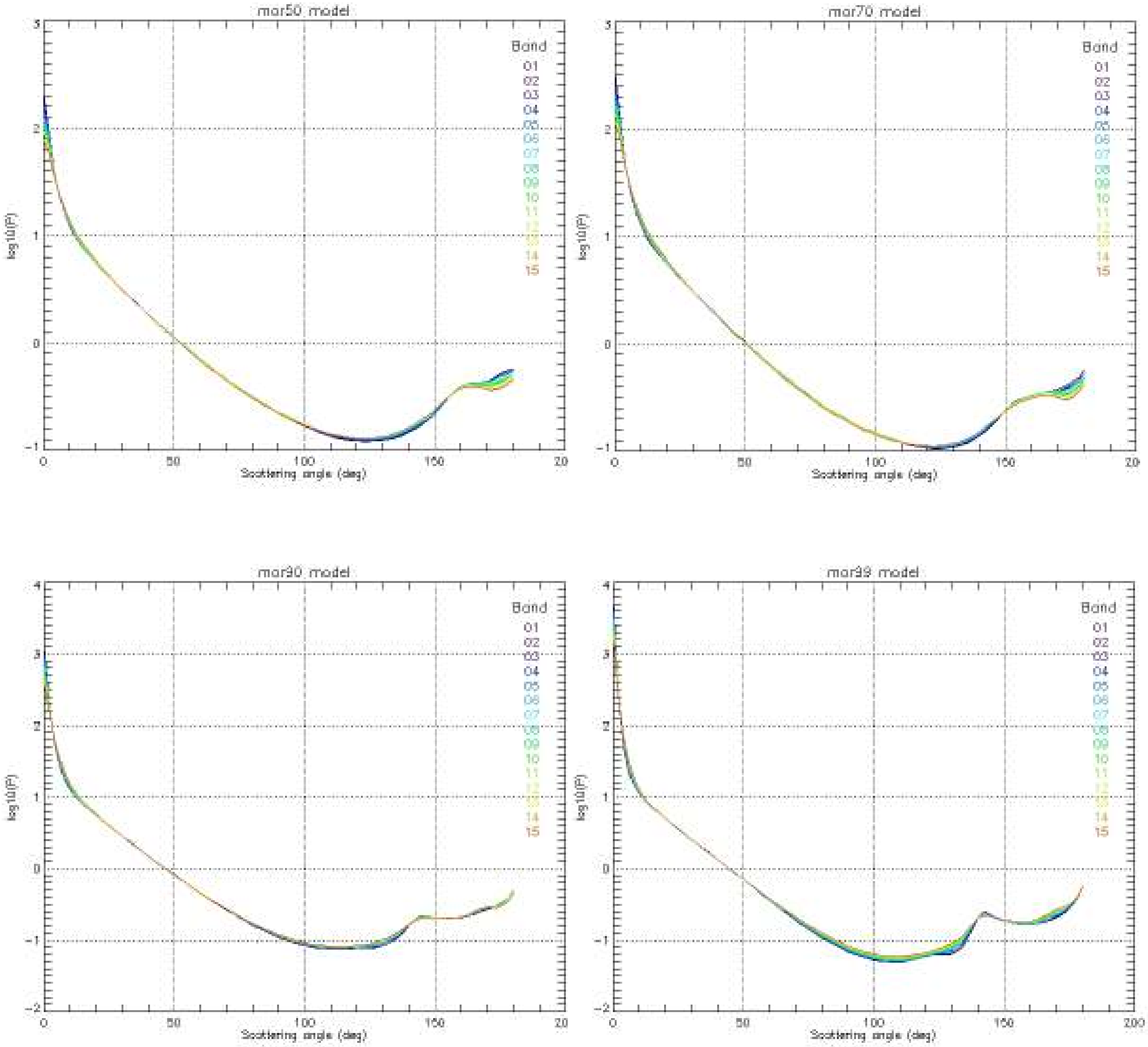

Figure 12-3: Scattering phase functions for the MAR models in the 15 MERIS bands.

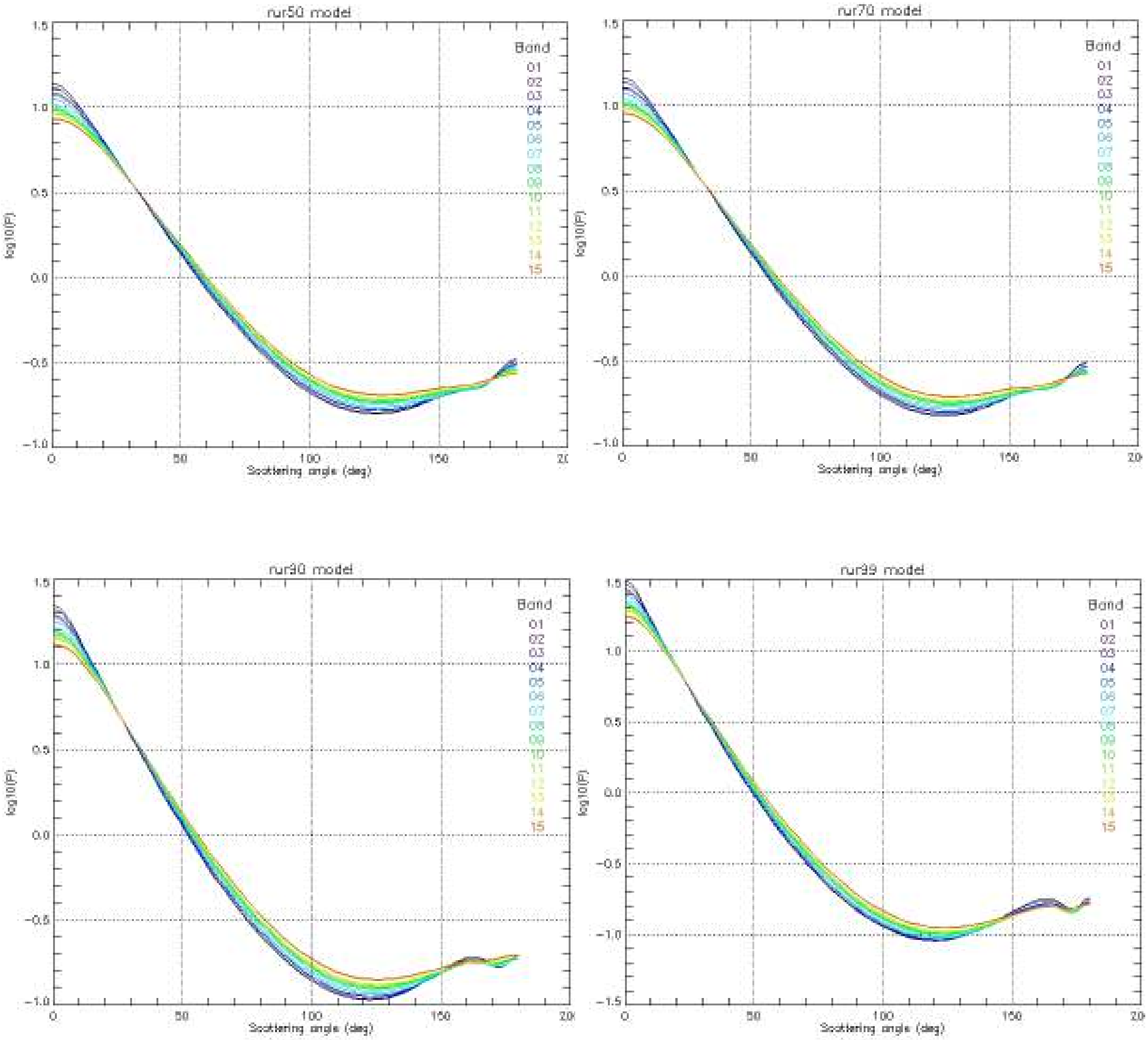

Figure 12-4: Scattering phase functions for the RUR models in the 15 MERIS bands.

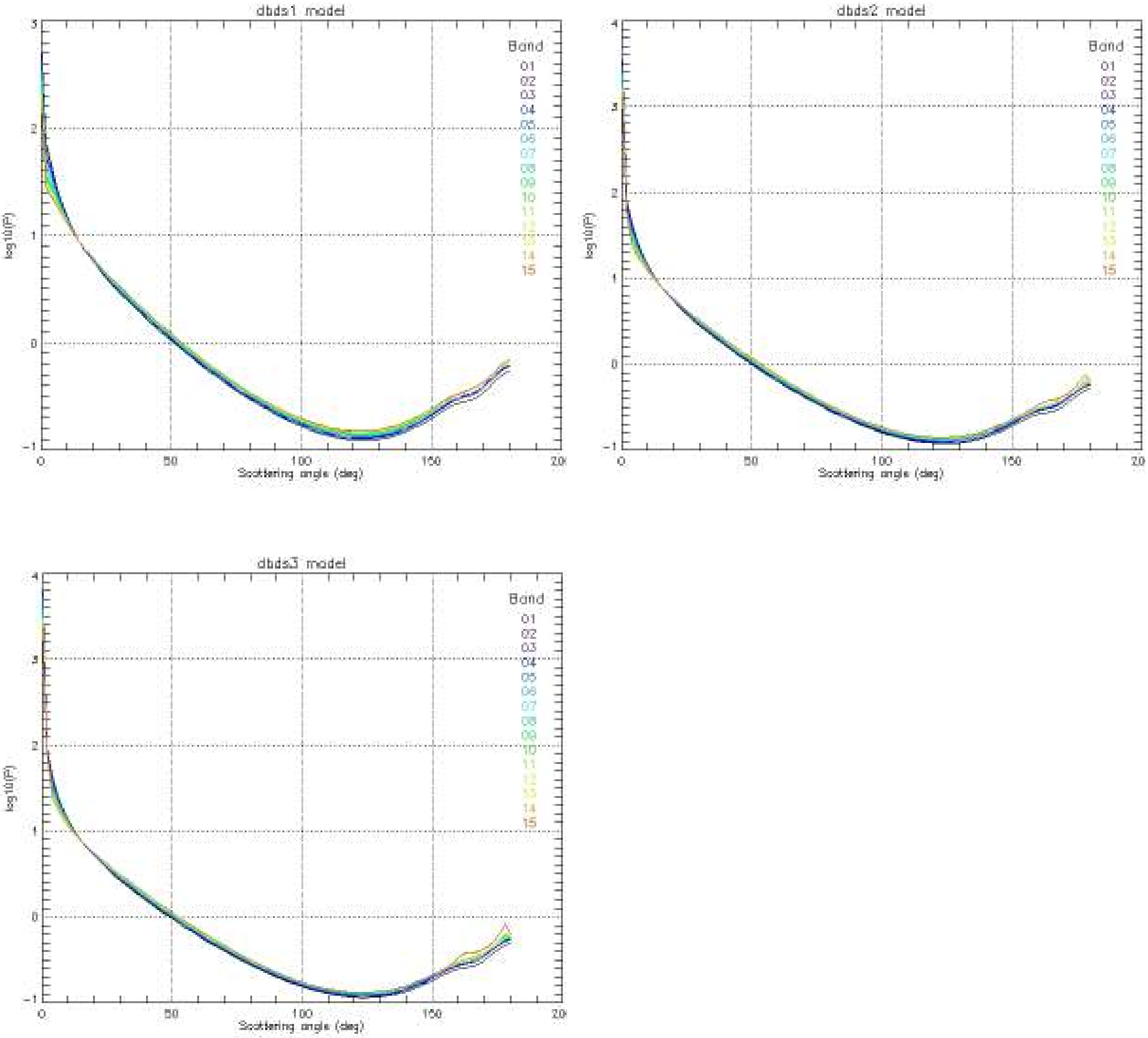

Figure 12-5: Scattering phase functions for the DBDS models in the 15 MERIS bands.

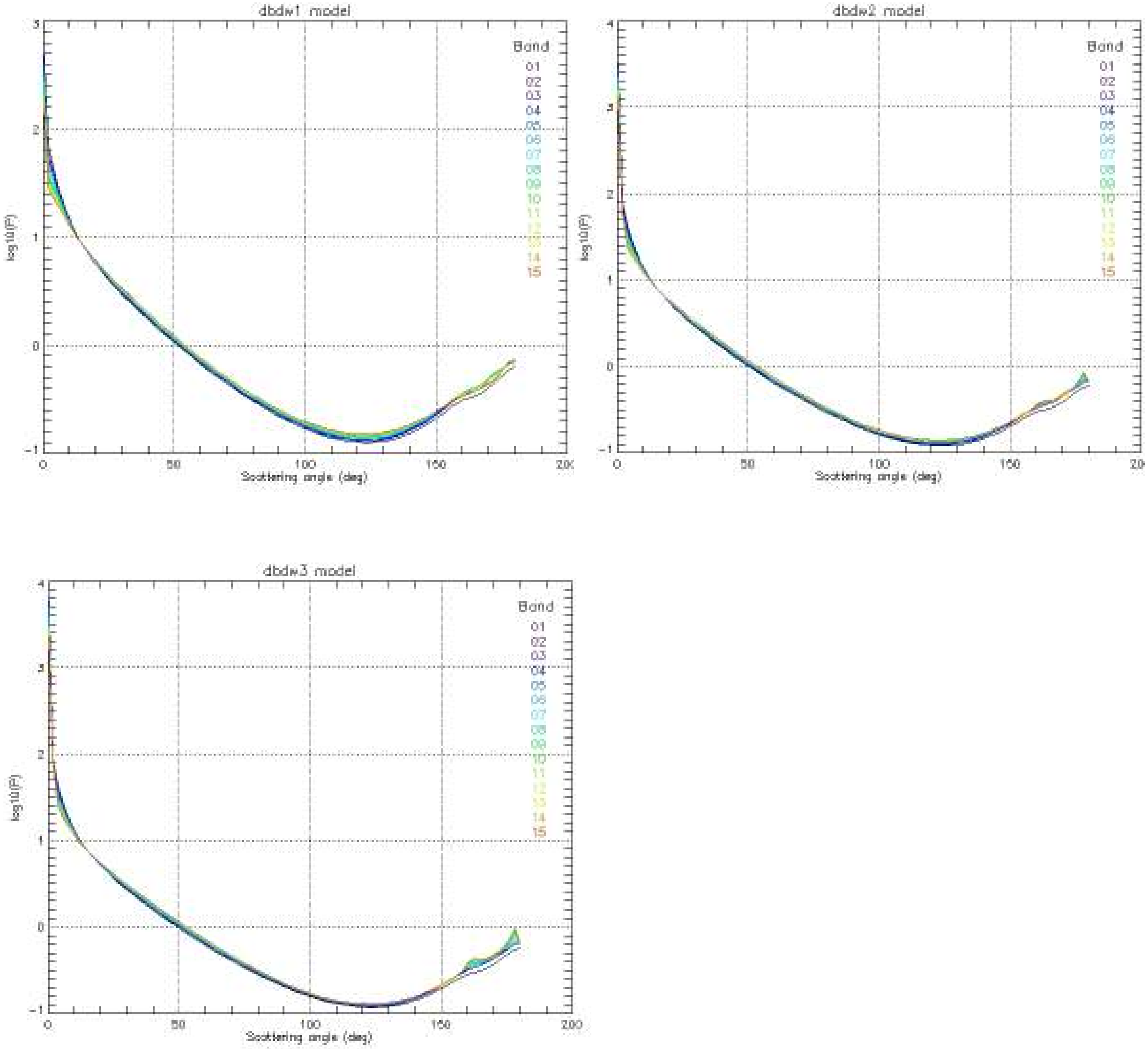

Figure 12-6: Scattering phase functions for the DBDW models in the 15 MERIS bands.

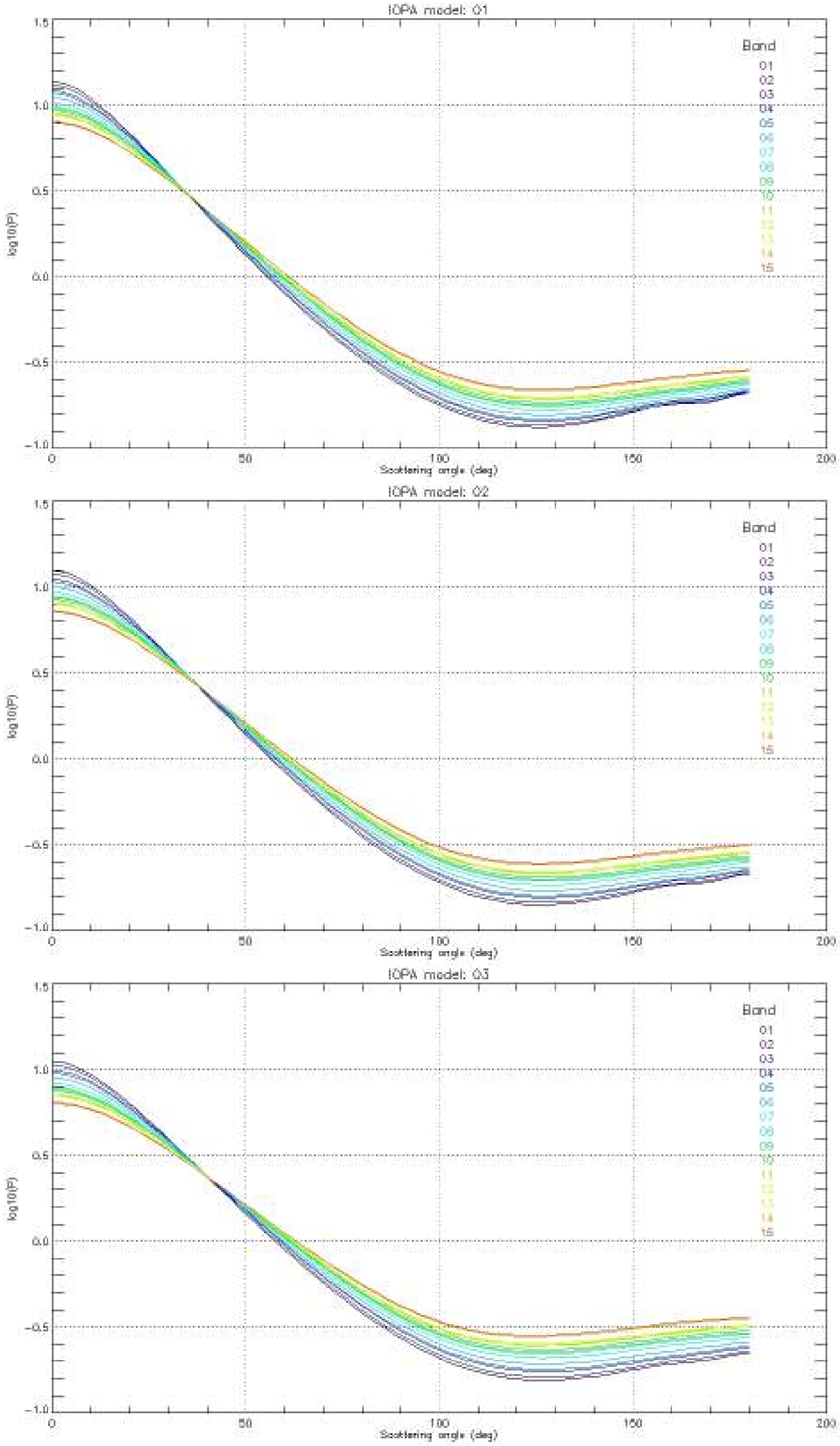

Figure 12-7: Scattering phase functions for the BLU-IOP models in the 15 MERIS bands

13. Spectral dependence of the aerosol optical thickness

13.1 – OCEAN-AEROSOLS

For the 34 aerosol assemblages listed in Table 11-1, the spectral dependence of the optical thickness is tabulated at 13 MERIS wavelengths (2 strongly absorbing bands being discarded here, *i.e.*, band#11 for O_2 absorption and band#15 for H_2O absorption) for a set of 6 aerosol optical thicknesses at 550 nm ($\tau_a(550)$) in Table 13-1.

Table 13-1: Spectral dependence of AOT for assemblages #0 through to #33

Spectral dependence of optical thickness for assemblage #0					
λ(nm) \ τ_a(550)	***0.03***	***0.10***	***0.30***	***0.50***	***2.00***
412.50	0.03102	0.10339	0.31017	0.51694	2.06777
442.50	0.03077	0.10256	0.30769	0.51281	2.05125
490.00	0.03040	0.10133	0.30399	0.50664	2.02657
510.00	0.03025	0.10082	0.30247	0.50411	2.01644
560.00	0.02994	0.09979	0.29936	0.49894	1.99576
620.00	0.02961	0.09870	0.29610	0.49349	1.97397
665.00	0.02941	0.09804	0.29413	0.49022	1.96086
681.25	0.02935	0.09782	0.29347	0.48911	1.95646
708.75	0.02924	0.09746	0.29238	0.48729	1.94918
778.75	0.02900	0.09666	0.28999	0.48331	1.93324
865.00	0.02879	0.09597	0.28791	0.47986	1.91943
Spectral dependence of optical thickness for assemblage #1					
λ(nm) \ τ_a(550)	***0.03***	***0.10***	***0.30***	***0.50***	***2.00***
412.50	0.07593	0.15627	0.38582	0.61537	2.33700
442.50	0.07194	0.14967	0.37176	0.59384	2.25949
490.00	0.06625	0.14031	0.35189	0.56348	2.15036
510.00	0.06408	0.13674	0.34433	0.55193	2.10890
560.00	0.05906	0.12846	0.32673	0.52500	2.01203
620.00	0.05377	0.11974	0.30823	0.49671	1.91036
665.00	0.05036	0.11411	0.29626	0.47841	1.84452
681.25	0.04922	0.11221	0.29220	0.47218	1.82208
708.75	0.04733	0.10905	0.28542	0.46180	1.78457
778.75	0.04303	0.10182	0.26980	0.43778	1.69763
865.00	0.03871	0.09441	0.25355	0.41269	1.60626

Table 12-1 Continued: Spectral dependence of AOT for assemblages #2, 3 & 4

Spectral dependence of optical thickness for assemblage #2

λ(nm) \ τ_a(550)	***0.03***	***0.10***	***0.30***	***0.50***	***2.00***
412.50	0.07510	0.15353	0.37759	0.60165	2.28213
442.50	0.07134	0.14765	0.36570	0.58375	2.21911
490.00	0.06591	0.13915	0.34842	0.55768	2.12719
510.00	0.06385	0.13597	0.34203	0.54809	2.09353
560.00	0.05910	0.12860	0.32716	0.52572	2.01491
620.00	0.05409	0.12081	0.31142	0.50203	1.93163
665.00	0.05084	0.11572	0.30109	0.48647	1.87677
681.25	0.04977	0.11404	0.29769	0.48134	1.85871
708.75	0.04797	0.11121	0.29190	0.47259	1.82776
778.75	0.04391	0.10474	0.27854	0.45235	1.75590
865.00	0.03982	0.09812	0.26469	0.43125	1.68050

Spectral dependence of optical thickness for assemblage #3

λ(nm) \ τ_a(550)	***0.03***	***0.10***	***0.30***	***0.50***	***2.00***
412.50	0.07361	0.14856	0.36269	0.57682	2.18282
442.50	0.07022	0.14392	0.35451	0.56510	2.14450
490.00	0.06535	0.13731	0.34290	0.54850	2.09044
510.00	0.06347	0.13471	0.33827	0.54182	2.06846
560.00	0.05921	0.12895	0.32821	0.52748	2.02195
620.00	0.05473	0.12294	0.31782	0.51270	1.97429
665.00	0.05182	0.11899	0.31090	0.50281	1.94213
681.25	0.05086	0.11770	0.30865	0.49961	1.93179
708.75	0.04928	0.11558	0.30499	0.49440	1.91499
778.75	0.04570	0.11071	0.29647	0.48223	1.87541
865.00	0.04216	0.10590	0.28802	0.47015	1.83607

Spectral dependence of optical thickness for assemblage #4

λ(nm) \ τ_a(550)	***0.03***	***0.10***	***0.30***	***0.50***	***2.00***
412.50	0.07251	0.14488	0.35166	0.55844	2.10926
442.50	0.06940	0.14119	0.34632	0.55144	2.08988
490.00	0.06491	0.13584	0.33850	0.54116	2.06109
510.00	0.06318	0.13376	0.33540	0.53705	2.04938
560.00	0.05926	0.12911	0.32868	0.52826	2.02508
620.00	0.05511	0.12420	0.32159	0.51899	1.99947
665.00	0.05245	0.12108	0.31716	0.51325	1.98390
681.25	0.05156	0.12004	0.31569	0.51133	1.97867
708.75	0.05011	0.11833	0.31325	0.50816	1.97005
778.75	0.04683	0.11450	0.30782	0.50115	1.95108
865.00	0.04363	0.11081	0.30275	0.49470	1.93426

Table 12-1 Continued: Spectral dependence of AOT for assemblages #5, 6 & 7

Spectral dependence of optical thickness for assemblage #5					
λ(nm) \ τ_a(550)	***0.03***	***0.10***	***0.30***	***0.50***	***2.00***
412.50	0.07808	0.16345	0.40735	0.65126	2.48055
442.50	0.07356	0.15505	0.38791	0.62076	2.36714
490.00	0.06709	0.14311	0.36031	0.57750	2.20645
510.00	0.06462	0.13855	0.34976	0.56097	2.14508
560.00	0.05893	0.12803	0.32545	0.52286	2.00349
620.00	0.05296	0.11704	0.30013	0.48321	1.85634
665.00	0.04911	0.10995	0.28377	0.45759	1.76124
681.25	0.04782	0.10757	0.27829	0.44900	1.72933
708.75	0.04570	0.10364	0.26919	0.43473	1.67633
778.75	0.04089	0.09468	0.24838	0.40208	1.55480
865.00	0.03607	0.08561	0.22715	0.36870	1.43026
Spectral dependence of optical thickness for assemblage #6					
λ(nm) \ τ_a(550)	***0.03***	***0.10***	***0.30***	***0.50***	***2.00***
412.50	0.07723	0.16062	0.39888	0.63713	2.42403
442.50	0.07293	0.15298	0.38167	0.61036	2.32557
490.00	0.06673	0.14191	0.35669	0.57147	2.18235
510.00	0.06438	0.13774	0.34736	0.55697	2.12907
560.00	0.05898	0.12819	0.32592	0.52365	2.00663
620.00	0.05329	0.11815	0.30344	0.48873	1.87841
665.00	0.04961	0.11162	0.28880	0.46598	1.79483
681.25	0.04839	0.10947	0.28397	0.45847	1.76725
708.75	0.04637	0.10587	0.27586	0.44586	1.72083
778.75	0.04178	0.09765	0.25729	0.41693	1.61422
865.00	0.03720	0.08939	0.23848	0.38757	1.50575
Spectral dependence of optical thickness for assemblage #7					
λ(nm) \ τ_a(550)	***0.03***	***0.10***	***0.30***	***0.50***	***2.00***
412.50	0.07537	0.15440	0.38021	0.60603	2.29962
442.50	0.07154	0.14832	0.36772	0.58711	2.23256
490.00	0.06605	0.13965	0.34991	0.56018	2.13716
510.00	0.06392	0.13622	0.34279	0.54936	2.09864
560.00	0.05910	0.12860	0.32716	0.52571	2.01490
620.00	0.05405	0.12067	0.31102	0.50137	1.92899
665.00	0.05075	0.11542	0.30020	0.48498	1.87081
681.25	0.04967	0.11371	0.29669	0.47967	1.85203
708.75	0.04788	0.11091	0.29101	0.47110	1.82177
778.75	0.04381	0.10442	0.27760	0.45078	1.74962
865.00	0.03979	0.09801	0.26435	0.43069	1.67823

Table 12-1 Continued: Spectral dependence of AOT for assemblages #8, 9 & 10

Spectral dependence of optical thickness for assemblage #8					
***λ(nm)* \ τ_a(550)**	***0.03***	***0.10***	***0.30***	***0.50***	***2.00***
412.50	0.07364	0.14863	0.36291	0.57719	2.18426
442.50	0.07026	0.14407	0.35494	0.56582	2.14741
490.00	0.06538	0.13739	0.34313	0.54887	2.09194
510.00	0.06349	0.13476	0.33842	0.54207	2.06947
560.00	0.05919	0.12888	0.32800	0.52712	2.02053
620.00	0.05464	0.12264	0.31693	0.51121	1.96834
665.00	0.05172	0.11864	0.30984	0.50105	1.93508
681.25	0.05074	0.11730	0.30746	0.49762	1.92383
708.75	0.04914	0.11510	0.30356	0.49202	1.90547
778.75	0.04550	0.11007	0.29454	0.47900	1.86251
865.00	0.04193	0.10514	0.28575	0.46636	1.82090
Spectral dependence of optical thickness for assemblage #9					
***λ(nm)* \ τ_a(550)**	***0.03***	***0.10***	***0.30***	***0.50***	***2.00***
412.50	0.08319	0.18046	0.45840	0.73634	2.82089
442.50	0.07738	0.16782	0.42619	0.68456	2.62238
490.00	0.06909	0.14976	0.38025	0.61074	2.33943
510.00	0.06591	0.14283	0.36262	0.58241	2.23084
560.00	0.05863	0.12702	0.32241	0.51780	1.98324
620.00	0.05104	0.11064	0.28091	0.45119	1.72826
665.00	0.04615	0.10007	0.25415	0.40823	1.56380
681.25	0.04453	0.09658	0.24530	0.39403	1.50946
708.75	0.04185	0.09081	0.23070	0.37058	1.41971
778.75	0.03581	0.07775	0.19759	0.31743	1.21620
865.00	0.02981	0.06475	0.16457	0.26438	1.01302
Spectral dependence of optical thickness for assemblage #10					
***λ(nm)* \ τ_a(550)**	***0.03***	***0.10***	***0.30***	***0.50***	***2.00***
412.50	0.08317	0.18041	0.45824	0.73608	2.81983
442.50	0.07739	0.16782	0.42621	0.68459	2.62249
490.00	0.06904	0.14960	0.37977	0.60994	2.33620
510.00	0.06587	0.14270	0.36223	0.58175	2.22818
560.00	0.05863	0.12703	0.32245	0.51788	1.98354
620.00	0.05107	0.11072	0.28117	0.45162	1.72997
665.00	0.04618	0.10020	0.25452	0.40885	1.56629
681.25	0.04457	0.09671	0.24571	0.39470	1.51214
708.75	0.04190	0.09096	0.23113	0.37130	1.42259
778.75	0.03585	0.07790	0.19802	0.31814	1.21905
865.00	0.02989	0.06502	0.16537	0.26572	1.01837

Table 12-1 Continued: Spectral dependence of AOT for assemblages #11, 12 & 13

Spectral dependence of optical thickness for assemblage #11					
***λ(nm)* \ τ_a(550)**	***0.03***	***0.10***	***0.30***	***0.50***	***2.00***
412.50	0.08200	0.17651	0.44655	0.71659	2.74188
442.50	0.07654	0.16500	0.41773	0.67046	2.56597
490.00	0.06871	0.14849	0.37644	0.60439	2.31403
510.00	0.06564	0.14194	0.35993	0.57793	2.21289
560.00	0.05870	0.12726	0.32315	0.51904	1.98820
620.00	0.05148	0.11210	0.28529	0.45849	1.75746
665.00	0.04670	0.10192	0.25969	0.41746	1.60074
681.25	0.04514	0.09861	0.25139	0.40418	1.55005
708.75	0.04259	0.09327	0.23806	0.38286	1.46882
778.75	0.03667	0.08061	0.20616	0.33171	1.27333
865.00	0.03083	0.06813	0.17470	0.28128	1.08059
Spectral dependence of optical thickness for assemblage #12					
***λ(nm)* \ τ_a(550)**	***0.03***	***0.10***	***0.30***	***0.50***	***2.00***
412.50	0.07997	0.16974	0.42622	0.68270	2.60632
442.50	0.07512	0.16025	0.40351	0.64676	2.47115
490.00	0.06798	0.14607	0.36917	0.59228	2.26557
510.00	0.06518	0.14042	0.35537	0.57033	2.18250
560.00	0.05880	0.12760	0.32416	0.52072	1.99494
620.00	0.05201	0.11388	0.29065	0.46742	1.79318
665.00	0.04760	0.10490	0.26863	0.43237	1.66036
681.25	0.04611	0.10187	0.26117	0.42047	1.61523
708.75	0.04369	0.09693	0.24905	0.40117	1.54206
778.75	0.03803	0.08515	0.21977	0.35440	1.36410
865.00	0.03236	0.07325	0.19006	0.30687	1.18297
Spectral dependence of optical thickness for assemblage #13					
***λ(nm)* \ τ_a(550)**	***0.03***	***0.10***	***0.30***	***0.50***	***2.00***
412.50	0.11332	0.27248	0.59079	0.90910	2.18235
442.50	0.11146	0.26884	0.58359	0.89834	2.15734
490.00	0.10852	0.26267	0.57099	0.87930	2.11255
510.00	0.10729	0.26006	0.56560	0.87114	2.09330
560.00	0.10446	0.25374	0.55230	0.85086	2.04510
620.00	0.10124	0.24609	0.53579	0.82550	1.98431
665.00	0.09897	0.24058	0.52380	0.80703	1.93991
681.25	0.09819	0.23863	0.51951	0.80039	1.92390
708.75	0.09691	0.23534	0.51221	0.78908	1.89656
778.75	0.09375	0.22711	0.49384	0.76056	1.82745
865.00	0.09035	0.21785	0.47286	0.72787	1.74790

Table 12-1 Continued: Spectral dependence of AOT for assemblages #14, 15 & 16

Spectral dependence of optical thickness for assemblage #14					
λ*(nm)* **** τ_a**(550)**	***0.03***	***0.10***	***0.30***	***0.50***	***2.00***
412.50	0.11332	0.27248	0.59079	0.90910	2.18235
442.50	0.11146	0.26884	0.58359	0.89834	2.15734
490.00	0.10852	0.26267	0.57099	0.87930	2.11255
510.00	0.10729	0.26006	0.56560	0.87114	2.09330
560.00	0.10446	0.25374	0.55230	0.85086	2.04510
620.00	0.10124	0.24609	0.53579	0.82550	1.98431
665.00	0.09897	0.24058	0.52380	0.80703	1.93991
681.25	0.09819	0.23863	0.51951	0.80039	1.92390
708.75	0.09691	0.23534	0.51221	0.78908	1.89656
778.75	0.09375	0.22711	0.49384	0.76056	1.82745
865.00	0.09035	0.21785	0.47286	0.72787	1.74790
Spectral dependence of optical thickness for assemblage #15					
λ*(nm)* **** τ_a**(550)**	***0.03***	***0.10***	***0.30***	***0.50***	***2.00***
412.50	0.11332	0.27248	0.59079	0.90910	2.18235
442.50	0.11146	0.26884	0.58359	0.89834	2.15734
490.00	0.10852	0.26267	0.57099	0.87930	2.11255
510.00	0.10729	0.26006	0.56560	0.87114	2.09330
560.00	0.10446	0.25374	0.55230	0.85086	2.04510
620.00	0.10124	0.24609	0.53579	0.82550	1.98431
665.00	0.09897	0.24058	0.52380	0.80703	1.93991
681.25	0.09819	0.23863	0.51951	0.80039	1.92390
708.75	0.09691	0.23534	0.51221	0.78908	1.89656
778.75	0.09375	0.22711	0.49384	0.76056	1.82745
865.00	0.09035	0.21785	0.47286	0.72787	1.74790
Spectral dependence of optical thickness for assemblage #16					
λ*(nm)* **** τ_a**(550)**	***0.03***	***0.10***	***0.30***	***0.50***	***2.00***
412.50	0.11304	0.27137	0.58803	0.90469	2.17133
442.50	0.11124	0.26795	0.58138	0.89480	2.14850
490.00	0.10839	0.26218	0.56974	0.87731	2.10758
510.00	0.10721	0.25973	0.56477	0.86981	2.08998
560.00	0.10448	0.25383	0.55252	0.85120	2.04595
620.00	0.10139	0.24670	0.53732	0.82794	1.99042
665.00	0.09922	0.24158	0.52629	0.81100	1.94986
681.25	0.09848	0.23977	0.52234	0.80492	1.93523
708.75	0.09725	0.23671	0.51564	0.79456	1.91026
778.75	0.09424	0.22908	0.49876	0.76843	1.84714
865.00	0.09101	0.22051	0.47951	0.73851	1.77452

Table 12-1 Continued: Spectral dependence of AOT for assemblages #17, 18 & 19

Spectral dependence of optical thickness for assemblage #17					
λ(nm) \ τ_a(550)	***0.03***	***0.10***	***0.30***	***0.50***	***2.00***
412.50	0.11304	0.27137	0.58803	0.90469	2.17133
442.50	0.11124	0.26795	0.58138	0.89480	2.14850
490.00	0.10839	0.26218	0.56974	0.87731	2.10758
510.00	0.10721	0.25973	0.56477	0.86981	2.08998
560.00	0.10448	0.25383	0.55252	0.85120	2.04595
620.00	0.10139	0.24670	0.53732	0.82794	1.99042
665.00	0.09922	0.24158	0.52629	0.81100	1.94986
681.25	0.09848	0.23977	0.52234	0.80492	1.93523
708.75	0.09725	0.23671	0.51564	0.79456	1.91026
778.75	0.09424	0.22908	0.49876	0.76843	1.84714
865.00	0.09101	0.22051	0.47951	0.73851	1.77452

Spectral dependence of optical thickness for assemblage #18					
λ(nm) \ τ_a(550)	***0.03***	***0.10***	***0.30***	***0.50***	***2.00***
412.50	0.11304	0.27137	0.58803	0.90469	2.17133
442.50	0.11124	0.26795	0.58138	0.89480	2.14850
490.00	0.10839	0.26218	0.56974	0.87731	2.10758
510.00	0.10721	0.25973	0.56477	0.86981	2.08998
560.00	0.10448	0.25383	0.55252	0.85120	2.04595
620.00	0.10139	0.24670	0.53732	0.82794	1.99042
665.00	0.09922	0.24158	0.52629	0.81100	1.94986
681.25	0.09848	0.23977	0.52234	0.80492	1.93523
708.75	0.09725	0.23671	0.51564	0.79456	1.91026
778.75	0.09424	0.22908	0.49876	0.76843	1.84714
865.00	0.09101	0.22051	0.47951	0.73851	1.77452

Spectral dependence of optical thickness for assemblage #19					
λ(nm) \ τ_a(550)	***0.03***	***0.10***	***0.30***	***0.50***	***2.00***
412.50	0.11279	0.27034	0.58546	0.90057	2.16104
442.50	0.11103	0.26712	0.57931	0.89150	2.14024
490.00	0.10828	0.26171	0.56858	0.87545	2.10293
510.00	0.10713	0.25942	0.56400	0.86858	2.08689
560.00	0.10450	0.25391	0.55272	0.85152	2.04675
620.00	0.10153	0.24727	0.53875	0.83022	1.99612
665.00	0.09945	0.24250	0.52861	0.81472	1.95916
681.25	0.09874	0.24083	0.52499	0.80916	1.94583
708.75	0.09757	0.23799	0.51884	0.79968	1.92307
778.75	0.09470	0.23092	0.50336	0.77580	1.86555
865.00	0.09163	0.22300	0.48574	0.74847	1.79941

Table 12-1 Continued: Spectral dependence of AOT for assemblages #20, 21 & 22

Spectral dependence of optical thickness for assemblage #20

***λ(nm)* \ τ_a(550)**	***0.03***	***0.10***	***0.30***	***0.50***	***2.00***
412.50	0.11279	0.27034	0.58546	0.90057	2.16104
442.50	0.11103	0.26712	0.57931	0.89150	2.14024
490.00	0.10828	0.26171	0.56858	0.87545	2.10293
510.00	0.10713	0.25942	0.56400	0.86858	2.08689
560.00	0.10450	0.25391	0.55272	0.85152	2.04675
620.00	0.10153	0.24727	0.53875	0.83022	1.99612
665.00	0.09945	0.24250	0.52861	0.81472	1.95916
681.25	0.09874	0.24083	0.52499	0.80916	1.94583
708.75	0.09757	0.23799	0.51884	0.79968	1.92307
778.75	0.09470	0.23092	0.50336	0.77580	1.86555
865.00	0.09163	0.22300	0.48574	0.74847	1.79941

Spectral dependence of optical thickness for assemblage #21

***λ(nm)* \ τ_a(550)**	***0.03***	***0.10***	***0.30***	***0.50***	***2.00***
412.50	0.11279	0.27034	0.58546	0.90057	2.16104
442.50	0.11103	0.26712	0.57931	0.89150	2.14024
490.00	0.10828	0.26171	0.56858	0.87545	2.10293
510.00	0.10713	0.25942	0.56400	0.86858	2.08689
560.00	0.10450	0.25391	0.55272	0.85152	2.04675
620.00	0.10153	0.24727	0.53875	0.83022	1.99612
665.00	0.09945	0.24250	0.52861	0.81472	1.95916
681.25	0.09874	0.24083	0.52499	0.80916	1.94583
708.75	0.09757	0.23799	0.51884	0.79968	1.92307
778.75	0.09470	0.23092	0.50336	0.77580	1.86555
865.00	0.09163	0.22300	0.48574	0.74847	1.79941

Spectral dependence of optical thickness for assemblage #22

***λ(nm)* \ τ_a(550)**	***0.03***	***0.10***	***0.30***	***0.50***	***2.00***
412.50	0.11333	0.27252	0.59090	0.90927	2.18278
442.50	0.11148	0.26893	0.58383	0.89872	2.15830
490.00	0.10852	0.26270	0.57106	0.87941	2.11283
510.00	0.10731	0.26012	0.56574	0.87136	2.09385
560.00	0.10446	0.25373	0.55228	0.85082	2.04500
620.00	0.10123	0.24605	0.53570	0.82535	1.98394
665.00	0.09896	0.24054	0.52371	0.80688	1.93955
681.25	0.09818	0.23859	0.51941	0.80022	1.92347
708.75	0.09689	0.23528	0.51206	0.78884	1.89596
778.75	0.09372	0.22699	0.49354	0.76009	1.82627
865.00	0.09030	0.21766	0.47238	0.72710	1.74598

Table 12-1 Continued: Spectral dependence of AOT for assemblages #23, 24 & 25

Spectral dependence of optical thickness for assemblage #23

***λ(nm)* \ τ_a(550)**	***0.03***	***0.10***	***0.30***	***0.50***	***2.00***
412.50	0.11333	0.27252	0.59090	0.90927	2.18278
442.50	0.11148	0.26893	0.58383	0.89872	2.15830
490.00	0.10852	0.26270	0.57106	0.87941	2.11283
510.00	0.10731	0.26012	0.56574	0.87136	2.09385
560.00	0.10446	0.25373	0.55228	0.85082	2.04500
620.00	0.10123	0.24605	0.53570	0.82535	1.98394
665.00	0.09896	0.24054	0.52371	0.80688	1.93955
681.25	0.09818	0.23859	0.51941	0.80022	1.92347
708.75	0.09689	0.23528	0.51206	0.78884	1.89596
778.75	0.09372	0.22699	0.49354	0.76009	1.82627
865.00	0.09030	0.21766	0.47238	0.72710	1.74598

Spectral dependence of optical thickness for assemblage #24

***λ(nm)* \ τ_a(550)**	***0.03***	***0.10***	***0.30***	***0.50***	***2.00***
412.50	0.11333	0.27252	0.59090	0.90927	2.18278
442.50	0.11148	0.26893	0.58383	0.89872	2.15830
490.00	0.10852	0.26270	0.57106	0.87941	2.11283
510.00	0.10731	0.26012	0.56574	0.87136	2.09385
560.00	0.10446	0.25373	0.55228	0.85082	2.04500
620.00	0.10123	0.24605	0.53570	0.82535	1.98394
665.00	0.09896	0.24054	0.52371	0.80688	1.93955
681.25	0.09818	0.23859	0.51941	0.80022	1.92347
708.75	0.09689	0.23528	0.51206	0.78884	1.89596
778.75	0.09372	0.22699	0.49354	0.76009	1.82627
865.00	0.09030	0.21766	0.47238	0.72710	1.74598

Spectral dependence of optical thickness for assemblage #25

***λ(nm)* \ τ_a(550)**	***0.03***	***0.10***	***0.30***	***0.50***	***2.00***
412.50	0.11305	0.27141	0.58814	0.90486	2.17174
442.50	0.11126	0.26804	0.58160	0.89516	2.14940
490.00	0.10840	0.26220	0.56981	0.87742	2.10784
510.00	0.10722	0.25978	0.56490	0.87002	2.09050
560.00	0.10448	0.25382	0.55249	0.85117	2.04586
620.00	0.10138	0.24666	0.53723	0.82780	1.99007
665.00	0.09921	0.24154	0.52620	0.81086	1.94951
681.25	0.09847	0.23973	0.52224	0.80476	1.93483
708.75	0.09723	0.23665	0.51549	0.79433	1.90969
778.75	0.09421	0.22897	0.49848	0.76799	1.84604
865.00	0.09097	0.22033	0.47906	0.73779	1.77272

Table 12-1 Continued: Spectral dependence of AOT for assemblages #26, 27 & 28

Spectral dependence of optical thickness for assemblage #26					
λ(nm) \ τ_a(550)	***0.03***	***0.10***	***0.30***	***0.50***	***2.00***
412.50	0.11305	0.27141	0.58814	0.90486	2.17174
442.50	0.11126	0.26804	0.58160	0.89516	2.14940
490.00	0.10840	0.26220	0.56981	0.87742	2.10784
510.00	0.10722	0.25978	0.56490	0.87002	2.09050
560.00	0.10448	0.25382	0.55249	0.85117	2.04586
620.00	0.10138	0.24666	0.53723	0.82780	1.99007
665.00	0.09921	0.24154	0.52620	0.81086	1.94951
681.25	0.09847	0.23973	0.52224	0.80476	1.93483
708.75	0.09723	0.23665	0.51549	0.79433	1.90969
778.75	0.09421	0.22897	0.49848	0.76799	1.84604
865.00	0.09097	0.22033	0.47906	0.73779	1.77272
Spectral dependence of optical thickness for assemblage #27					
λ(nm) \ τ_a(550)	***0.03***	***0.10***	***0.30***	***0.50***	***2.00***
412.50	0.11305	0.27141	0.58814	0.90486	2.17174
442.50	0.11126	0.26804	0.58160	0.89516	2.14940
490.00	0.10840	0.26220	0.56981	0.87742	2.10784
510.00	0.10722	0.25978	0.56490	0.87002	2.09050
560.00	0.10448	0.25382	0.55249	0.85117	2.04586
620.00	0.10138	0.24666	0.53723	0.82780	1.99007
665.00	0.09921	0.24154	0.52620	0.81086	1.94951
681.25	0.09847	0.23973	0.52224	0.80476	1.93483
708.75	0.09723	0.23665	0.51549	0.79433	1.90969
778.75	0.09421	0.22897	0.49848	0.76799	1.84604
865.00	0.09097	0.22033	0.47906	0.73779	1.77272
Spectral dependence of optical thickness for assemblage #28					
λ(nm) \ τ_a(550)	***0.03***	***0.10***	***0.30***	***0.50***	***2.00***
412.50	0.11280	0.27038	0.58556	0.90073	2.16142
442.50	0.11105	0.26721	0.57952	0.89183	2.14107
490.00	0.10828	0.26174	0.56864	0.87555	2.10318
510.00	0.10714	0.25947	0.56412	0.86877	2.08736
560.00	0.10450	0.25390	0.55269	0.85149	2.04667
620.00	0.10152	0.24724	0.53867	0.83009	1.99580
665.00	0.09944	0.24247	0.52853	0.81459	1.95883
681.25	0.09873	0.24079	0.52490	0.80901	1.94545
708.75	0.09756	0.23794	0.51871	0.79947	1.92254
778.75	0.09468	0.23082	0.50310	0.77539	1.86452
865.00	0.09159	0.22283	0.48532	0.74780	1.79773

Table 12-1 Continued: Spectral dependence of AOT for assemblages #29, 30 & 31

Spectral dependence of optical thickness for assemblage #29

λ(nm) \ τ_a(550)	*0.03*	*0.10*	*0.30*	*0.50*	*2.00*
412.50	0.11280	0.27038	0.58556	0.90073	2.16142
442.50	0.11105	0.26721	0.57952	0.89183	2.14107
490.00	0.10828	0.26174	0.56864	0.87555	2.10318
510.00	0.10714	0.25947	0.56412	0.86877	2.08736
560.00	0.10450	0.25390	0.55269	0.85149	2.04667
620.00	0.10152	0.24724	0.53867	0.83009	1.99580
665.00	0.09944	0.24247	0.52853	0.81459	1.95883
681.25	0.09873	0.24079	0.52490	0.80901	1.94545
708.75	0.09756	0.23794	0.51871	0.79947	1.92254
778.75	0.09468	0.23082	0.50310	0.77539	1.86452
865.00	0.09159	0.22283	0.48532	0.74780	1.79773

Spectral dependence of optical thickness for assemblage #30

λ(nm) \ τ_a(550)	*0.03*	*0.10*	*0.30*	*0.50*	*2.00*
412.50	0.11280	0.27038	0.58556	0.90073	2.16142
442.50	0.11105	0.26721	0.57952	0.89183	2.14107
490.00	0.10828	0.26174	0.56864	0.87555	2.10318
510.00	0.10714	0.25947	0.56412	0.86877	2.08736
560.00	0.10450	0.25390	0.55269	0.85149	2.04667
620.00	0.10152	0.24724	0.53867	0.83009	1.99580
665.00	0.09944	0.24247	0.52853	0.81459	1.95883
681.25	0.09873	0.24079	0.52490	0.80901	1.94545
708.75	0.09756	0.23794	0.51871	0.79947	1.92254
778.75	0.09468	0.23082	0.50310	0.77539	1.86452
865.00	0.09159	0.22283	0.48532	0.74780	1.79773

Spectral dependence of optical thickness for assemblage #31

λ(nm) \ τ_a(550)	*0.03*	*0.10*	*0.30*	*0.50*	*2.00*
412.50	0.09477	0.21907	0.57423	0.92938	3.59304
442.50	0.08494	0.19300	0.50173	0.81047	3.12599
490.00	0.07230	0.16046	0.41234	0.66423	2.55336
510.00	0.06782	0.14921	0.38176	0.61431	2.35842
560.00	0.05826	0.12579	0.31872	0.51165	1.95863
620.00	0.04912	0.10422	0.26165	0.41909	1.59986
665.00	0.04357	0.09147	0.22834	0.36521	1.39173
681.25	0.04178	0.08743	0.21785	0.34828	1.32645
708.75	0.03895	0.08112	0.20163	0.32214	1.22594
778.75	0.03281	0.06775	0.16758	0.26741	1.01614
865.00	0.02698	0.05530	0.13623	0.21715	0.82409

Table 12-1 Continued: Spectral dependence of AOT for assemblages #32 & 33

Spectral dependence of optical thickness for assemblage #32					
λ(nm) \ τ_a(550)	***0.03***	***0.10***	***0.30***	***0.50***	***2.00***
412.50	0.10279	0.24583	0.65449	1.06315	4.12813
442.50	0.09013	0.21030	0.55363	0.89696	3.47197
490.00	0.07449	0.16778	0.43431	0.70084	2.69980
510.00	0.06913	0.15359	0.39489	0.63620	2.44598
560.00	0.05801	0.12494	0.31617	0.50741	1.94166
620.00	0.04777	0.09972	0.24817	0.39661	1.50996
665.00	0.04174	0.08538	0.21006	0.33474	1.26985
681.25	0.03983	0.08092	0.19833	0.31573	1.19628
708.75	0.03683	0.07406	0.18045	0.28683	1.08471
778.75	0.03045	0.05990	0.14403	0.22816	0.85913
865.00	0.02455	0.04721	0.11196	0.17671	0.66231
Spectral dependence of optical thickness for assemblage #33					
λ(nm) \ τ_a(550)	***0.03***	***0.10***	***0.30***	***0.50***	***2.00***
412.50	0.11149	0.27480	0.74142	1.20803	4.70764
442.50	0.09557	0.22845	0.60808	0.98772	3.83500
490.00	0.07669	0.17511	0.45631	0.73751	2.84650
510.00	0.07043	0.15790	0.40781	0.65773	2.53211
560.00	0.05777	0.12414	0.31377	0.50341	1.92568
620.00	0.04655	0.09568	0.23604	0.37641	1.42913
665.00	0.04015	0.08007	0.19415	0.30822	1.16377
681.25	0.03815	0.07532	0.18152	0.28772	1.08423
708.75	0.03504	0.06810	0.16255	0.25700	0.96538
778.75	0.02855	0.05355	0.12498	0.19642	0.73217
865.00	0.02268	0.04099	0.09328	0.14558	0.53780

13.2 –AEROSOL FORWARD SCATTERING PROPORTION

For the 18 dust aerosol assemblages only, the aerosol forward scattering proportion (determined by the individual phase functions in the 4 aerosol layers) is tabulated at 11 MERIS bands (Table 13-2). The latter are used for estimating the atmospheric transmittances with the Gordon and Wang formulation in the third MERIS reprocessing.

Table 13-2: Aerosol forward scattering proportion in 11 MERIS bands for each of the 18 dust assemblages defined over ocean (*iaer* = 0-12, 31-33 are land aerosols and not included here).

iaer	*412.50*	*442.50*	*490.00*	*510.00*	*560.00*	*620.00*	*665.00*	*681.25*	*708.75*	*778.75*	*865.00*
13	0.912848	0.910016	0.908475	0.907741	0.905519	0.904598	0.903993	0.903750	0.903315	0.902107	0.900172
14	0.912848	0.910016	0.908475	0.907741	0.905519	0.904598	0.903993	0.903750	0.903315	0.902107	0.900172
15	0.912848	0.910016	0.908475	0.907741	0.905519	0.904598	0.903993	0.903750	0.903315	0.902107	0.900172
16	0.884346	0.883083	0.882889	0.882751	0.882195	0.882647	0.883092	0.883236	0.883463	0.884002	0.884535
17	0.884346	0.883083	0.882889	0.882751	0.882195	0.882647	0.883092	0.883236	0.883463	0.884002	0.884535
18	0.884346	0.883083	0.882889	0.882751	0.882195	0.882647	0.883092	0.883236	0.883463	0.884002	0.884535
19	0.855882	0.856153	0.857348	0.857827	0.859029	0.860967	0.862548	0.863114	0.864063	0.866524	0.869886
20	0.855882	0.856153	0.857348	0.857827	0.859029	0.860967	0.862548	0.863114	0.864063	0.866524	0.869886
21	0.855882	0.856153	0.857348	0.857827	0.859029	0.860967	0.862548	0.863114	0.864063	0.866524	0.869886
22	0.909263	0.905280	0.904401	0.903100	0.901661	0.900826	0.900287	0.900136	0.899902	0.899391	0.899377
23	0.909263	0.905280	0.904401	0.903100	0.901661	0.900826	0.900287	0.900136	0.899902	0.899391	0.899377
24	0.909263	0.905280	0.904401	0.903100	0.901661	0.900826	0.900287	0.900136	0.899902	0.899391	0.899377
25	0.882100	0.880093	0.880324	0.879900	0.88001	0.880612	0.881157	0.881365	0.881708	0.882577	0.884053
26	0.882100	0.880093	0.880324	0.879900	0.88001	0.880612	0.881157	0.881365	0.881708	0.882577	0.884053
27	0.882100	0.880093	0.880324	0.879900	0.88001	0.880612	0.881157	0.881365	0.881708	0.882577	0.884053
28	0.854892	0.854906	0.856346	0.856913	0.858817	0.861077	0.862882	0.863500	0.864499	0.866919	0.869917
29	0.854892	0.854906	0.856346	0.856913	0.858817	0.861077	0.862882	0.863500	0.864499	0.866919	0.869917
30	0.854892	0.854906	0.856346	0.856913	0.858817	0.861077	0.862882	0.863500	0.864499	0.866919	0.869917

- END OF DOCUMENT -